Modelling the terrestrial nitrogen and phosphorus biogeochemical cycles in an intermediate complexity Earth system climate model

by

© **Makcim Luis De Sisto Lelchitskaya**

A thesis submitted to the School of Graduate Studies in partial fulfillment of the requirements for the degree of Doctor of Philosophy.

Department of engineering and applied sciences

Memorial University

January 2024

St. John's, Newfoundland and Labrador, Canada

Abstract

The application of land nutrient limitation has been shown to improve the accuracy of carbon cycle estimates in Earth system models simulations. As the main limiting nutrients in terrestrial systems nitrogen and phosphorus cycles are crucial for the terrestrial carbon cycle representation. In this thesis a terrestrial nitrogen and phosphorus cycles modules were developed for Earth system models, utilizing the University of Victoria Earth System Climate Model. Both nitrogen and phosphorus cycles were then applied to assess the impact of nutrient limitation on remaining carbon budget estimations. Moreover, the nitrogen cycle representation was used to simulate terrestrial N_2O emissions. After coupling with an existing ocean N_2O emission module, the N_2O dynamics were used to project N_2O concentrations to the end of the 21st century. This represents the first fully coupled terrestrial-ocean N_2O dynamic module in existence. The terrestrial nutrient limitation reduced the capacity of terrestrial vegetation to uptake carbon, decreasing the land primary productivity. This decrease improved the representation of terrestrial productivity in comparison with observations. The remaining carbon budgets were reduced by 19 and 21% for the 1.5°C warming target with the application of nutrient limitation in different Shared Socioeconomic Pathways, re-enforcing the importance of nutrient limitation in the uncertainties of the carbon cycle. As remaining carbon budgets are an important decision-making metric, nutrient limitation is suggested to be taken into account when analyzing or estimating these budgets. The projection of N_2O concentration was between 401 to 418 ppb in the year 2100. These simulations show that N_2O concentrations are insensitive to mitigation efforts currently represented in the Shared Socioeconomic Pathways scenarios, showing similar values in low and high-emission scenarios. Overall, terrestrial nitrogen and phosphorus are an integral part of terrestrial systems and have improved the capacity of the University of Victoria Earth System Climate Model to represent the terrestrial carbon cycle.

Acknowledgements

I am grateful for the support from the Natural Sciences and Engineering Research Council of Canada's Discovery Grants programme and support from Compute Canada (now the Digital Research Alliance of Canada). I am indebted to Michael Eby for early advice on implementing the nitrogen version of the model and for providing the model code for the original N cycle version of UVic ESCM.

I want to express my gratitude to my supervisors Dr. Andrew MacDougall and Dr. Joseph Daraio. The supervision and guiding of Dr. Andrew MacDougall made this work possible, I am grateful and lucky to have such great supervisor. Furthermore, I would like to thank the supervisory committee members Dr. Lisa Kellman and Dr. Entcho Demirov for their invaluable support.

I am forever grateful and fortunate for the support I received from Sophia. Let this be an achievement that represents a victory for all our efforts. Without your support and encouragement this work would not exist.

Table of contents

List of tables

List of figures

Chapter 1

Introduction

Terrestrial nutrient biogeochemical cycles are sensitive to changes in atmospheric CO_2 concentrations and climate. Presently land biosphere absorbs around 25% of human CO_2 emissions (Friedlingstein et al. , 2022). In terrestrial ecosystems, carbon cycle feedbacks are constrained in part by the availability of nutrients (Fisher et al. , 2012; Zaehle et al. , 2014; Wieder et al. , 2015; Du et al , 2020). Among nutrients nitrogen and phosphorus are considered to be the most critical for limiting the primary productivity (Filipelli , 2002; Fowler et al. , 2013). Both are fundamental functional needs for plant biochemistry and their requirement is common in all vegetation taxa (Filipelli , 2002; Vitousek et al. , 2010; Du et al , 2020). Regionally, the scarcity of nutrients can impair the photosynthetic efficiency of terrestrial vegetation and consequently their response to increasing atmospheric CO_2 concentration. Hence, in Earth System Models (ESMs) the representation of nutrient limitations is imperative to improve the accuracy of carbon feedback projections and estimation of carbon budgets compatible with temperature guardrails, such as the 1.5 and 2.0 °C targets from the Paris Agreement (UNFCCC 2015).

The global distribution of N and P is dependent on the biogeochemical characteristics of each nutrient. N inputs are mainly from Biological Nitrogen Fixation (BNF) and atmospheric deposition (Fowler et al. , 2013; Du et al , 2020). In contrast, the main input of P comes from local rock weathering (mainly of the mineral apatite). The sourcing of P from local rocks are among the reasons for a global spatial pattern where young soils are usually N limited and old soil are usually P limited (Filipelli , 2002; Fowler et al. , 2013; Du et al , 2020). N accumulates rapidly from BNF where nitrogen fixers are abundant and slowly where atmospheric deposition is dominant. Thereby, old soils have a larger accumulation of N especially in regions where nitrogen fixers are abundant. On the other hand, P input is limited by the parent material and the bioavailability is further constrained by the retention of recalcitrant P in soils. Walker and Syers (1976) even suggested that P storage has a fixed total that cannot be rapidly replenished as parent material is limited.

These notions led to the common conceptualization that high latitudes are N-limited while tropical regions are P limited. While this generalization is correct in most observational studies, the complex pattern of limitation is more intricate, and P limitation could be more common than is commonly inferred. Du et al (2020) found that globally 43% of the terrestrial system is limited by P while only 18% is limited by N with the rest being co-limited by both. The addition of P has been shown to be positive for nitrogen fixation, leading to the replenishment of N in ecosystems (Eisele et al. , 1989). N supply on the other hand regulates the production of the enzyme phosphatase that cleaves ester-P bonds in soil organic matter (McGill and Cole , 1981; Olander and Vitousek , 2000; Wang et al. , 2007). Vegetation species variable adaption to nutrient concentrations also plays a role in the availability of nutrients in soils and the biogeography of terrestrial vegetation. Several studies have found that in some ecosystems lack of N in soil usually leads to dominance of woody

symbiotic nitrogen fixers (e.g. Menge et al. , 2012). The availability of P is also impacted by the geochemical interactions in terrestrial soils. Vitousek et al. (2010) defined six mechanisms by which P becomes limited: 1) driven (dissolved inorganic and organic phosphorus) loss by leaching; 2) soil barriers (soil layer that physically prevents access to roots); 3) transactional (slow release of mineral P forms); 4) P parent material; 5) sink driven (sequestration of P in soils and pools in the ecosystem); and 6) anthropogenic input of other nutrients (typically N input).

Earth system models represent biogeochemical processes such as the carbon cycle coupled to a physical climate system (Kawamiya et al. , 2020). Given the importance of terrestrial nitrogen and phosphorus on terrestrial ecosystems in Earth system models, the representation of nutrient limitation in terrestrial structure is thereby crucial to improve the representation of the terrestrial carbon cycle (Wang et al. , 2010; Goll et al. , 2017; Wang and Goll , 2021). The inclusion of nutrient limitation in Earth system models has been considered globally in several Earth system modelling groups with the recent Intergovernmental Panel on Climate Change (IPCC) report using six ESMs containing a terrestrial nitrogen cycle and only one containing a terrestrial phosphorus cycle (Spafford and MacDougall , 2021). However, the role of nutrient limitation in Earth system model global carbon cycle uncertainties is still understudied. Furthermore, the emission of N_2O from terrestrial systems from the nitrogen cycle is rarely simulated in Earth system model structures and no model has dynamically modelled a coupled terrestrial-ocean N_2O dynamics to project N_2O concentrations in the atmosphere.

1.1 Scientific questions

In this study, I address the role of terrestrial nutrient limitation in Earth system model projections and uncertainties. The most common issue is overestimating the land carbon sink in simulations without nutrient limitation. Other terrestrial nutrient limitation impacts on Earth system model uncertainties include: 1) missing anthropogenic impacts on terrestrial nutrient concentrations, 2) terrestrial phosphorus is rarely included in Earth system models but has been suggested to be necessary for accurate tropical forest representation and 3) missing non-CO_2 greenhouse gasses emissions simulation from terrestrial N_2O fluxes.

1.1.1 How does the terrestrial nutrient anthropogenic forcing impact Earth system model carbon cycle estimates?

The nitrogen and phosphorus cycles have been shown to be impacted by human activities (Filipelli , 2002; Fowler et al. , 2013). Human impact on ecosystems is altering the abundance of N and P globally (Harrison et al. , 2010; Beusen et al. , 2013; Harrison et al., 2019). A significant change in the export of particulate and dissolved nutrients from land to rivers, and ultimately to coastal seas, has been caused by human activities on land (Mayorga et al , 2010). For example, fertilizer application for agriculture is a key factor that has reduced nitrogen and phosphorus limitations in agricultural areas (Vitousek et al. , 1997; Tilman et al. , 2002). In nature, nitrogen input from biological nitrogen fixation is estimated to be between 52 to 130 TgN yr^{-1} and the input of phosphorus from rock weathering is estimated to be between 1 to 3 TgP yr^{-1} (Filipelli , 2002; Wang et al. , 2010; Fowler et al. , 2013). Globally, the rise of food demand has increased the application of agricultural fertilizer (Smil , 2002). The increasing and excessive use of fertilizers is resulting in a variety of

environmental problems (Bouwman et al. , 2016; Vitousek et al. , 2009). Lu and Tian (2017) show that synthetic N and P fertilizer use worldwide increased by 85 Tg N yr^{-1} and 10 Tg P N yr^{-1}, respectively, from 1960 to 2013. On a global scale, Southern Asia (which includes East Asia, South Asia, and Southeast Asia) accounted for 71 % of the increase in N fertilizer use, followed by North America (11 %), Europe (7 %), and South America (6 %). In addition, there has been a significant increase in the amount of P available in the environment due to mining and its use as fertilizer, detergent additives, sewage and animal feed supplements (Seitzinger et al. , 2010).

Furthermore, Beusen et al. (2022) projected increases in global river dissolve inorganic phosphorus export are projected in all sustainable socioeconomic pathways. This is primarily due to an increase in sewage, fertilizer, P-based detergents, and manure input. This has direct implications for the environment, affecting biological productivity, diversity and abundance of species (Modolo et al , 2018; Pesce et al. , 2018). A healthy ecosystem is dependent on biodiversity to maintain its functioning. Consequently, these alterations have profound effects on the carbon cycle and feedback in most ecosystems (Shibata et al. , 2015). Earth system models that lack nutrient cycles overlook the anthropogenic impact in terrestrial systems and thus, their effects on the carbon cycle.

1.1.2 What is the role of terrestrial nutrient limitation in Earth system models carbon cycle uncertainties?

The change of nutrient concentration in terrestrial systems is an uncertainty in determining the degree of nutrient limitation impact on land carbon sink over the next decades (Shibata et al. , 2010, 2015; Menge et al. , 2012). Anthropogenic input of N and P via agricultural fertilization (artificial and manure), atmospheric deposition

and urban waste waters account for a large portion of nutrient concentration in land and, for some regions, have even doubled the natural coastal input (Lu and Tian , 2017). This has resulted in unwanted ecosystem changes such as eutrophication, hypoxia, and anoxia (Selman et al. , 2008). Artificial and biogenic nitrogen fertilization data for different Shared Socioeconomic Pathways are already available for model use, but similar gridded data for P does not exist at present.

By 2050, global income levels and population levels are expected to increase. Consequently, there is a likelihood that the amount of food consumed and the number of livestock-based products will increase (Bodirsky et al. , 2015), thus increasing the environmental impact of agriculture. Future demand for agricultural goods, as well as land use dynamics, are uncertain. Increasing populations, changes in dietary preferences, and changes in trade patterns will increase the need for non-food products such as bioenergy, and the development of agricultural yields will be influenced by relevant policies that will lead to a further increase in these demands (Popp et al. , 2014).

Many of the critical processes involved in land biogeochemical models are difficult to parameterize due to a lack of observational datasets, thereby decreasing the quantitative understanding of key processes and their interactions (Wang and Goll , 2021). It is important to ensure that these models remain up to date with the increasing availability of observation-based data. Improvement and further development is required in Earth system models to ensure they remain relevant to the current state of knowledge in theory (Achad et al. , 2016).

1.1.3 How much will atmospheric N_2O increase by the end of the 21st century?

CO_2 emissions are the primary source of greenhouse gasses (GHGs) accumulation in the atmosphere. The total anthropogenic radiative forcing from greenhouse gasses between 1960-2019 was 63% for CO_2, 11% for CH_4, 6% for N_2O, and 17% for the halogenated species (Canadel et al. , 2021). CH_4 and N_2O are the most critical non-CO_2 GHGs emissions contributors accounting for between 11.5 - 14 and 5.8 - 6.8 % of global emissions respectively from 1990 to 2018 (Crippa et al. , 2021). In comparison to CH_4, N_2O has a longer atmospheric lifetime (Myhre et al. , 2013; Prather et al. , 2023). Considering that N_2O is one of the most significant contributors to net anthropogenic climate forcing, global climate change policies in the twenty-first century must take its fluxes into consideration. A number of factors are expected to contribute significantly to agricultural N_2O emissions, including population growth, per capita calorie intake, and livestock consumption. It is possible to improve estimates of current and future agricultural N_2O emissions around the world by simulating and quantifying the relationship between perturbations in N inputs and increases in N_2O emissions by simulating the nitrogen cycle and more precisely quantifying the effects of perturbations in N inputs in terrestrial systems. Projections from non-dynamic atmospheric N_2O concentration, where the N_2O is estimated with a simplified equation, show a significant increase of N_2O by the end of the century, dependent on the assumptions of different future projections N_2O management and overall model forcing (Meinhaussen et al. , 2020).

1.1.4 What is the impact of terrestrial nutrient limitation on the sensitivity of the terrestrial carbon cycle to changes in atmospheric CO_2 concentrations?

The response of terrestrial ecosystems to climate changes involves the model to represent the interactions between climate and carbon. N and P control, in part, the response of the carbon cycle to environmental disturbances. Hence, N and P are crucial for accurately representing the terrestrial system in Earth system models to changes in atmospheric CO_2 concentrations.

The simulations from first-generation ESMs with carbon-only schemes have very likely overestimated the response of the terrestrial ecosystem to the increase of atmospheric CO_2 concentrations (Hungate et al. , 2003; Thorton et al. , 2007), showing a high terrestrial carbon uptake response which would require an unrealistic large nutrient supply. The addition of a nitrogen cycle to the land system in ESMs has shown an overall reduction in the effect of CO_2 fertilization, especially in high latitudes, with a weaker response in low latitudes which are typically P limited in natural systems (Wang et al. , 2007, 2010; Du et al , 2020). However, the effect of N and P limitation on carbon budgets for given temperature guardrails has yet to be systematically quantified.

Despite its importance P terrestrial limitation has been neglected in Earth system modelling. The effect of P in tropical forests may be the key to better representing the vegetation biomass and the response to CO_2 fertilization, in these systems. The lack of P observational data is partly responsible for the difficulty of simulating P limitation in Earth system models (Spafford and MacDougall , 2021). However, several studies have attempted to provide reliable global P datasets (Yang et al. , 2013; Hartmann et al. , 2014; He et al. , 2021) that could be used to develop more accurate models.

Furthermore, many studies have shown that the inclusion of P into ESM structures is possible and that it improves the representation of vegetation biomass in tropical regions (Wang et al. , 2007, 2010; Goll et al. , 2017; Nakhavali et al. , 2021).

1.2 Purpose of study

The current generation Earth system models are developing or have already developed nitrogen and phosphorus cycles and nutrient limitation to their model structure. While carbon-nitrogen (CN) models are more common, carbon-nitrogen-phosphorus (CNP) models remain rarer. However, P cycles have been suggested to be included in Earth system model for their importance in tropical regions (Wang et al. , 2010; Goll et al. , 2012). The first attempt to include nutrient limitation in the University of Victoria Earth system climate model (UVic ESCM) was done by Wania et al. (2012) but was not included in the current publically available version of the model due to the need of further improvement. In order to improve the carbon cycle projections here I intend to improve the current state of the previous N cycle, develop a new P cycle and couple CNP in the UVic ESCM version 2.10. Thereby, allowing the assessment of carbon budget uncertainties and the simulation of terrestrial N_2O emissions and atmospheric N_2O concentrations in long-term projections. The assessment of terrestrial N and P limitations on the estimation of carbon budgets, and the coupling of terrestrial N_2O emissions modules with ocean N_2O emissions presented here are the first study of their kind. The following specific objectives set in the present study are:

1. Develop an improved nitrogen cycle for the UVic ESCM version 2.10.
2. Develop a phosphorus cycle for the UVic ESCM version 2.10.
3. Add agricultural fertilization to the terrestrial nitrogen and phosphorus cycles.

4. Determine the impact of nutrient limitation on the global carbon cycle in future projections.
5. Determine the impact of nutrient limitation on remaining carbon budgets derived from future projections.
6. Assess the modelled N_2O flux estimations in future climate projections.

1.3 Thesis outline

The following chapters describe the development and application of a terrestrial nitrogen and phosphorus cycles in an Earth system model of intermediate complexity. Chapter two is a relevant literature review on the terrestrial nitrogen and phosphorus cycles and a short description of the current modelling approaches. Chapter three contains details of the development of terrestrial nitrogen and phosphorus cycles on an intermediate complexity Earth system climate model. Chapter four applies the nitrogen and phosphorus modules to assess the impact of terrestrial nutrient limitation on the estimation of remaining carbon budgets. Finally, chapter five applies the new terrestrial nutrient modules to project of atmospheric N_2O concentrations. The projection of atmospheric N_2O using a coupled terrestrial and marine N_2O modules in an Earth system model, is, to my knowledge, the first of its kind.

Chapter 2

Literature review

In this chapter, I will review the importance of nitrogen and phosphorus for plant biochemistry and their terrestrial biogeochemical cycles. The importance of N and P in terrestrial ecosystems is widely known. Nutrient limitation occurs globally and impacts the potential plant growth. Thereby, affecting human activities such as agriculture and placing a natural constraint on global terrestrial vegetation productivity.

2.1 Nutrients in plants

Nutrients play a crucial role in the metabolism of plants. Organic molecules such as sugar, nucleic acids, and proteins are generally synthesized through biochemical processes involving just six elements (C, H, O, N, P, and S) (Maathuis , 2009; Travers and Muskhelishvili , 2015). Nutrients are divided into macronutrients and micronutrients according to their concentration requirements (de Bang et al. , 2021). Plants, for example, utilize macronutrients (K, Ca, C, P, N and Mg) to control pH, osmotic pressure, and enzyme activity. Six micronutrients (Fe, Mn, Zn, Cu, Mo, and Ni) are metals that are essential for oxidative, reductive reactions in enzymes or heme.

Plant metabolism is consequently affected by the concentration of core nutrients in plant structures and the availability to obtain said elements from their environment (Maathuis , 2009; DalCorso et al. , 2014).

2.2 Nitrogen impacts on plant growth

Various environmental factors affect plant growth, including temperature, water supply, nutrients, and light intensity (Atilio and Causin , 1995). Nitrogen availability in soil is essential for plant growth (Gruber and Galloway , 1995). Hence, the supply of nitrogen has been linked to the growth of vegetation (Coskun et al. , 2016). It is essential for plant development that N is available to roots during the plant's life cycle. Nitrogen influences a wide range of physiological processes (Atilio and Causin , 1995; Munawar et al. , 2017). The growth and development of leaves stems, and parts are promoted by N. With abundant N, leafy vegetables grow more rapidly, and early growth is accelerated (Leghari et al. , 2016). Additionally, it facilitates the uptake and utilization of other nutrients, such as potassium and phosphorus (Duncan et al. , 2018), and regulates the growth of the plant as a whole. All organisms, both prokaryotes and eukaryotes, rely on N for several essential compounds, including membrane lipids, amino acids, proteins, nucleic acids (DNA, RNA), nicotinamide adenine dinucleotide, nicotinamide adenine dinucleotide phosphate, co-enzymes, secondary metabolites, photosynthesis pigments, and many others (Maathuis , 2009).

2.3 Nitrogen in soils

There are two predominant forms of inorganic nitrogen in soils, nitrate (NO_3^-) and ammonium (NH_4^+) (Bronson et al. , 2008) as well as organic nitrogen compounds. In general, organic nitrogen consists of urea, free amino acids, and short peptides

(Farzadfar et al. , 2021). In aerobic soils, NO_3^- is the most abundant form of inorganic nitrogen and is readily leached (Bronson et al. , 2008). While NH_4^+ tends to be adsorbed strongly to soil particles(Kothawala and Moore , 2009). Due to soil heterogeneity and dynamic microbial conversions, as well as agronomic practices and environmental conditions, the availability of these resources by roots varies considerably over time and space (Farzadfar et al. , 2021).

2.4 Terrestrial nitrogen cycle

Nitrogen is an essential element for the survival of terrestrial life. Therefore, it is evident that the N biogeochemical cycle plays a significant role in terrestrial ecosystems. Overall, the N cycle is driven by microbial and plant processes (Fowler et al. , 2013; Isobe and Nobuhito , 2014). Furthermore, there are a number of physicochemical processes that contribute to the distribution of nitrogen concentrations on land. These processes include diffusion, emission, volatilization, leaching, and erosion. A variety of nitrogen transformations take place in terrestrial ecosystems, including the uptake and immobilization of nitrogen by microbes and plants, as well as the production and decomposition of litter (McNeill and Unkovich , 2007; Fowler et al. , 2013). The following short review of the N cycle will show the flow of N through the terrestrial system.

2.4.1 Inputs of N to terrestrial systems

The primary natural source of nitrogen in the terrestrial N cycle is biological fixation, followed by wet and dry deposition of N, with lightning providing a relatively minor contribution (Fowler et al. , 2013). Anthropogenic sources of nitrogen include

agriculture fertilizers (artificial and manure), wastewater from urban areas and atmospheric deposition (Lu and Tian , 2017). N input is primarily derived from BNF in the absence of human influences (Fowler et al. , 2013; Vitousek et al. , 2013).

2.4.2 Biological nitrogen fixation

Despite of the fact that nitrogen gas (N_2) makes up 78% of the Earth's atmosphere and is indispensable for the survival of all life forms, biological systems cannot utilize atmospheric nitrogen directly. In order to break the triple bond of N_2, substantial amounts of energy are required, as well as the addition of three hydrogen atoms to each N atom to produce ammonium (Ward , 2012). Prokaryotes, including Archaea and Bacteria, are the only organisms capable of fixing nitrogen. These use the energy derived from the oxidation of carbohydrates to reduce molecular nitrogen (N_2) to ammonia (NH_3) (Halbleib et al , 2000). The chemical reaction for the fixation of atmospheric N is:

$$N_2 + 16\text{ATP} + 8\text{e}^- + 8\text{H}^+ \rightarrow 2NH_3 + \text{H}_2 + 16\text{ADP} + 16\text{P}, \tag{2.1}$$

where ATP is Adenosine Triphosphate and ADP is Adenosine Diphosphate, both of which have an important role in cellular energy. A substantial amount of N_2 can be converted into organic N by biological N fixers, which is sufficient for maintaining N pools in ecosystems and replenishing N losses (Fowler et al. , 2013). A variety of factors constrain nitrogen-fixer organisms, including individual biochemistry and environmental conditions. For example: 1) Abiotic controls such as temperature, moisture, and pH can impact the enzymatic rate. 2) The presence of O_2 can inhibit the biochemical nitrogen fixation pathway. 3) Molybdenum is required for the function of most nitrogenases. 4) High concentrations of nitrogen can also inhibit the synthesis

and/or activity of nitrogenase (Vitousek et al. , 2002). However, there is currently no consensus regarding the limitations on biological nitrogen fixation (Barnard and Friedlingstein , 2020)

2.4.3 Organic matter decomposition, mineralization and immobilization

Litter production and decomposition are key contributors to the turnover of nitrogen in the terrestrial environment (Giweta , 2020). Through internal nitrogen cycling, nitrogen enters the soil organic matter pool. The decomposition of organic matter is largely mediated by soil microbes. This ultimately results in the release of nutrients in mineral form and the loss of carbon from the soil (Khatoon et al. , 2017). The bioavailable nitrogen resulting from macromolecule cleavage can be utilized by both plants and microorganisms. The mineralization of nitrogen in soil involves the release of NH_3 or NH_4^+ by heterotrophic soil microbial communities (Giweta , 2020). Mineralization of nitrogen occurs in biologically active horizons of soils that contain a large amount of dead and decomposing plants and other organisms (Ward , 2012). N can be immobilized by microbial assimilation (Bengston and Bengtson , 2005). Alternatively, adsorption to organic matter or fixation in clay can immobilize ammonium and reduce concentrations in soil.

2.4.4 Nitrification

The process of nitrification involves the oxidation of reduced nitrogen forms in order to produce nitrate (NO_3^-) yielding energy to microbes. There are two steps involved: 1) Ammonia is oxidized to hydroxylamine by the enzyme ammonia monooxygenase. 2) Hydroxylamine is oxidized by hydroxylamine oxidoreductase using oxygen from

water. Ammonia oxidation requires two electrons, while the remaining electrons pass through the electron transport chain (Norton , 2008). The process is mediated by three types of microorganisms: 1) autotrophic ammonia oxidizers, (2) autotrophic nitrite oxidizers, and (3) heterotrophic nitrifiers (Ward , 2008).

2.4.5 Plant uptake

Abiotic factors such as temperature and soil pH influence the acquisition of nitrogen by plants, in addition to the genetic characteristics of the plant species (Santoyo et al. , 2017). N can be acquired by plants from the soil in the form of NH_4^+, NO_3^- or NO_2^-, or as simple organic compounds (Bronson et al. , 2008). Generally, plants prefer inorganic N forms, and some species may show a preference for NH_4^+ or NO_3^-. Regulation of nutrient uptake by roots is governed by root system architecture and mechanisms that control transport system activity (Masclaux et al. , 2010). Allocation of nutrients to plant structures will depend on the metabolic health of plants.

2.4.6 Denitrification

Nitrate is converted into gaseous nitrogen compounds such as N_2O, NO, and N_2 during denitrification under anaerobic conditions. NO_3 is reduced to NO_2, followed by NO, N_2O, and N_2. Nitrogen oxides serve as electron acceptors during the process, which is similar to the electron transport chain involved in aerobic respiration (Spanning and Delgado , 2006). There are four stages involved in denitrification: reducing nitrates, reducing nitrites, reducing nitric oxides, and reducing nitrous oxides. They are catalyzed by a specific reductase enzyme. An incomplete process results in the emission of NO and N_2O, which are major atmospheric pollutants (MacDuffie et al. , 2020). The emission of intermediates is caused when electron fluxes are unbalanced over the

four subsequent steps of denitrification or when incomplete pathways are expressed or present in denitrifying organisms (Ward , 2012). Multiple promoters regulate gene expression during the induction of the denitrification pathway after oxygen depletion. In spite of the fact that many types of bacteria have similar promoters, the exact mechanism of regulation varies from one species to another (Carreira et al. , 2018). Specific environmental factors such as oxygen and nitrogen oxide concentrations, as well as metal ions, affect gene expression.

2.5 Phosphorus impacts on plant growth

For terrestrial plants, phosphorus availability in soils is a significant challenge (Du et al , 2020; Hou et al. , 2020). The availability of P is limited for plant uptake (Penn and Camberato , 2019). P deficiency generally results in a reduction in plant growth due to a decrease in the photosynthetic rate (Cartensen et al. , 2018). In cells, it maintains the structure of the cell membrane, and phospholipids are an essential component of the membrane. A vital role is also played by phosphorus in the synthesis and formation of biomolecules. There are many energy-rich compounds that contain this compound, such as adenosine triphosphate (ATP), cytidine triphosphate (CTP), guanosine triphosphate (GTP), uridine triphosphate (UTP), phosphoenol pyruvate, and others. By transferring energy to acceptor molecules, these phosphate-containing compounds serve as cellular energy carriers. Furthermore, it participates in the division of cells, the activation and inactivation of enzymes, and the metabolism of carbohydrates. As a result, P promotes the germination of seeds, the development of roots, stalks, and stems, the production of flowers and seeds, the quality and yield of crops, and the production of the seed itself (Malhotra et al. , 2018). Plant growth parameters and photosynthesis are sensitive to P concentration in plant structures.

Walker et al. (2014) found a significant correlation between leaf phosphorus concentration and photosynthetic rate. A low concentration of cytoplasmic P inhibits photosynthesis as a result of end-product inhibition (Rychter et al. , 2016). It has also been demonstrated that P is essential for the activation of RuBisCO, the key enzyme used to fix CO_2 for photosynthesis (Marcus et al. , 2011).

2.6 Phosphorus in soils

Various forms of phosphorus are found in soils, and their distribution changes with time and soil development (Walker and Syers , 1976; Yang et al. , 2013). P in soil can be divided into inorganic and organic. Inorganic phosphorus is predominantly present as $H_2PO_4^-$ and HPO_4^{-2} adsorbed onto oxides or hydroxides of Fe or Al, organic matter, or bound to calcium (Muindi , 2019). The pH and clay minerals of soil affect the adsorption of P in soil (Lopez and Burnham , 2006). A low pH value results in insoluble compounds with iron and aluminium, a neutral pH value results in more soluble compounds with calcium and magnesium, and a higher pH value results in insoluble compounds with calcium. Soil inorganic P compounds are grouped as calcium, magnesium-bound, iron and aluminium-bound (Muindi , 2019).

In soils, native phosphorus is mainly derived from disintegrated and transformed rocks containing mineral apatite, $Ca_{10}(PO_4)_6(F.Cl.OH)_2$. Due to its low solubility and rate of solubilization, apatite in its primary form does not provide available phosphate to plants. Apatites, strengite, and variscite, are generally stable in acidic soils and release a minimum amount of P into the soil solution when weathered. Depending on particle size and soil pH, secondary phosphate minerals containing calcium, iron, and/or aluminium dissolve differently. In general, increasing soil pH increases the solubility of iron and aluminum phosphates, but decreases the solubility of calcium

phosphates until pH values are above 8, at which point the solubility of calcium phosphates begins (Muindi , 2019). As the soil weathers, bases, silicates, and carbonates are removed, iron and aluminum are concentrated, and phosphorus is released into the soil solution (Filipelli , 2002; Hartmann et al. , 2014). The soluble P can also be sorbed or desorbed into or out of secondary minerals, becoming available as labile P or unavailable for plant uptake (Wang et al. , 2010; Yang et al. , 2013). A variety of mechanisms retain P in soils, including ligand exchange, adsorption, and precipitation. These mechanisms vary with soil pH. In acid soils, adsorption of P occurs primarily via a complex formed between orthophosphate anions and metal cations or metal oxyhydroxides (such as Fe and Al). P retention in alkaline and calcareous soils usually occurs as a result of precipitation of calcium phosphate minerals or as a result of adsorption on iron impurities within the carbonates (Muindi , 2019).

2.7 Terrestrial phosphorus cycle

The P cycle, as N, plays an important role in terrestrial ecosystems. A deep understanding of P soil chemistry is essential in order to understand the flow of P through life and the soil. P speciation varies in relation to soil pH, mineral content, temperature, and other soil characteristics (Walker and Syers , 1976; Hartmann et al. , 2014). There is typically a low concentration of P that is available for uptake by plants and microbes (Filipelli , 2002). According to the climate, the type of soil, and the level of the ecosystem, P is generally vigorously recycled to varying extents in ecosystems (Yang et al. , 2013).

2.7.1 Phosphorus input

P is released primarily from apatite minerals and is made soluble and bioavailable by weathering (Filipelli , 2002). Unlike this chemical weathering process, physical weathering and erosion of continents release P that is typically not available for life on Earth. The chemistry and structure of apatite minerals vary greatly depending on the environments in which the apatite-bearing rocks where form, including igneous, metamorphic, sedimentary, and biogenic environments (Malhotra et al. , 2018). P is also added to the ecosystem by human influence. Fertilizers and urban wastewater are both significant inputs that some studies have identified to surpass natural inputs (Lu and Tian , 2017).

2.7.2 Mineralization and immobilisation

P mineralization includes biological and biochemical processes (McGill and Cole , 1981). The process of biological mineralization involves the conversion of organic P into bioavailable orthophosphates as a result of the oxidation of carbon by soil organisms (Samal et al , 2020). Biochemical mineralization is the process of releasing inorganic P from organic compounds by way of enzymatic hydrolysis outside of the cell membrane. The need for phosphate by microorganisms is thought to control this type of mineralization because of the negative feedback between P availability in the organism and phosphatase biosynthesis in the cell (Oehl et al , 2004). Finally, P immobilization by biological processes refers to the assimilation of P in soil by microorganisms. Due to this conversion, the P becomes inaccessible to plants as organic forms. In the course of time, microbial P will become available as the microbes die (Waithaisong et al. , 2022).

2.8 Modelling the terrestrial nitrogen and phosphorus cycles in Earth system models

In terrestrial Earth system model structures, the representation of nutrient limitation on the carbon cycle is a major factor that needs to be considered, as it constrains the capacity of plants to uptake carbon (Wang et al. , 2010; Goll et al. , 2017; Wang and Goll , 2021). The lack of nutrient limitation usually leads to high estimations of terrestrial carbon uptake, as shown in Wieder et al. (2015). The uncertainty of nutrient limitation has been addressed in Earth system models in the last two decades but has only begun to be systematically included in Earth system models in the previous decade (Wang et al. , 2007; Yang et al. , 2009; Wang et al. , 2010; Yang et al. , 2013; Goll et al. , 2017; Wang and Goll , 2021). The latest Intergovernmental Panel on Climate Change report (IPCC) included six models with terrestrial nitrogen and one with a terrestrial nitrogen-phosphorus cycle (Arora et al. , 2020; Spafford and MacDougall , 2021)

Developing modules for Earth system models is closely linked to the availability of observational and experimental studies that provide model equations to represent nature processes and datasets to calibrate and validate model outputs. Globally, the terrestrial nitrogen and phosphorus cycles generally lack observational and experimental studies (Wang and Goll , 2021). Hence, the estimation of the global nitrogen and phosphorus cycle is challenging and large ranges of uncertainty are embedded in global attempts to improve their representation. These uncertainties plague the accuracy of estimations. Intermediate complexity models suffer, especially as validation through downscaling to site scale may not be used due to low resolution. However, new studies are emerging showing global terrestrial nutrient datasets processed with artificial intelligence (He et al. , 2021). Again, these studies are challenged by the

lack of global data as input to train machine learning processes.

Early attempts to include nutrients in model structures consisted of the use of constant carbon-to-nutrient ratios e.g.(Mengis et al. , 2020). This has gradually has been shifting to dynamic carbon-to-nutrient ratios. The advantage is the capture of the time-variation of nutrients and, thereby, a more accurate representation of nutrient limitation in terrestrial systems that can reflect changes to global warming, land use change and agricultural activities (Wang et al. , 2010; Goll et al. , 2017).

The nitrogen inputs in Earth system models generally consist of biological nitrogen fixation, atmospheric nitrogen deposition and fertilizers inputs, with rock weathering and lightning sources being disregarded in most cases (Yang et al. , 2009; Gerber et al. , 2010; Wang et al. , 2010; Zaehle et al. , 2010; Wania et al. , 2012; Goll et al. , 2017; Wang et al. , 2020). Biological nitrogen fixation can be represented through empirical relationships with ecosystem productivity (Gerber et al. , 2010; Wania et al. , 2012). The uptake of inorganic nutrients by plant roots can be simulated by direct plant uptake or/and by mycorrhizae symbiosis (Wang et al. , 2010; Wania et al. , 2012; Braghiere et al. , 2021, 2022). The carbon cost for nitrogen uptake by mycorrhizae is also considered in some models as a constraint to the amount of nitrogen plants can uptake (Braghiere et al. , 2022)

The plant structural division varies among models. The simplest models contain three basic compartments: roots, wood and leaves with a constant or flexible stoichiometry (Wang et al. , 2010; Gerber et al. , 2010; Wania et al. , 2012; Goll et al. , 2017; Wang and Goll , 2021). These three compartments are connected to a litter pool, and this pool can be divided further into metabolic, structural and coarse woody debris in some models (Wang et al. , 2010). The litter is usually dependent on plant functional types parameterization and temperature-dependent equations (Wania et

al. , 2012). The resorption of nutrients during senescence is usually constant (Gerber et al. , 2010; Wania et al. , 2012). However, Reed et al. (2012) has shown interesting patterns of nutrient resorption which suggest the need for a dynamic structure. The recycling of nutrients in leaves is an important uncertainty as some models define nutrient limitation based on nutrient concentrations in leaves (Wania et al. , 2012; Mengis et al. , 2020). In soils, the recycling of soil organic matter is controlled by environmental conditions and soil type, with microbial processes being simplified as most Earth system models do not represent microbes explicitly (Wang and Goll , 2021).

The loss of nutrients varies among models containing leaching, harvesting, fire, nitrification and denitrification processes (Yang et al. , 2009; Wang et al. , 2010; Gerber et al. , 2010; Wania et al. , 2012; Goll et al. , 2017). The leaching of nitrogen is generally dependent on the inorganic nitrogen concentration in soils, drainages and soil moisture (Wang and Goll , 2021). The flux of leach nitrogen is further controlled by the runoff of water through the soil structures (Wania et al. , 2012). Gaseous loss from nitrification and denitrification represents much of the total nitrogen loss (Fowler et al. , 2013). Denitrification can only be simulated in land model structures with the capacity to estimate a low fraction of oxygen in soils. The requirement is often the simulation of aquatic-terrestrial interfaces such as wetlands or inundated soil grids (Grosso et al. , 2020).

The phosphorus cycle inputs generally consist of constant rates applied to global soil type order distribution maps (Wang et al. , 2010; Yang et al. , 2013). The release rate of P is differentiated in low-high weathered soils and given a constant value (Wang et al. , 2010; Goll et al. , 2017). These values are then applied to global maps. Another way of simulating global phosphorus inputs is by estimating

the phosphorus release from parent material as a function of runoff, temperature and wind as shown in (Hartmann et al. , 2014). In soil, sorption-desorption processes are generally accounted for. In equilibrium, sorption-desorption processes can be determined using non-linear Langmuir equations, while in disequilibrium, kinetic-type Langmuir equations are better suited (Wang et al. , 2010, 2020). Usually, models assume rapid equilibrium on each time step. Others, such as Goll et al. (2017), use a much simpler approach, where the amount of phosphorus sorbed out of the labile solution is determined by global constant rates per soil type. Furthermore, there can be a division between sorption and strong sorption, where the strongly sorbed is considered to be a loss of phosphorus of the terrestrial structure (Wang et al. , 2010). The microbial turnover of phosphorus in soils also depends on soil types and environmental conditions, mainly soil moisture and temperature (Wang et al. , 2010; Goll et al. , 2017; Wang et al. , 2020). Some models account for the nitrogen cost for phosphorus-related enzymes (Wang et al. , 2010). This represents a subtle co-limitation in Earth system models. The outputs of phosphorus consist mainly of strong sorption and leaching (Wang et al. , 2010; Goll et al. , 2017; Wang et al. , 2020). Leaching is generally modelled as a function of soluble phosphorus and runoff flux (Goll et al. , 2017).

2.9 Applicability of Earth system models and the development of nitrogen and phosphorus cycles modules to engineering

There are several uses of Earth system models in engineering and these are mostly dependent on model resolution. As tools for projecting long-term changes in the

Earth systems, Earth system models are valuable to assess future impacts caused by anthropogenic climate change. Hence, Earth system models can be used to predict threats to livelihood and infrastructure, and can be used to project conditions in long-term scenarios (Gelbrecht et al. , 2023). The different projections are dependent on the forcing data input fed into the model simulations (Meinhaussen et al. , 2020). Important variables, such as sea level rise, storm surges and other extreme events can be predicted with a reasonable uncertainty (Siahaan et al. , 2022). In coastal regions, for example, the improvement of infrastructure resilience is imperative under climate change (Chester et al. , 2021). However, the regional application of global models with downscaling approaches is limited to relatively high-resolved models (Rockel , 2015).

The following studies tackle uncertainties in the global carbon cycle with the development and application of terrestrial nutrient limitation and the addition of atmospheric N_2O forcing. These uncertainties affect our prediction for future warming and hence, the prediction of variables related to human activities and infractures. While the following terrestrial nitrogen and phosphorus cycle is applied in an intermediate complexity Earth system and climate model, by itself, it represents a stand-alone coding structure that can be ported to other models, improving their capacity to represent the global carbon cycles and allowing for the estimation of N_2O emissions. Hence, improving the accuracy of models to predict future warming, climate extremes and important variables for the life of humans, their activities and their infractures.

Finally, Earth system models can be used to assess the effect of climate engineering schemes to reduce the amount of CO_2 in the atmosphere or to directly reduce atmospheric temperatures (Keller et al. , 2014). Earth system models have been used

to assess a wide array of climate geoengineering schemes such as ocean iron fertilization, artificial ocean alkalinization, direct air capture and storage, afforestation and bioenergy with carbon capture and storage (Keller et al. , 2014; Feng et al. , 2016; Richter et al. , 2022) Giving Earth system models great value as tools to test and idealize climate geoengineering ideas, their impacts on the global environment and their potency to mitigate climate change.

Chapter 3

Modelling the terrestrial nitrogen and phosphorus cycle in the UVic ESCM version 2.10

Preface.

A version of this chapter has been published in the Journal of Geoscientific model development issued in 2023, 16: 4113–4136. I am the primary author. Along with Co-authors, Andrew MacDougall, Nadine Mengis and Sophia Antoniello. I developed the model code for the terrestrial nitrogen and phosphorus cycle. I have carried out the simulations and validations of the model outputs. I have prepared the first draft of the manuscript and subsequently revised the manuscript, based on the feedback from Co-authors and also peer review process. As Co-author, Andrew MacDougall assisted in the development of the concept and provided supervisory feedback by reviewing and revising the manuscript. Nadine Mengis contributed to the calibration of the terrestrial modules. Sophia Antoniello contributed to the visualization of

the new terrestrial nutrient modules. The article can be access with the following link https://doi.org/10.5194/gmd-16-4113-2023.

3.1 Abstract

Nitrogen (N) and Phosphorus (P) biogeochemical dynamics are crucial for the regulation of the terrestrial carbon cycle. In Earth System Models (ESMs) the implementation of nutrient limitations has been shown to improve the carbon cycle feedback representation and hence, improve the fidelity of the response of land to simulated atmospheric CO_2 rise. Here we aimed to implement a terrestrial N and P cycle in an Earth system model of intermediate complexity to improve projections of the future CO_2 fertilization feedback. The N cycle is an improved version of the Wania et al. (2012) N module, with enforcement of N mass conservation and the merger with a deep land-surface and wetland module that allows for the estimation of N_2O and NO fluxes. The N cycle module estimates fluxes from three organic (litter, soil organic matter and vegetation) and two inorganic (NH_4^++and NO_3^-) pools, accounts for inputs from biological N fixation and N deposition. The P cycle module contains the same organic pools with one inorganic P pool, it estimates the influx of P from rock weathering and losses from leaching and occlusion. Two historical simulations are carried out for the different nutrient limitation setups of the model: Carbon and Nitrogen (CN) and Carbon, Nitrogen and Phosphorus (CNP), with a baseline carbon-only simulation. The improved N cycle module now conserves mass and the added fluxes (NO and N_2O), along with the N and P pools are within the range of other studies and literature. For the years 2001-2015 the nutrient limitation resulted in a reduction of GPP from the Carbon-only value of 143 PgC yr^{-1} to 130 PgC yr^{-1} in the CN version and 127 PgC yr^{-1} in the CNP version. This implies that the model

efficiently represents a nutrient limitation over the CO_2 fertilization effect. CNP simulation resulted in a reduction of 11% of the mean GPP and a reduction of 23% of the vegetation biomass compared to baseline C simulation. These results are in better agreement with observations, particularly in tropical regions where P limitation is known to be important. In summary, the implementation of the N and P cycle have successfully enforced a nutrient limitation in the terrestrial system, which now has reduced the primary productivity and the capacity of the land to uptake atmospheric carbon better-matching observations.

3.2 Introduction

Terrestrial biogeochemical cycles are sensitive to changes in atmospheric CO_2 concentrations and climate. Their global evolution will determine the capacity of vegetation and soils to store anthropogenic carbon (Goll et al. , 2012). In terrestrial ecosystems, carbon cycle feedbacks are constrained in part by the availability of nutrients (Fisher et al. , 2012; Zaehle et al. , 2014; Wieder et al. , 2015; Du et al , 2020). Among nutrients Nitrogen (N) and Phosphorus (P) are considered to be the most critical for limiting the primary productivity (Filipelli , 2002; Fowler et al. , 2013). Both are fundamental functional needs for plant biochemistry and their requirement is common in all vegetation taxa (Filipelli , 2002; Vitousek et al. , 2010; Du et al , 2020). Regionally, the availability of nutrients can impair the photosynthetic efficiency of terrestrial vegetation and consequently their response to increasing atmospheric CO_2. Hence, in Earth System Models (ESMs) the representation of nutrient limitations is imperative to improve the accuracy of carbon feedback projections and estimation of carbon budgets.

The simulations from first-generation ESMs with carbon-only schemes have very likely

overestimated the response of the terrestrial ecosystem to the increase of atmospheric CO_2 concentrations (Hungate et al. , 2003; Thorton et al. , 2007), showing a high terrestrial carbon uptake response which would require an unrealistic large nutrient supply. The addition of a N cycle to the land system in ESMs has shown an overall reduction in the effect of CO_2 fertilization especially in high latitudes, with a weaker response in low latitudes which are typically P limited in natural systems (Wang et al. , 2007, 2010; Goll et al. , 2017; Du et al , 2020; Wang et al. , 2020).

The global distribution of N and P is dependent on the biogeochemical characteristics of each nutrient. N inputs are mainly from Biological Nitrogen Fixation (BNF) and atmospheric deposition with little addition from rock weathering (Du et al , 2020). There are two types of N deposition from the atmosphere: wet (precipitation) and dry (particles). Among the two, wet deposition represents most of the atmospheric N input (Fowler et al. , 2013; Dynarski et al. , 2019). In contrast, the main input of P comes from rock weathering (mainly apatite) with lesser inputs from atmospheric deposition as dust particles. These characteristics are among the reasons of a global spatial pattern where young soils are usually N limited and old soil are P limited (Filipelli , 2002; Fowler et al. , 2013; Du et al , 2020). N accumulates rapidly from BNF where N fixers are abundant and slowly where atmospheric deposition is dominant. Thereby, old soils have a larger accumulation of N especially in regions where N fixers are abundant. On the other hand, P input is limited by the parent material and the bioavailability is further constrained by the retention of recalcitrant P in soils. Walker and Syers (1976) even suggested that P storage has a fixed total that cannot be rapidly replenished as parent material is limited.

These notions led to the common conceptualization that high latitudes are N-limited

while tropical regions are P limited. While this generalization is correct in most observational studies, the complex pattern of limitation is more intricate, and P limitation could be more common than is commonly inferred. Du et al (2020) found that globally 43% of the terrestrial system is relatively limited by P while only 18% is limited by N with the rest being co-limited by both. Biochemically, the availability of N and P can directly limit one another. The addition of P has been shown to be positive for the N fixation, leading to the replenishment of N in ecosystems (Eisele et al. , 1989). N supply on the other hand regulates the production of the enzyme phosphatase that cleaves ester-P bonds in soil organic matter (McGill and Cole , 1981; Olander and Vitousek , 2000; Wang et al. , 2007).

Biodiversity plays a crucial role in biogeochemical cycles. The fluxes and availability of N and P in soils depend on the interactions between soil mineral matrix, plants and microbes (Cotrufo et al. , 2013). For example, N input from atmospheric N_2 fixation is mediated by a specialized group of microorganisms. Furthermore, the recycling of N from plants-soil-microbes determines the availability of N for plant uptake. Overall, the land biota dynamics impact productivity, ecosystem resilience and stability (Yang et al. , 2018). High diversity has been linked to enhanced vegetation productivity (Wagg et al. , 2014). The diversity in terrestrial ecosystems is determined by biological, environmental and physicochemical processes. Anthropogenic activities can influence soil diversity, impacting the availability and cycling of N and P (Chen et al. , 2019). For example, N and P fertilization, have been shown to affect soil microbial biomass and composition (Ryan et al. , 2009). Plant diversity is linked to soil health and functioning, and is core for the N and P cycles. Vegetation species variable adaption to nutrient concentrations also plays a role in the availability of nutrients in soils and the biogeography of terrestrial vegetation. Overall, biodiversity constitutes an environmental resilience factor to abrupt changes (Van Oijen et al. , 2020). However,

implementing such dynamics remains far beyond the capabilities of the present generation Earth systems models. Several studies have found that in some ecosystems lack of N in soil usually leads to dominance of woody symbiotic N fixers (e.g. Menge et al. , 2012). The availability of P is also impacted by the geochemical interactions in terrestrial soils, Vitousek et al. (2010) defined six mechanisms by which P is driven to limitation: loss by leaching, soil barriers that physically prevent access to roots, slow release of mineral P forms, P parent material, sequestration of P in soils and pools in the ecosystem and finally, anthropogenic input of nutrients.

Despite its importance P terrestrial limitation has been rare in Earth system modelling. The effect of P in tropical forests may be the key to better representing the vegetation biomass and the response to CO_2 fertilization. The lack of P observational data is partly responsible for the difficulty of simulating P limitation in Earth system models (Spafford and MacDougall , 2021). However, several studies have attempted to provide reliable global P datasets (Yang et al. , 2013; Hartmann et al. , 2014; He et al. , 2021) that could be used to develop more accurate models. Furthermore, many studies have shown that the inclusion of P into ESM structures is possible and that it improves the representation of vegetation biomass in tropical regions (Wang et al. , 2007, 2010; Goll et al. , 2012, 2017; Fleischer et al. , 2019; Thum et al. , 2019; Yang et al. , 2019; Wang et al. , 2020; Nakhavali et al. , 2021). The addition of nutrient limitation has been observed to mainly affect the capacity of vegetation to uptake carbon (Wang et al. , 2010; Goll et al. , 2017; Wang et al. , 2020). Therefore, the accumulation of carbon in the atmosphere is enhanced, leading to increases in temperature in simulations. These temperature changes are likely to have some impact on variables sensitive to atmospheric temperature changes. Furthermore, the decrease in vegetation biomass affects variables affected by the distribution and composition of plant functional types, such as changes in terrestrial albedo.

Intermediate complexity Earth system models have a lower spatial representation, and model structures that have been intentionally simplified in one or more ways. This simplification allows for long-term simulations that are typically not feasible in higher-complexity models. This class of model is not suitable for studying processes at small spatial scales. Hence, they are used in research questions that require large spatial and temporal scales (Weber , 2010). Current generation Earth system models are or have already developed nutrient limitation to their model structure (e.g., Community Land Model (Lawrence et al. , 2019), Joint UK Land Environment Simulator (Clark et al. , 2011), Community Atmosphere–Biosphere Land Exchange model (Haverd et al. , 2018), Australian Community Climate and Earth System Simulator (Ziehn et al. , 2020)). While CN models are more common CNP models remain to be rarer. However, P cycles have been suggested to be included into Earth system model for its importance in tropical regions (Wang et al. , 2010; Goll et al. , 2012). The first attempt to include nutrient limitation in the University of Victoria Earth system and climate model (UVic ESCM) was done by Wania et al. (2012) but was not included in the current publically available version of the model due to the need of further improvement. We aim to describe a terrestrial N and P cycle adapted, developed and implemented for the UVic ESCM version 2.10. The main dynamics captured in this study are in the terrestrial system, especially vegetation. Furthermore, I intend to improve the current state of the previous N cycle implement in the UVic ESCM, develop a new P cycle and couple carbon N and P, in order to improve the carbon cycle feedbacks projections.

3.3 Methodology

3.3.1 Model description

The UVic ESCM is a climate model of intermediate complexity (ver. 2.10, Weaver et al. (2001); Mengis et al. (2020)), it contains a simplified moisture-energy balance atmosphere coupled with a three-dimensional ocean general circulation (Pacanowski , 1995) and a thermodynamic sea-ice model (Bitz et al. , 2001). The model has a common horizontal resolution of 3.6° longitude and 1.8° latitude and the oceanic module has a vertical resolution of 19 levels with a varying vertical thickness (50 m near the surface to 500 m in the deep ocean).

In version 2.10, the soil is represented by 14 subsurface layers with thickness exponentially increasing with depth with a surface layer of 0.1 m, a bottom layer of 104.4 m and a total layer of 250 m. Only the first 8 layers have active hydrological processes (top 10 m), below that lays bedrock with thermal characteristics of granitic rocks. The soil carbon cycle is active in the top 6 layers up to a depth of 3.35 m (Avis , 2012; MacDougall et al. , 2012) the soil respiration is a function of temperature and moisture (Meissner et al. , 2003). The terrestrial vegetation is simulated by a top-down representation of interactive foliage and flora including dynamics (TRIFFID) representing vegetation interaction between 5 functional plant types: broadleaf trees, needleleaf trees, shrubs, C3 grasses, and C4 grasses that compete for space in the grid following the Lotka-Volterra equations (Cox , 2001). Net carbon fluxes estimated in the model update the total areal coverage, leaf area indexes and canopy height for each PFT. For each PFT the carbon fluxes are derived from a photosyntesis-stomatal conductance model (Cox et al. , 1998). The carbon uptake through photosynthesis is allocated into growth and respiration and the vegetation carbon is transferred to the

soil via litter fall and allocated in the soil as a decreasing function of depth (proportional to root distribution) and except for the top layer is only added to soil layers with temperature above 1°C.

Furthermore, permafrost carbon is prognostically generated within the model using a diffusion-based scheme meant to approximate the process of cryoturbation (MacDougall and Knutti , 2016). The sediment processes are modelled using an oxic-only calcium carbonate scheme (Archer , 1996). Terrestrial weathering is diagnosed from the spin-up net sediment flux and stays fixed at the preindustrial equilibrium value (Meissner et al. , 2012). Mengis et al. (2020) merged the previous version of the UVic ESCM and evaluated its performance representing carbon and heat fluxes, water cycle and ocean tracers. A full description of the model can be found in Mengis et al. (2020).

3.3.2 Nitrogen cycle

Nitrogen uptake

The new N cycle module was adapted from Wania et al. (2012). The module contains three organic (litter, soil organic matter and vegetation) and two inorganic ($NH4^+$, $NO3^-$) N pools. The base structure is based on Gerber et al. (2010) with further modifications to fit the UVic ESCM scheme. $NH4^+$ is produced both from BNF and mineralization of organic N, it can be taken up by plants (vegetation), leached, or transformed into $NO3^-$ via nitrification. $NO3^-$ is produced through nitrification, and can be taken up by plants, leached or denitrified into NO, N_2O or N_2. The inorganic N is distributed between leaf, root and wood, with wood having a fixed stoichiometry ratio and variable ratios for the leaf and root pools. Organic N leaves the living pools via litter-fall into the litter pool, which is either mineralized or transferred to the

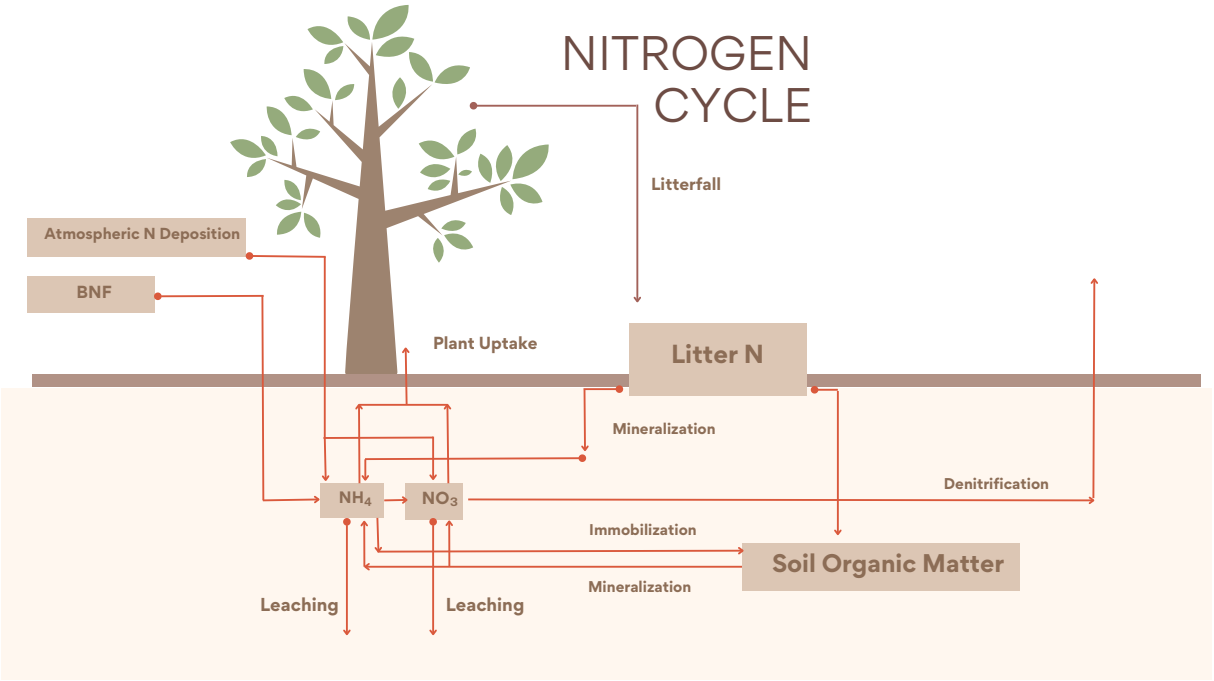

Figure 3.1: Diagram representing the UVic ESCM nitrogen cycle.

organic soil pool, part of this N can be mineralized into the inorganic N pools. At the same time, N can flow from the inorganic to the soil organic pool via immobilization. The CN ratios in leaves are determined by Eq. (1):

$$CN_{leaf} = \frac{C_{leaf}}{N_{leaf}}, \tag{3.1}$$

where C_{leaf} is the carbon content in leafs and N_{leaf} is the N content in leafs. CN_{leaf} is one of the most important nutrient limitations in the model. It controls the maximum carboxylation rate of RuBISCO. Furthermore, it controls vegetation biomass. If leaf C:N ratio is higher than $CN_{leafmax}$ (the maximum CN ratio parameter) terrestrial vegetation biomass is reduced.

The new version of the N cycle has been merged with a deep land-surface (MacDougall and Knutti , 2016) and a new wetland module (Nzotungicimpaye et al. , 2021). Both

inorganic N pools are transferred between soil layers following ground-water flow. Given this flow, the distribution of N in layers was taken into account in the uptake calculations in Eq. (2) and (3), a root fraction was added (4) fixing the amount of root biomass per PFTs per layer depth. The equations governing N uptake are:

$$NH_4^{UP} = \sum_{PFT} (\frac{V_{maxn} C_{root} [NH_4(av)] Froot}{K_{n,1/2} + [Nmin(av)]} + [NH_4(av)] * Qt), \tag{3.2}$$

$$NO_3^{UP} = \sum_{PFT} (\frac{V_{maxn} C_{root} [NO_3(av)] Froot}{K_{n,1/2} + [Nmin(av)]} + [NO_3(av)] * Qt), \tag{3.3}$$

where NH_4^{UP} and NO_3^{UP} represent the N uptake, the left term is the active uptake while the right term is the passive uptake (see table 3.1), the latter is the transport of N via the transpiration water stream. V$maxn$ is the maximum uptake rate for N, C$root$ is the root carbon biomass, [$NH_4(av)$], [$NO_3(av)$] and [Nmin(av)] are the NH_4, NO_3 and mineral N concentrations, $K_{n,1/2}$ is the half saturation constant for N and Qt is the transpiration rate. av represents the available portion of NH_4 and NO_3 in soil. This fraction is calculated as the total concentration of NH_4 and NO_3 divided by sorption factors (10 and 1 respectively) following Wania et al. (2012). The equation for root fraction is:

$$Froot_{,PFT} = \frac{e^{z_{top,n}/d_{r,PFT}} - e^{z_{bot,n}/d_{r,PFT}}}{1 - e^{D/d_{r,PFT}}}, \tag{3.4}$$

where Z_{top} and Z_{bot} represent the top layer and bottom layer depth respectively, while D and d_r are the depth of the soil layer and the root depth. The depth of the soil layer represents the depth of each specific soil layer. Root depth is a PFT-based parameter that represents the depth of the roots. Given the multiple soil layer setup, the root fraction modifies the value of root carbon, creating a more realistic representation of

the uptake root depth reaches for each PFT given the multiple soil layer setup.

Denitrification

The N cycle was merged with a wetland module that allowed the estimation of anoxic fractions for each soil layer, based on Gedney and Cox (2003). The anoxic fraction is taken to be the saturated fraction of the soil layer that is shielded from O_2 by the saturated soil layer above. The Anoxia representation led to denitrification to be added to the N model, accounting for the largest exit pathway for N in the terrestrial biosphere. The anaerobic respiration is estimated from eq. (5):

$$R_{an} = K_{rNO_3} f_t f_m C_s A_f \ \frac{[NO_3(av)]}{[NO_3(av)] + K_n}, \tag{3.5}$$

where R_{an} is the anaerobic respiration, K_{rNO3} is the ideal respiration rate via NO_3 reduction, f_t and f_m are temperature and moisture functions, C_s is the concentration of organic carbon, Af is the anaerobic fraction, K_n is the half-saturation of N-oxides (Li et al. , 2000). The temperature and moisture soil functions are taken directly from Cox (2001), and are represented by the following equations:

$$f_t = q_{10}^{0.1(t_s - 25)}, \tag{3.6}$$

$$f_m = \begin{cases} 1 - 0.8(S - S_0) & \text{for S} > \text{S}_0, \\ 0.2 + 0.5(\frac{S - S_W}{S_0 - S_W}) & \text{for S}_W < \text{S} \ \ \text{S}_0, \\ 0.2 & \text{for S} \ \ \text{S}_W, \end{cases}$$

(3.7)

where in f_t, $q_{10} = 2$ and t_s is the soil temperature in °C. In f_m, S is the soil moisture, S_W is the wilting point of soil moisture, S_0 is the optimum soil moisture. Fluxes of N_2O and NO to the atmosphere are computed based on the 'leaky-pipe' conceptualization of soil-nitrogen processes (Firestone and Davidson , 1989). In the leaky pipe conceptual model N_2O and NO leak out of reactions of one species of nitrogen into another, namely nitrification (NH_4 to NO_3) and denitrification (NO_3 to N_2). The size of the holes is determined by the soil processes. For implementation in the UVic ESCM the size of the holes is fixed but the partitioning ratio between NO and N_2O changes based on water-filled pore space of the soil layer. The ratio is parameterized based on an empirical relationship derived by Davidson et al. (2000):

$$\frac{N_2O}{NO} = 10^{2.6S_U - 1.66}, \tag{3.8}$$

where S_U is the water-filled pore space. Thus, the model produces a total flux of both NO and N_2O for nitrification and denitrification, which is partitioned between the two species based on the above relationship. The NO flux is added to the atmosphere and redeposited as part of the N deposition flux. The N_2O flux is added to the N_2O pool in the atmosphere which has a characteristic half-life of 90.78 years (Myhre et al. , 2013). Decayed N_2O is assumed to become part of the atmospheric N_2 pool.

Mass balance N cycle

In Wania et al. (2012) N cycle module, under N limitation ($CN_{leaf} > CN_{leafmax}$) the N available was increased artificially by reducing the leaching by up to 100% and if

necessary, the immobilization by 50%. These mechanics created an unrealistic increase of N in soils and thereby, defying the mass balance conservation of the module.

Here, the vegetation can no longer uptake extra N from leaching or immobilization under nutrient limitation. Instead, under nutrient limitation wood and root carbon mass is transferred as litter (emulating a dying vegetation) until the correct ratio is met. Section 2.4 presents a detailed explanation of nutrient limitation for N and P.

Table 3.1: Updated nitrogen cycle module pools, rates and variables.

Variables	Units	Type	Descriptions
NH_4^{UP}	kg N m^{-2} yr^{-1}	Rate	NH_4 vegetation uptake
NO_3^{UP}	kg N m^{-2} yr^{-1}	Rate	NO_3 vegetation uptake
Croot	Kg C m^{-2}	Pool	Root carbon
$[NH_4(av)]$	kg N m^{-3}	Pool	Available NH_4 concentration
$[NO_3(av)]$	kg N m^{-3}	Pool	Available NO_3 concentration
Froot	-	Variable	Root fraction
$[Nmin(av)]$	kg N m^{-3}	Pool	Available mineral N concentration
R_{an}	kg C m^{-3} s^{-1}	Rate	Anaerobic respiration rate
C_s	kg C m^{-3}	Pool	Density of soil carbon in each layer
A_f	-	Variable	Anaerobic saturation fraction
N_2O	kg N m^{-2} yr^{-1}	Rate	Nitrous oxide flux
NO	kg N $m^{-2}yr^{-1}$	Rate	Nitric oxide flux

3.3.3 Phosphorus cycle

The P cycle is based on Wang et al. (2007, 2010) and Goll et al. (2017) with some equations where modified from Wania et al. (2012) to have better consistency with N estimations in the new soil layer model. The module contains four inorganic (labile, sorbed, strongly sorbed and occluded) and three organic P pools: Vegetation (leaf, root and wood), litter and soil organic P.

Table 3.2: Updated nitrogen cycle parameters.

Variables	Units	Value	Description	Source
$K_{n,1/2}$	kg N m^{-3}	0.003	Half saturation constant for N uptake	Gerber et al. (2010)
$Vmaxn$	kg N (kg root C^{-1})yr^{-1}	Varies with PFTs	Maximum uptake rate for N	Wania et al. (2012)
D	m	Varies with soil layer	Soil layer depth	MacDougall and Knutti (2016)
Qt	m yr^{-1}	Varies with PFTs	Transpiration rate	Wania et al. (2012)
$z_{top,n}$	m	Varies with soil layer	Top layer soil depth	Avis (2012)
$z_{bot,n}$	m	Varies with soil layer	Bottom soil layer depth	Avis (2012)
d_r	m	Varies with PFTs	Root depth	Avis (2012)
K_{rNO_3}	10^{-9} s^{-1}	5	Soil respiration rate for Nitrate respiration	
K_n	kg N m_{-3}	0.083	Half saturation constant for N-oxides	Li et al. (2000)
$CN_{leafmax}$	kg C $(kg N)^{-1}$	Varies with PFTs	Maximum CN ratio	Wania et al. (2012)

Input

The P module estimates weathering input following Wang et al. (2010) and is driven by a fixed estimate (Table 3.3) of P release assigned by soil order divided in 12 classes from U.S. department of agriculture (USDA) soil order map.

Additionally, an extra input structure was tested in the model but was not used for the P results in this study. It was implemented to compare the benefits of a static and a dynamic weathering scheme into the P pool. In this method weathering depends on runoff following Hartmann et al. (2014) using the lithological world map with 16 different classes generated by Hartmann and Moosdorf (2012). Eq. 9 shows the estimation of the chemical weathering rate:

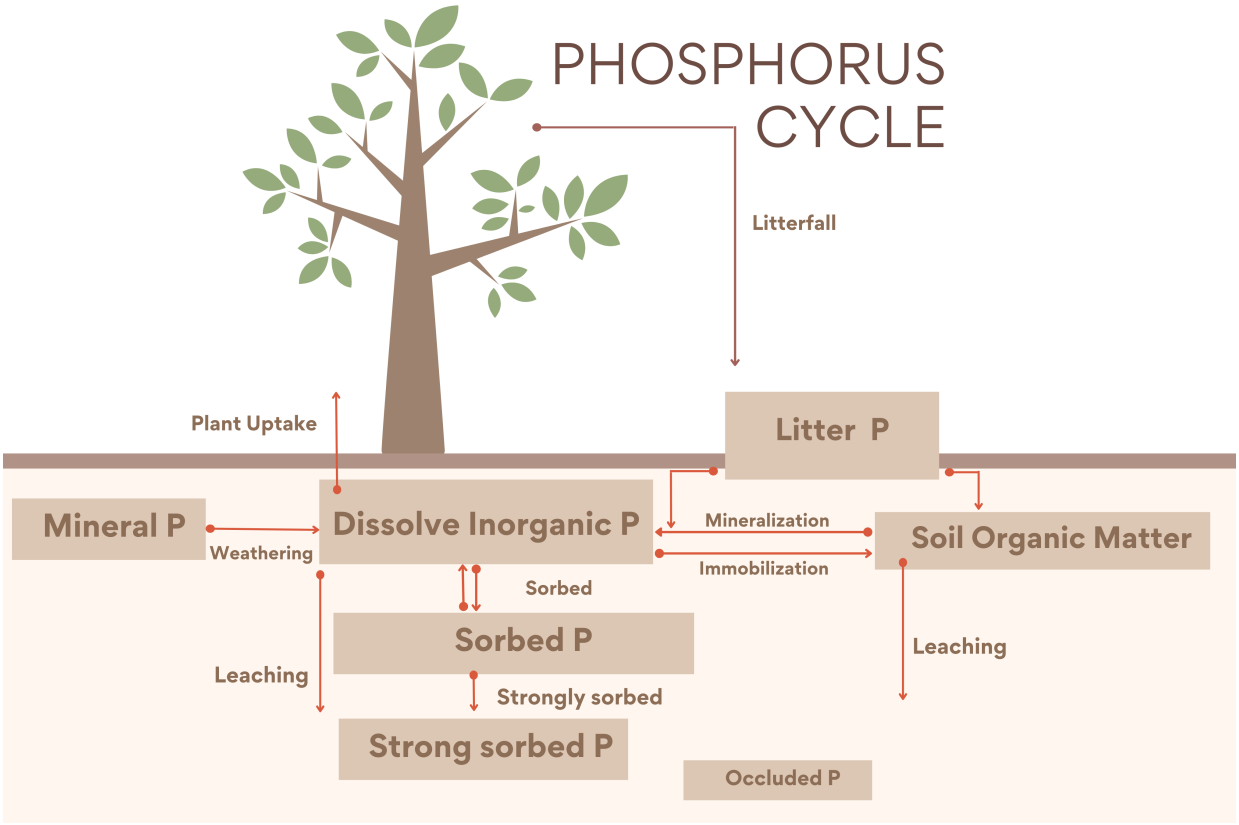

Figure 3.2: Diagram representing the UVic ESCM CNP P cycle. Weathering from mineral P is the only input into the soils. There are 4 inorganic pools (Dissolved inorganic, adsorbed, stronged sorbed and occluded P) and 3 organic pools (vegetation (root, wood and leaf), litter and soil organic matter). As in Wang et al. (2010) the flux from strongly sorbed P to the occluded pool is not represented here, instead it is assumed to be a fraction of total soil P.

$$F_{CW} = b_i q, \tag{3.9}$$

$$b_i = b_{carbonate} + b_{silicate}, \tag{3.10}$$

where F_{CW}(t km^{-2} yr^{-1}) is the chemical weathering rate, q is the runoff (mm yr^{-1}) and b_i is the factor for each lithological class i; shielding correction functions were not applied. The chemical weathering is defined as the total fluvial export of Ca

Table 3.3: Constants for P input from Wang et al. 2010. The values change depending on the weathering state of the soil type. Highly weathered soils have lower values.

Soil order	Value (gP m^{-2} yr^{-1})
Entisol	0.05
Inceptisol,Gellisol,Histosol	0.05
Vertisol	0.01
Aridisol,Andisol	0.01
Mollisol	0.01
Alfisoil,Spodosol	0.01
Ultisoil	0.005
Oxisoil	0.003

+ Mg + K + SiO_2 and carbonate derived CO_3, $b_{carbonate}$ and $b_{silicate}$ are chemical weathering parameters associated to carbonate and silicate rocks respectively found in Hartmann et al. (2014). Here we only apply Wang et al. (2010) approach as we found it to be more controllable and an advantage to the planned coupling of P flux from land into the ocean. Hartmann et al. (2014) requires the estimation of runoff by the model structure. Hence, while representing a dynamical P release it needs to be carefully assessed so that no extreme overestimation or underestimation are represented regionally. Wang et al. (2010) approach provides constant input without variability which in this particular case is favorable.

Inorganic soil phosphorus

Inorganic P (Psoil) in soil follows the dynamics described in (Goll et al. , 2017) in eq. (11), where each time step a fix fraction (k_s) of P is adsorbed and the rest is dissolved (1-k_s). This fraction is based on Hedley fractionation method (Hedley and Stewart , 1982) which is dependent on soil orders, the dataset has been commonly used to assess the different P forms in soil. The adsorbed P is regulated by k_s in eq. (12) as determined by the soil order in Hedley dataset:

$$\frac{dPsoil}{dt} = (1 - K_s)(P_{wea} + P_{litmin} + P_{orgmin} - P_{leach} - P_{up} - \tau_{sorb} P_{sorb} - P_{imm}), \quad (3.11)$$

$$\frac{dPsorb}{dt} = K_s \frac{dPsoil}{dt}, \quad (3.12)$$

where P_{wea} is the P released by rock weathering, P_{litmin} is the P mineralized from the P litter pool, P_{orgmin} is the P mineralized from the soil organic P, $P_{leach}$is the leached inorganic P, P_{up} is the P uptake by plants, P_{sorb} is the amount of P sorbed, τ_{sorb} is the rate of strong sorption and P_{imm} is the P immobilized from the inorganic P pool. The estimation of P*soil* based on Goll et al. (2017), is originally taken from Goll et al. (2012). Here, the sum P_{sorb} and P_{soil} constitute the inorganic P pool in soil. Hence, the loss given by the rate of strong sorption is applied to the total inorganic P pool. The estimation of occluded P followed Wang et al. (2010) approach, based in Cross and Schlesinger (1995) the pool was assumed to be 35 % of the total soil P. P_{leach} and P_{up} were determined as in eq. (13), (14) based on an adaptation of Wania et al. (2012) representation of leaching and uptake of N in the new soil layer model version:

$$P_{leach} = Q_D P_{soil}, \quad (3.13)$$

$$P_{UP} = \sum_{PFT} \left(\frac{V_{maxp} C_{root} [P_{soil}] F_{root}}{K_{p,1/2} + [P_{soil}]} \right), \quad (3.14)$$

where Q_D is the runoff. V_{maxp} is the P maximum uptake rate, $K_{p,1/2}$ is the half-saturation constant for P, C_{root} is the root carbon and F_{root} is the root fraction.

Organic soil phosphorus

After uptake, P is distributed in three vegetation compartments: leaf, root and wood. Leaf and root have a dynamic value that varies between a minimum and a maximum, while wood has a fix CP ratio. The vegetation P biomass dynamics is determined from the difference between the amount of uptake and the loss from litterfall as in eq. (15) and the litterfall is estimated as the CP ratio of the original model litterfall as in eq. (16):

$$\frac{dVegp}{dt} = P_{UP} - P_{LF}, \tag{3.15}$$

$$P_{LF} = \sum_{PFT} \frac{Lit_{leaf}}{CP_{leaf}} (1 - R_{leafp}) + \frac{Lit_{root}}{CP_{root}} + \frac{Lit_{wood}}{CP_{wood}}, \tag{3.16}$$

where V_{egp} is the vegetation P change over time, P_{LF} is the P litterfall and Lit_{leaf}, Lit_{root}, Lit_{wood} are the carbon litterfall rates for vegetation carbon. The leaf CP ratio is determined as:

$$CP_{leaf} = \frac{C_{leaf}}{P_{leaf}}, \tag{3.17}$$

where C_{leaf} is the carbon content in leafs and P_{leaf} is the P content in leafs. CP_{leaf} is one of the most important nutrient limitation in the model. The limiting effect of CP_{leaf} is when its value is higher than the maximum CP_{leaf} ratio parameter $CP_{leafmax}$. This leads to biomass reduction. In contrast to CN_{leaf}, CP_{leaf} does not control the maximum carboxylation rate of RuBISCO. A more detailed description of nutrient limitation can be found in section 2.4. The litter biomass is added to the P litter pool (P_{lit}), and its dynamic is based on Wang et al. (2007) as in eq. (18):

$$\frac{dP_{Lit}}{dt} = P_{LF} - \tau_{lit} P_{lit} - \ P_{litmin}, \tag{3.18}$$

$$P_{litmin} = \ \frac{P_{lit}}{P_{som} + P_{lit}} \ P_{tase}, \tag{3.19}$$

$$P_{tase} = U_{tase} \frac{\lambda_{up} \ - \ \lambda_{Ptase}}{\lambda_{up} \ - \ \lambda_{Ptase} \ + \ K_{ptase}}, \tag{3.20}$$

where τ_{lit} is a rate constant for litter carbon decomposition (0.42 yr^{-1}), P_{litmin} is the biochemical P litter mineralization, P_{tase} is the biochemical P mineralization rate, U_{tase} is the maximum rate of P biochemical mineralization, λ_{up} is the N plant root cost to uptake P, λ_{Ptase} is the critical value of N cost of root P uptake above which phosphate production starts and K_{ptase} is the Michaelis-Menten constant for biochemical P mineralization. Here, the N cost refers to the N required for protein structures involved in the metabolization of P in plants. P_{tase} is a constant value.

The soil litter decomposed is transferred to the soil organic P pool (P_{som}); the dynamics of P_{som} are adapted from Wang et al. (2007) as in eq. (21):

$$\frac{dP_{som}}{dt} = \tau_{lit} P_{lit} \varepsilon - \ \tau_s P_{som} - P_{orgmin}, \tag{3.21}$$

$$P_{orgmin} = \ \frac{P_{som}}{P_{lit} + P_{som}} \ P_{tase}, \tag{3.22}$$

where the first term represents the litter P input, while the other two are the P_{som} decomposition and mineralization. ε is a microbial growth efficiency (0.6), τ_s is the

rate constant for soil carbon decomposition and P_{orgmin} is the biochemical P mineralization. The immobilization is determined from the NP ratio of the N immobilization estimated by Wania et al. (2012).

3.3.4 Nitrogen and phosphorus limitation

The N cycle limits the terrestrial vegetation productivity in two distinct ways: the first limits the photosynthesis efficiency by controlling the maximum carboxylation rate of Rubisco (V_{cmax}). The Rubisco enzyme plays a crucial role in the photosynthesis biochemistry by catalyzing the carboxylation reactions in the Calvin cycle and has been found to be linearly related to the N leaf content (Walker et al. , 2014). The original equation for V_{cmax} takes into account a fix N leaf (Cox et al. , 1999), this was replaced by Wania et al. (2012) implemented in the first N cycle where it is replaced by the calculated inverse average canopy leaf C/N ratio ($CN_{invleaf}$), in this representation the plant productivity is reduced when CN_{leaf} increases. V_{cmax} is calculated as:

$$V_{cmax} = \lambda CN_{invleaf}, \tag{3.23}$$

where λ is a constant of proportionality, 0.004 for C3 and 0.008 for C4 PFTs (Cox et al. , 1999). N and P both share the second form of limitation, where stoichiometrically N and P limitation reduce the vegetation biomass. If C:N ratios is too high, wood and root carbon biomass is transferred to the litter pool until the normal C:N ratio is reached (See table 3.4).

The model assumes nutrient limitation when the estimated CN and CP leaf ratio is higher than the maximum CN ($CN_{leafmax}$) and CP ($CP_{leafmax}$) ratio in leaves. For grids with nutrient limitation, the carbon in leaves is reduced to match the maximum

CN or CP ratios in leaves. The carbon that is reduced is transferred to the litter pool. This reduction can happen for one or both nutrients until the ratio is met. The following equations regulate the reduction of biomass based on nutrient limitation:

$$C_{leaflimitedn} = N_{leaf} CN_{leafmax}, \tag{3.24}$$

$$C_{leafdiffn} = C_{leaf} - C_{leaflimitedn}, \tag{3.25}$$

$$C_{leaflimitedp} = N_{leaf} CP_{leafmax}, \tag{3.26}$$

$$C_{leafdiffp} = C_{leaf} - C_{leaflimitedp}, \tag{3.27}$$

where $C_{leaflimitedn}$ and $C_{leaflimitedp}$ are the carbon concentration in leaves if the system is considered to be limited. $C_{leafdiffn}$ and $C_{leafdiffp}$ are the carbon lost due to nutrient limitation and their value are the sum in the litterfall equation when the system is in nutrient limitation.

Table 3.4: Maximum leaf C:P and C:N in the CNP simulation by PFTs.

Variables	Broadleaf trees	Needleleaf trees	C3	C4	Shrubs
$CP_{leafmax}$	225	250	500	500	450
$CN_{leafmax}$	70	80	60	80	80

3.3.5 Model runs and validation

The three different terrestrial biogeochemical versions: C, CN and CNP, were run for a historical simulation from 1850 to 2020. The C version served as a baseline run representing the original version of the UVic ESCM ver. 2.10 (Mengis et al. , 2020), the CN version is the modified version of Wania et al. (2012) N model, and CNP is the newest coupled model that includes P. Historical simulations are forced with fossil CO_2 emissions, dynamically determined land use change emissions, non-CO_2

GHG forcing, sulphate aerosol forcing, volcanic anomalies forcing, and solar forcing. Furthermore, 24 historical simulations were run to assess the model sensitivity of 6 key parameters ($CP_{leafmax}$, $CN_{leafmax}$, R_{leafp}, R_{leafn}, V_{maxp}, V_{maxn}) in N and P limitation over terrestrial vegetation. The parameters were perturbed by increasing and reducing their value by 10 % and 20 % individually. $CP_{leafmax}$ and $CN_{leafmax}$ are the maximum leaf CP or CN ratios respectively. If the values of CP_{leaf} and CN_{leaf} are above these thresholds the model will take the system to be nutrient limited by either P or N. R_{leafN} and R_{leafP} are parameters that represent the resorption of N and P in leaves. This partly controls the loss of N and P from vegetation to the litter pool. V_{maxp} and V_{maxn} are the P and N maximum uptake rates.

It should be noted that the porting of the N cycle from version 2.9 to 2.10 of the UVic ESCM and later model spin-up, could slightly alter the results presented in Mengis et al. (2020). Hence, the baseline model is slightly different from the standard UVIC ESCM ver. 2.10. The N cycle is compared to Zaehle et al. (2010); Li et al. (2000) and Yang et al. (2009) as well as Wania et al. (2012). The N_2O flux was compared with the Emissions Database for Global Atmospheric Research (EDGAR ver. 6.0, Crippa et al. (2021)) dataset, it provides emission time series from 1970 until 2015 for non-CO2 GHGs for all countries.

For the P cycle, I used as a benchmark for the carbon cycle the UVic ESCM version 2.10 model calibration values and references, which included the Le Quere et al. (2018) datasets. The total soil P was calibrated with the He et al. (2021) dataset. The labile and sorbed pools were calibrated using Yang et al. (2013) P distributions map dataset. For the use of He et al. (2021) dataset, I transformed the units with Eq. 28:

$$P_{soil} = Bk_{density} * SL_D * P_{dataset}, \tag{3.28}$$

where P_{soil} is the total P soil concentration (kg P m^{-2}), $Bk_{density}$ (kg m^{-3}) is the bulk density taken from International Geosphere-Biosphere Programme Data and Information System (IGBP-DIS) (Global Soil Data Task Group , 2014), SL_D (m) is the soil layer depth and $P_{dataset}$ (kg P (kg soil)1) is He et al. (2021) dataset. The foliar stoichiometry was compared to the latitudinal trend from Reich and Oleksyn (2004) N:P observations.

One of the challenges of modelling nutrients in terrestrial systems is the lack of observations and validation datasets. Furthermore, the existing range of values for N and P variables are highly uncertain. This large range in values makes it difficult to accurately tune models. Although, improvements are in sight, with new artificial intelligence-derived global datasets beginning to become available (He et al. 2021). Model validation has been advancing quickly in the last decade (Spafford and MacDougall , 2021) with tools such as the International Land Model Benchmarking (Collier et al. , 2018) that significantly improves terrestrial model validation. However, there are limited variables available to compare to nutrient model development. The increase of the addition of nutrient structures in ESMs (Arora et al. , 2020) suggests the need of terrestrial nutrient validation tools to improve model accuracy in the developmental phase. Moreover, a terrestrial nutrient model intercomparison project would unify global efforts to improve the representation of N and P in ESMs.

Table 3.5: Phoshorus cycle model pools and variables.

Variables	Units	Descriptions
P_{litmin}	kg P m^{-2} yr^{-1}	P litter mineralization
P_{orgmin}	kg P m^{-2} yr^{-1}	P organic matter mineralization
P_{leach}	kg P m^{-2} yr^{-1}	P leaching
P_{up}	kg P m^{-2} yr^{-1}	P uptake
P_{sorb}	kg P m^{-2} yr^{-1}	P sorbtion
P_{imm}	kg P m^{-2} yr^{-1}	P immobilization
$[P_{soil}]$	kg P m^{-3}	Soil layers labile P concentration
P_{soil}	kg P m^{-2}	Labile P
Lit_{leaf}	kg C m^{-2} yr^{-1}	Leaf literfall rate
CP_{leaf}	kg C (kg P)$^{-1}$	CP leaf ratio
Lit_{root}	kg C m^{-2} yr^{-1}	Root literfall rate
CP_{root}	kg C (kg P)$^{-1}$	CP root ratio
Lit_{wood}	kg C m^{-2} yr^{-1}	Wood literfall rate
CP_{wood}	kg C (kg P)$^{-1}$	CP wood ratio
F_{tase}	kg P m^{-2} yr^{-1}	Rate of P biochemical mineralization
P_{som}	kg P m^{-2}	P soil organic matter pool
P_{lit}	kg P m^{-2}	P litter pool

Table 3.6: Phosphorus cycle model parameters.

Variables	Units	Value	Description	Source
K_s	-	Varies with soil order	Fraction of P sorbed	Goll et al. (2017)
P_{wea}	kg P m^{-2} yr^{-1}	Varies with soil order	P flux from weathering	Wang et al. (2010)
τ_{sorb}	yr^{-1}	0.067	Rate of P strong soil sorption	Wang et al. (2010)
$K_{p,1/2}$	kg P m^{-3}	0.002	Half saturation constant for P uptake	Machado and Furlani (2004)
V_{maxp}	kg P (kg root C^{-1})yr^{-1}	0.46	Maximum uptake rate for P	Tuned
R_{leaf}	-	0.5	Leaf P readsorption rate	Tuned
U_{tase}	kg P m^{-2} yr^{-1}	0.0001	Maximum biochemical mineralization rate	Wang et al. (2007)
λ_{up}	kg C (kg P)$^{-1}$	25	N cost of plant root P uptake	Wang et al. (2007)
λ_{ptase}	kg C (kg P)$^{-1}$	15	Critical N cost of root P uptake	Wang et al. (2007)
K_{ptase}	kg C (kg P)$^{-1}$	150	Constant for biochemical P mineralization	Wang et al. (2007)
τ_{lit}	yr^{-1}	0.42	Rate constant for litter C decomposition	Wang et al. (2007)
ε	-	0.6	Microbial growth efficiency	Wang et al. (2007)
τ_s	yr^{-1}	0.02	Constant for soil carbon decomposition	Wang et al. (2007)
λ	-	Varies with PFTs	Constant of proportionality	Cox et al. (1999)
$CP_{leafmax}$	kg C (kg P)$^{-1}$	Varies with PFTs	Maximum CP ratio	Tuned

3.4 Results and Discussions

3.4.1 Carbon cycle

Land global primary productivity

The global gross productivity in CN and CNP resulted in a better agreement with the FLUXCOM GPP dataset (Jung et al. , 2019) as shown in Fig. 3.3, with both CN and CNP overestimating the terrestrial global GPP average less than the baseline simulation. Compared to the baseline simulation (143 Pg yr^{-1}) both nutrient-limited model versions showed a reduced mean GPP from the years 2001-2015 with CN at 130 Pg yr^{-1} and CNP at 127 Pg yr^{-1}. Furthermore, the modifications for the N cycle in regards to the mass balance changes resulted in the reduction of mean GPP from 129 Pg yr^{-1} (Wania et al. , 2012) to 122 Pg yr^{-1} in the 1990s. The GPP distribution from Baseline, CN and CNP reproduce FLUXCOM dataset values reasonably well (Fig. 3.4). The seasonal pattern of GPP is also well represented within the UVic ESCM simulations as shown in Fig. 3.4. The addition of nutrients improves the representation of GPP, where CNP had the highest correlation with FLUXCOM GPP dataset. The high GPP in the baseline simulation can be explained by the overestimation of the vegetation biomass especially broadleaf trees in tropical regions stated in Mengis et al. (2020). The representation of vegetation biomass is linked to the PFTs fractions in the model. In the CN and CNP simulations, the reduction of biomass is critical for the reduction of terrestrial productivity, especially in tropical regions where P availability has been shown to be a limiting factor for GPP (Du et al , 2020). Similar to Wania et al. (2012), Bonan and Levis (2010), and Zaehle et al. (2010) the addition of nutrient limitation in ESM seems to reduce GPP. Furthermore, locally in Amazonia soils, Nakhavali et al. (2021) found that the inclusion of P reduces the model GPP and NPP outputs by 5.1 and 4.5% respectively for a site simulation.

Similar to Nakhavali et al. (2021) I found an overall reduction of GPP in the Amazon region.

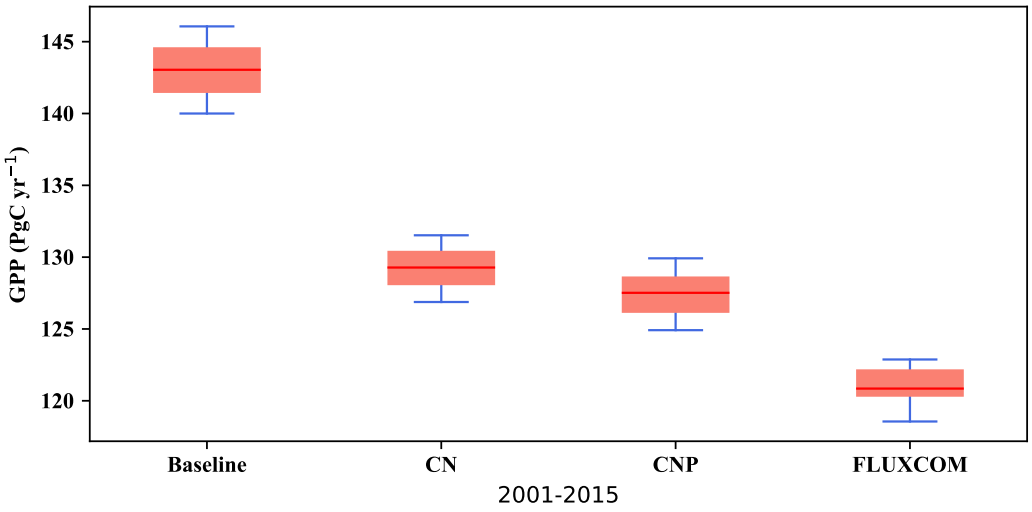

Figure 3.3: Modelled yearly Gross Primary Productivity (GPP) from 2001 to 2015 versus FLUXCOM GPP dataset (Jung et al. , 2019).

The nutrient limitation reduced the amount of land-atmosphere carbon flux in the simulations. The cumulative land uptake from 1850-2005 was 150 Pg C yr^{-1} in CNP, lower than version 2.10 calibration in Mengis et al. (2020) (177 PgC yr^{-}1). This change in response is crucial for understanding the future dynamics in the Shared Socio-Economic Pathways Projections as terrestrial vegetation is expected to decrease its capacity to store carbon in the future (Goll et al. , 2012). Overall, the carbon feedback values are in concordance with the ranges of the global carbon project used in Mengis et al. (2020) (Le Quere et al. , 2018) where the cumulative carbon flux was estimated to be 141 PgC yr^{-1} from 1850-2005. The atmosphere-to-land carbon flux follows the GCP dataset (Le Quere et al. , 2018) magnitude closely.

Similar to Wania et al. (2012), I found higher values of NPP for CN (77.4 Pg C yr^{1}) compared to the baseline simulation (74.2 Pg C yr^{1}). While CNP (72 Pg C yr^{1})

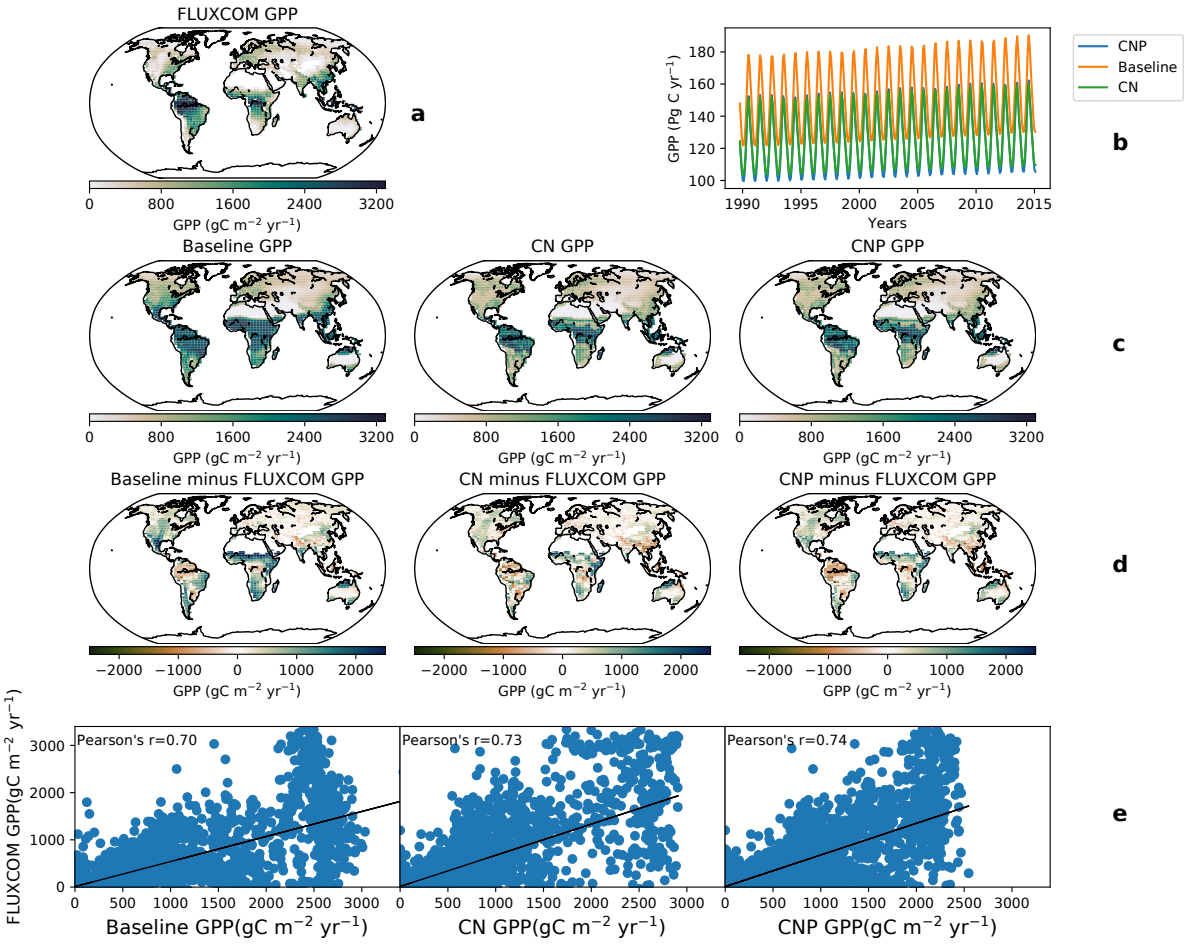

Figure 3.4: a. FLUXCOM GPP dataset from 2000-2010, b. Seasonal GPP from 1990-2015 for Baseline, CN and CNP. c. Second line shows the global GPP from 2000-2010 for Baseline, CN and CNP. d. The third line shows the difference between Baseline, CN and CNP and FLUXCOM GPP datasets. e. Shows the correlation of Baseline, CN and CNP to FLUXCOM GPP dataset.

resulted in lower values, due to the reduction of tropical vegetation biomass. CN and CNP results are close to the upper range (21.5 to 69.3 Pg C yr^1) of simulated NPP showed in Li et al. (2015). The reduction of tropical biomass mainly in broadleaf trees carbon is reflected in the fraction of the PFT shown in the model output. Wania et al. (2012), argued that the reason behind the high NPP was the dependence of autotrophic respiration on N content in leaf, root and stem which are based on the original MOSES/TRIFFID version (Cox et al. , 1999). In CN and CNP, the reduction of wood CN ratios and higher leaf content than in CN and CNP which fluctuates from a minimum to a maximum value gives place to the reduction of the maintenance respiration which reduces the autotrophic respiration and consequently NPP. Furthermore, in the new CNP version while wood CN remains to be fixed the stoichiometric reduction of wood carbon by the lack of P availability decreases wood carbon even more especially in tropical forests and other tropical ecosystems.

Atmospheric CO_2 concentration

The simulated CNP atmospheric CO_2 concentration matches observations very closely and the addition of N and P has shown an improvement in the representation of the model accumulation of carbon in the atmosphere. The CO_2 concentration has improved compared to the evaluated 2.10 version of the UVic ESCM where from 1960 to 2010 the simulation deviates above the observed curve (Δ78 ppm in the simulation compared to Δ73 ppm observations; Mengis et al. (2020)). Compared with the CN and baseline simulations (Fig. 3.5), CNP provides a more accurate representation of the atmospheric CO_2 concentration. Thus the nutrient limitation has effectively reduced the CO_2 fertilization effect on the terrestrial vegetation. Consequently, the CN and CNP show a larger pool of atmospheric CO_2.

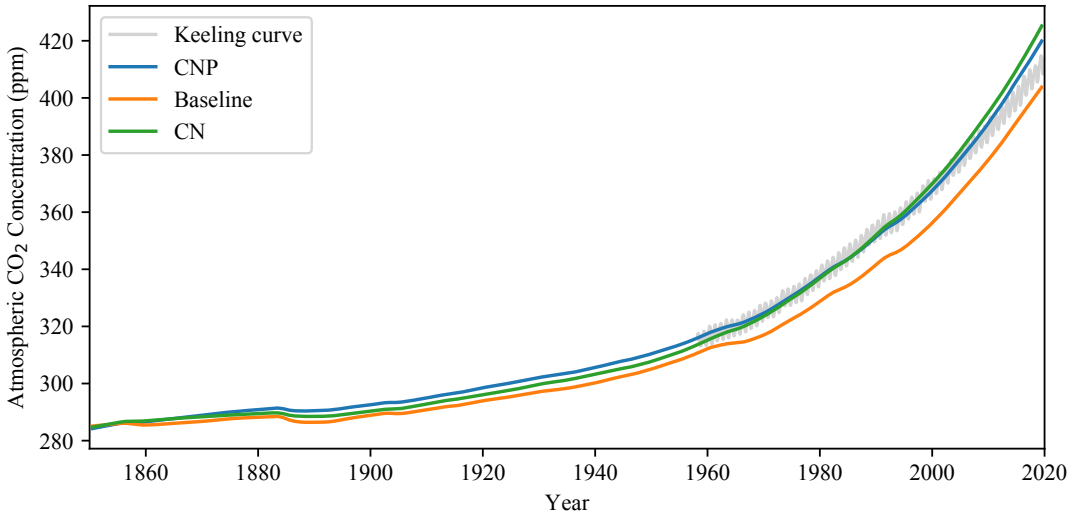

Figure 3.5: Atmospheric CO_2 concentration in CNP, CN and baseline simulations compared to the keeling curve from the Mauna Loa observatory (Keeling et al., 2005; grey line).

Terrestrial vegetation

Given that tropical forests and savannas are commonly limited by the availability of P, the simulated vegetation biomass representation is affected by the absence of nutrient limitation in ESMs. Nakhavali et al. (2021) found that the addition of P improved the vegetation estimations and the carbon cycle response to rising CO_2 for the Amazonian region, basing their study in a site representative for 60% of the Amazon soils.

In the CNP version of the model, Broadleaf trees coverage declined in tropical and subtropical latitudes (Fig. 3.6) with the largest changes located in South East Asia, Africa and South America. The reduction of vegetation biomass ranged from 6-20 % in South America and Africa, while a higher reduction of 20-30% was present in South Eastern Asia. The magnitude of continental difference can be attributed to the base internal vegetation biomass model version bias (Mengis et al. , 2020). Additionally,

CN and CNP show a shift of coverage where broadleaf trees is taken over by C3 grass. Needleleaf trees were reduced in North America and Europe. Both CN and CNP simulations of vegetation carbon resulted in a decrease of vegetation biomass with 456 Pg C and 525 Pg C respectively compared to baseline simulation (594 Pg C), similar to Zaehle et al. (2010). Overall CNP shows a high correlation with all PFTs coverage when compared with Poulter et al. (2015) PFTs dataset. In tropical regions, the UVic ESCM seems to represent vegetation closely to the data (Fig. 3.7, 3.8).

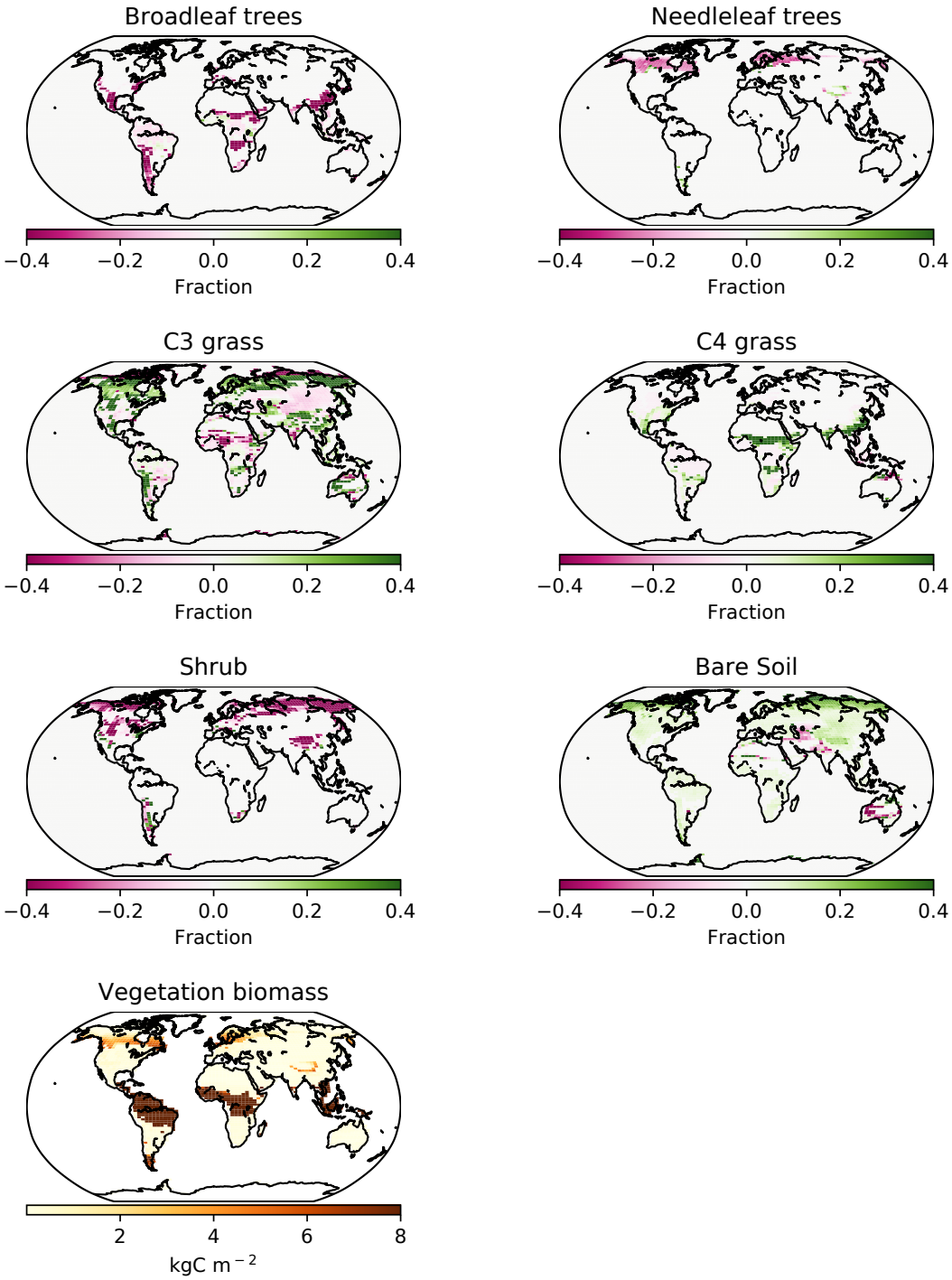

Figure 3.6: PFTs fractions in the UVic ESCM for 1980-2010, CNP minus baseline. The bottom last plot shows CNP global biomass distribution.

The total vegetation carbon is similar to Wania et al. (2012), with tropical forest having a range from 8-16 kgC m^{-2} and 4-12 kgC m^{-2} in temperate and boreal forest with means of 10.50 and 6.7 kgC m^{-2} respectively compared to 12-16 kgC m^{-2} and 4-12 kgC m^{-2} and means of 13.4 and 7.3 kgC m^{-2}. The latitudinal mean shows a decrease in the range of vegetation carbon in tropical latitudes of 1-1.5 kgC m^{-2} and 0.4-0.8 kgC m^{-2} in northern template latitudes. These results indicate that the main reduction of vegetation carbon is in the tropics, which agrees with the general N and P global pattern (Du et al , 2020). Consistent with Wania et al. (2012) the vegetation carbon outputs are similar to 12.1 kgC m^{-2} for tropical and 5.7–6.4 for temperate and boreal forests to Malhi et al. (1999).

3.4.2 Nitrogen cycle

Nitrogen distribution

The soil N ranges from 0 to 1.5kgN m^{-2} with lower N in the tropics increasing towards the temperate regions. Globally, the CNP simulated soil N is reduced compared to the original N structure in the UVic ESCM version 2.9 presented by Wania et al. (2012). The primary differences between Wania et al. (2012) N cycle and the current version are the soil layer structure and the stochiometry response to N limitation. In the former, N could be transferred from other pools when N was outside of the ratio threshold and thereby be considered to be limiting vegetation.

This result is also lower than the 0 to 4.8 kgN m^{-2} from IGBP-DIS data base (Global Soil Data Task Group , 2000). Wania et al. (2012) stated that the N content in the model is dependent to soil carbon fixed via a fixed CN ratio. Given this, lower carbon values can lower soil N values in CN simulations. Thereby, lower carbon in soil could be a strong reason why these results have less N than IGBP-DIS database (Global

Soil Data Task Group , 2000) and Wania et al. (2012). However, the values of this study fall within the range of uncertainty. The UVic ESCM estimates a mean BNF for 2010-2020 of 119 Tg N yr^{-1}. This value is above 35 Tg N yr^{-1} from Braghiere et al. (2022) and within the range of 52–130 Tg N yr^{-1} presented by Barnard and Friedlingstein (2020)

Vegetation nitrogen

The total amount of vegetation N (2.20 Pg N) was lower than the previous N cycle (2.94 Pg N, Wania et al. (2012)). These values are similar to Zaehle et al. (2010) (3.8 Pg N) and Wang et al. (2018) (3.9 PgN) but lower than Li et al. (2000) (16Pg N) and Yang et al. (2009) (18 Pg N). The tropical (30 to 45gN m^2) and boreal forest vegetation N (20 to 35gN m2) results are lower than from Wania et al. (2012) (30 to 40gN m^2), and those of Xu-ri and Prentice (2008) and Yang et al. (2009) (both studies ranged between of 150 to 400 gN m^2)

The global pattern of CN ratio is similar to Wania et al. (2012) structure with the highest located in tropical regions especially South America and South East Asia. Tropical forests show a value that ranges from 230-280 C:N (Figure 3.9) compared to 250-300 C:N to Wania et al. (2012). The reduction in wood carbon in tropics by P limitation in CNP lowered the C:N ratios. The values simulated are within the observational range of uncertainty (95-730) stated in Martius (1992).

The distribution of vegetation N resembles the results of Du et al (2020) where N primary effect in higher latitudes. The PFTs fraction changes show that N mainly limits North and central America (BR and NL), Chile (BR), Argentinian Patagonia (BR), North Europe (NL) and East Asia (BR)(Fig. 3.6). However, there seems to be N limitation in the tropical Africa and Asia in the model simulations. Even though

the model does not represent co-limitation the stochiometric limitation does seem to indirectly capture this effect.

N_2O fluxes

The multilayer model has allowed the estimations of anoxic regions and hence, a major improvement in the model is the quantification of terrestrial N_2O flux. Figure 3.10 shows CN and CNP N_2O fluxes from 1990 to 2018. Compared to EDGAR version 6 dataset (Crippa et al. , 2021) the UVic ESCM simulates N_2O fluxes relatively well, agreeing mostly in the last 10 years of the values. However, I observed an overestimation from 1990 to 2010. The CN version of the model fits within the lower natural (Natural soil, Atmospheric N deposition on land) + anthropogenic (Agriculture, Fossil fuel and industry) emission range (8.9 -14.3 Tg N yr^{-1}) given by the global carbon project (Tian et al. , 2020) while CNP falls just below the lower range value. The reduction of N in the model system by P effect is shown by these results, the reduction of vegetation biomass and then litterfall reduces the amount of N transfer to the N soil pool limiting the natural denitrification. The lack of oceanic production of N_2O in the model makes the comparison with the global total N_2O flux impossible at the moment. The total estimates for N_2O emissions being 4.2 to 11.4 Tg N yr^{-1} anthropogenic and 8.0 to 12.0 Tg N yr^{-1} natural given by global carbon project (Tian et al. , 2020). Assuming an ocean output of a mid-range emission (3.4 Tg N yr^{-1}) the model simulations are close to the lower range of the emission reported with CN (13.3 Tg N yr^{-1}) and CNP (12.1 Tg N yr^{-1}). Lighting and atmospheric production, biomass burning (addition of N_2O to the atmospheric pool) and post-deforestation pulse effect are not taken into account in the model structure and that could improve the fit of the simulation to a mid-range level value.

3.4.3 Phosphorus cycle

Inputs and losses

The P global weathering rate estimated is 3 Tg P yr^{-1} similar to 2 Tg P yr^{-1} in Wang et al. (2010). Fertilization inputs of 1 Tg P yr^{-1} (Filipelli , 2002) were added as an option to the model but were not used for the current simulations and dust deposition is not accounted for. Hence, the only P input into the system in this experimental setup comes from rock weathering. Regarding the P weathering representation Hartmann et al. (2014) approach was tested at first, but Wang et al. (2010) weathering scheme resulted in a better, simplified and controllable input. Although, Hartmann et al. (2014) was found to be superior since P input is dynamic, incorporating model runoff and lithological map distribution. A dynamic P input will also require a better representation of P losses in order to maintain a steady state.

The P weathering was set so the loss by leaching (3 Tg P yr^{-1}) was in accordance with the rates of was comparable with to the riverine input stated in Filipelli (2002) of 4-6 Tg P yr^{-1}. The gap corresponds to anthropogenic inputs not included here, the pre-industrial P input to the ocean from riverine input is 2-3 Tg P yr^{-1} and the human activities, especially agriculture (fertilizers) and water wastes, roughly correspond to a doubling of the P input.

Land P pools and storages

The total inorganic and organic P values are similar to those shown in the results of Smil (2000), Mackenzie (2002) and Wang et al. (2010) (Table 3.7), although organic P is slightly underestimated in the model (3.5 Pg P). This underestimation is likely the result of the lack of P fertilization on land. The labile, sorbed, strongly sorbed P and occluded pools are comparable values to Wang et al. (2010).

Globally the total soil P distribution (Fig. 3.11) is comparable to the He et al. (2021) dataset, which is one of the few terrestrial P concentrations maps available. Overall, the model simulates less global P, especially in northern latitudes most likely due to the oversimplified weathering scheme that underestimated the inputs in higher latitudes.

Latitudinally, the tropical soils showed the lowest P with the exception of highlands and mountains while increasing sequentially to the northern latitudes as showed in He et al. (2021). The labile P shows a similar distribution to Yang et al. (2013) with tropical regions being relatively depleted compared to other regions due to the high adsorption and occlusion by the soils.

In contrast with N, P inputs are limited by the mineral (apatite) concentration and weathering rate rather than biologically fixed. Most of the P is retained by soils leaving a small labile fraction for biological uptake. Because P mineral weathering and chemical recycling in the soils are so constraining, the linear model approach for adsorption based on Goll et al. (2017) might overestimate the impact of adsorption and occlusion in tropical soils. It is also worth noting that the biological impact on the adsorption-desorption dynamics is missing in most P modules in ESMs. The release of P from mineral grains can be enhanced by either the reduction of pH due to respiration, or the direct addition of organic acids by plants roots Schlesinger (1997).

Phosphorus in vegetation

The terrestrial vegetation shows a slight underestimation in comparison with other models. The new stochiometry limitation scheme of the model plays an important role in the vegetation biomass and could be the reason for the underestimated values especially for tropical regions. However, the range of P in terrestrial vegetation is

still uncertain with several studies showing a range from 1.8-3.0 Pg P (Smil , 2000). Although Wang et al. (2010) have dismissed those values as overestimations given an overall N:P ratio of 10-20 gN gP $^{-1}$, 3 Pg P is simply too high to be met.

Table 3.7: Phosphorus cycle model pools and values for literature.

Variables	Value (Pg P)	References (Pg P)
Total inorganic P	20.8	35-40 Smil (2000)
Total organic P	3.5	36 Mackenzie (2002) 26.5 Wang et al. (2010) 13.7 Wang et al. (2018) 5-10 Smil (2000)
Labile P	1.4	5 Mackenzie (2002) 5.7 Wang et al. (2010) 8.6 Yang et al. (2013) 1.5 Wang et al. (2010)
Sorbed P	1.1	3.6 Yang et al. (2013) 1.7 Wang et al. (2010)
Strongly sorbed P	12	7.6 Wang et al. (2010)
Occluded	6.3	9.0 Wang et al. (2010)
Vegetation P	0.2	0.4 Wang et al. (2010) 0.5 Smil (2000) 0.5 Wang et al. (2018) 0.2 Wang et al. (2018)
P Litter	0.01	0.5 Mackenzie (2002) 0.04 Wang et al. (2010) 0.03 Wang et al. (2018)

The foliar stoichiometry seems to approximately follow the N:P ratio field measurements of Reich and Oleksyn (2004) (Fig. 3.12). The tropical regions show some underestimated values in the UVic ESCM, the low amount of labile P and the latter decrease in broadleaf trees biomass could be responsible for the low numbers. Similarly, Nakhavali et al. (2021) show model values of 4-15 gP m^{-}2 for an Amazonian site which surpasses the results of this study.

A more complex adsorption–desorption scheme might be beneficial to solve the underestimation for tropical latitudes as those regions are heavily sorbed and lose most

of the input P, even though, the need of a proper global P vegetation dataset is imperative to have proper ranges in global distributions. The mechanical reduction of vegetation stoichiometrically by the model structure might also be too simplistic to represent P limitation in the tropics.

3.4.4 Parameter sensitivity

I perturbed 6 parameters ($CP_{leafmax}$, $CN_{leafmax}$, R_{leafp}, R_{leafn}, V_{maxp}, V_{maxn}) over historical simulations to assess the model sensitivity in terms of limitation of N and P. All of the above parameters play an important role in the nutrient limitation structure of the model. $P_{leafmax}$, $N_{leafmax}$ control when the stochiometrical limitation is set to be enforced on terrestrial vegetation and R_{leafp}, R_{leafp}, V_{maxp} and V_{maxn} control the uptake, litterfall and allocation of nutrients in leaves. In each case, default values were increased and decreased by 10% and 20% while holding other parameters constant. The results were compared to model simulations with all parameters held constant and set to default values. The cumulative atmosphere-land carbon flux was used to measure the effect of the perturbation since the limitation directly affects this flux.

The results of the sensitivity study show that model sensitivity varies with different parameters (Table 3.8). The UVic ESCM is most sensitive to perturbations of $CP_{leafmax}$ and $CN_{leafmax}$ because both determine directly the threshold by which vegetation carbon is reduced and nutrient limitation is defined. The model seems to be most sensitive to changes in $CP_{leafmax}$. The regulation of this parameter is very useful to calibrate woody vegetation in tropical regions to improve cover representation. The other parameters have a lower impact on the atmosphere-land carbon flux ranging from -3.23% to +1.60%.

Table 3.8: Cumulative atmosphere-land carbon flux anomaly from baseline (%). The parameters were perturbed by increasing and reducing 10 and 20 % of their value.

Parameters	-20%	-10%	+10%	+20%
$CP_{leafmax}$	-16.04%	-3.03%	+0.25%	+0.26%
$CN_{leafmax}$	-6.46 %	-2.10 %	+8.63%	+12.58%
R_{leafp}	-0.23%	-0.12%	+0.22%	+0.26%
R_{leafn}	-0.98%	-0.76%	+1.20%	+1.60%
V_{maxp}	-3.23%	-0.94%	+0.18%	+0.22%
V_{maxn}	-1.30%	-1.10%	+0.95%	+1.45%

3.5 Limitations and applications of the terrestrial nutrient modules

The UVic ESCM has been a critical tool in developing the cumulative emissions framework for climate mitigation (Zickfeld et al. , 2009; Matthews et al. , 2009; Matthews and Weaver , 2009; MacDougall and Knutti , 2016; Mengis et al. , 2018; Tokarska et al. , 2019) due to its low computations cost and strict enforcement of matter and energy conservation the model is capable of conducting a host of simulation beyond the limits of most other models, but with higher resolution than other EMICs (e.g. Montenegro et al. (2007); Matthews and Caldeira (2008); Keller et al. (2014); MacDougall and Knutti (2016); MacDougall (2017); Kvale et al. (2021)). As terrestrial nutrient limitation constrains the carbon cycle in nature, the new N and P modules allow addressing research questions relating to carbon budgets, carbon cycle and CH_4 feedbacks, carbon dioxide removal and permafrost carbon cycle, among other questions. Furthermore, the N and P cycles can represent environmental and climate critical processes such as the release of N_2O, agricultural impacts on terrestrial soils and coastal lines, eutrophication, anoxic events and nutrient fluxes from land to ocean.

A number of limitations have been identified with the developed N and P modules that relate to the degree of complexity or the lack of large-scale datasets available. Due to

the lack of global estimates of nutrient pools and fluxes based on field measurements, many of the parameters or parameterizations in this model are poorly constrained. In general, these are the following model limitation that is plan to be improved in future model development projects:

1. The model does not include a dynamic nutrient leaf resorption rate. Under nutrient limitations, this rate can increase as a strategy to conserve nutrients (Reed et al. , 2012). Thus, the effect of limitation in the UVic ESCM might be overestimated.

2. There is a static input of P from weathering. To control the P input I chose to estimate weathering flux by adding a fixed amount. This oversimplification could add more uncertainty to the P pools and can be overcome using a runoff-based weathering scheme. Moreover, I do not account for P atmospheric dust deposition.

3. The sorption-desorption dynamics of P in soil are oversimplified. We chose Goll et al. (2017) approach because it was a simpler way to represent this process. However, a more complex solution might improve the distribution of P globally.

4. The absence of an ocean N_2O output. Consequently, I am unable to estimate the total amount of a dynamically evolving N_2O concentration at this time. As N_2O is the 3rd most important greenhouse gas (IPCC , 2022), its incorporation into the model is a priority.

5. The model does not account for root uptake constraints of N and P on terrestrial vegetation. This includes spatial representations of mycorrhizal associations and the carbon cost of nitrogen and phosphorus uptake from soil (Shi et al. , 2016; Braghiere et al. , 2021, 2022).

The CNP model is primarily designed to improve carbon cycle feedback under current and future climate conditions. The use of nutrient limitation improves the land-atmosphere dynamics. In simulations, this improvement has a significant impact on atmospheric CO_2 concentrations. In future studies, I intend to assess the impact of nutrient limitation on different SSP scenarios and key carbon cycle benchmark metrics. Furthermore, the model can be used to improve the vegetation representation in ESMs. Finally, the CNP model may be used to generate coastal nutrient input and integrate terrestrial nutrient biogeochemical processes with oceanic processes.

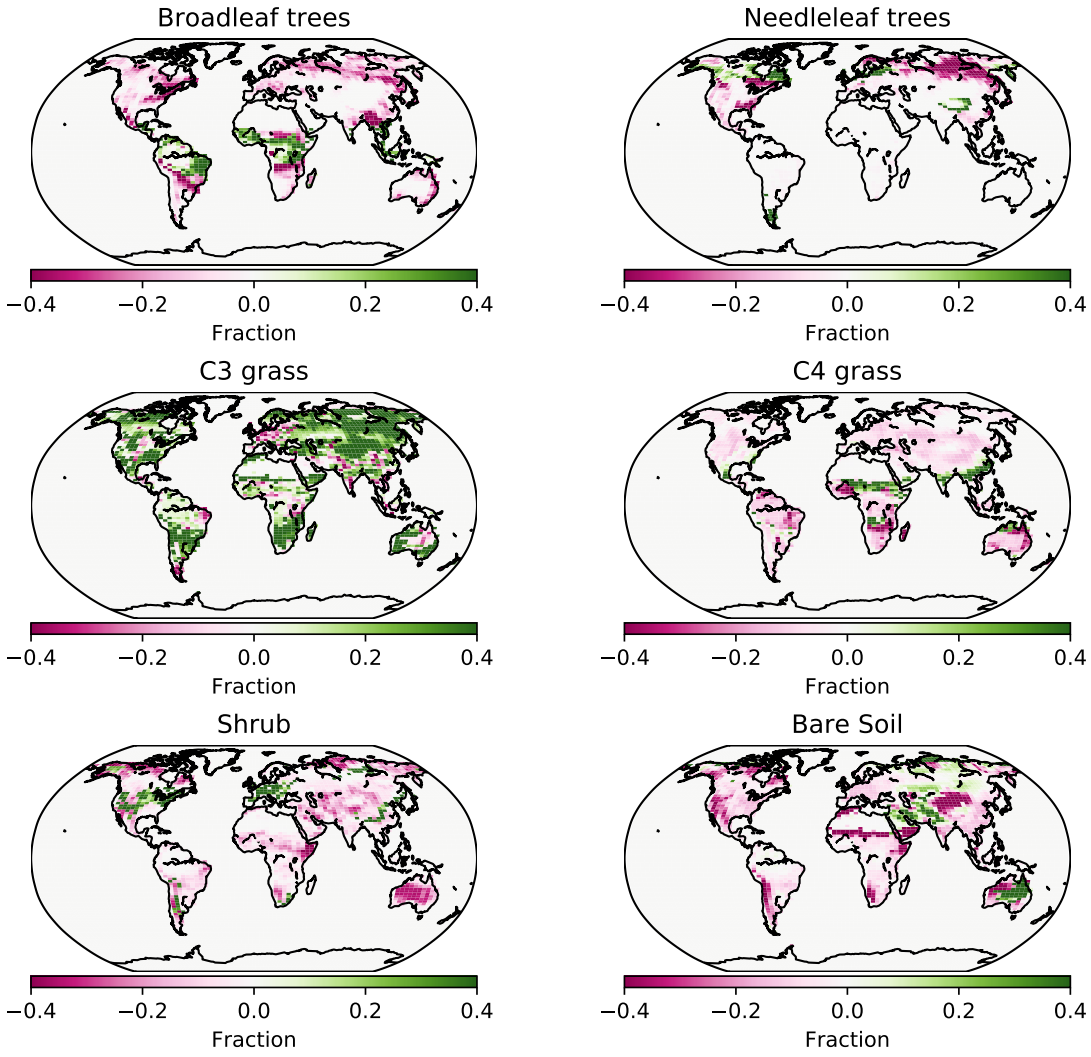

Figure 3.7: PFTs fractions in the UVic ESCM for 2008-2012, CNP minus Poulter et al. 2015 PFTs dataset.

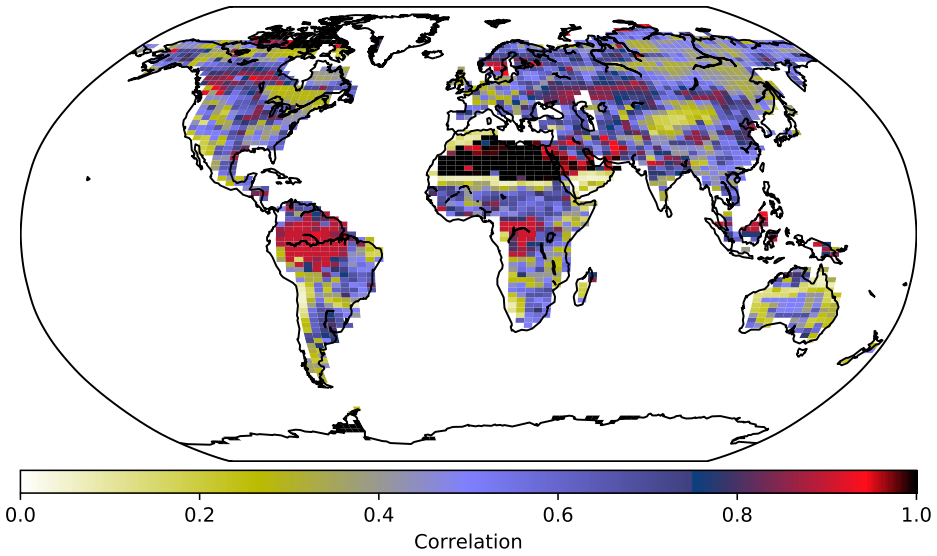

Figure 3.8: PFTs fractions across grid cells in the UVic ESCM for 2008-2012, CNP correlation to Poulter et al. (2015) PFTs dataset.

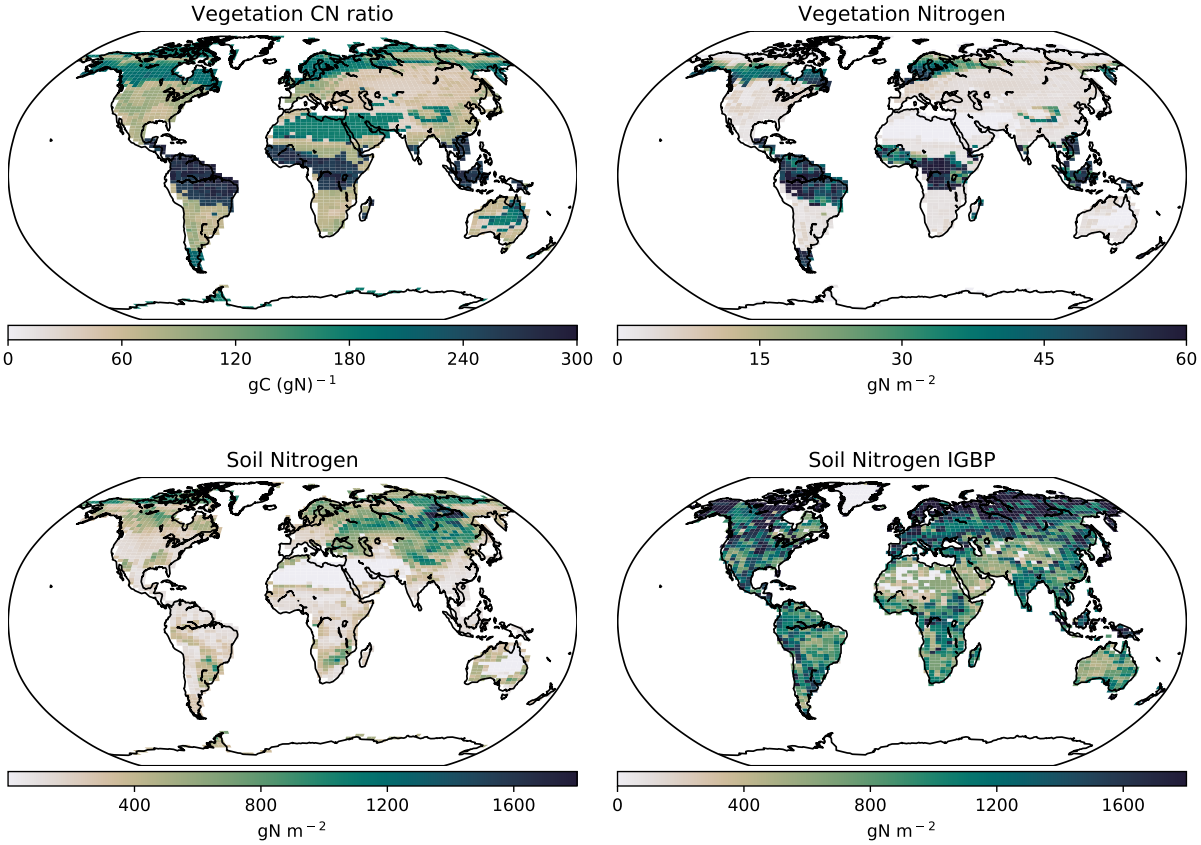

Figure 3.9: Modelled global soil and vegetation N in the CNP version of the UVic ESCM from 1980-1999. Lower right map corresponds to the soil N from the IGBP-DIS dataset (Global Soil Data Task Group , 2000)

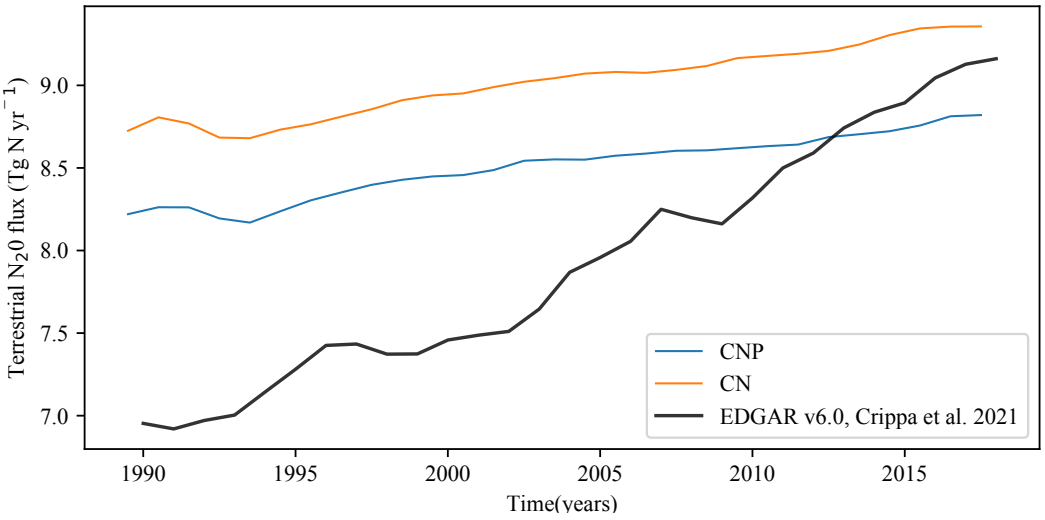

Figure 3.10: CNP and CN global soil N_2O emissions vs EDGAR version 6.0 N_2O dataset (Crippa et al. , 2021).

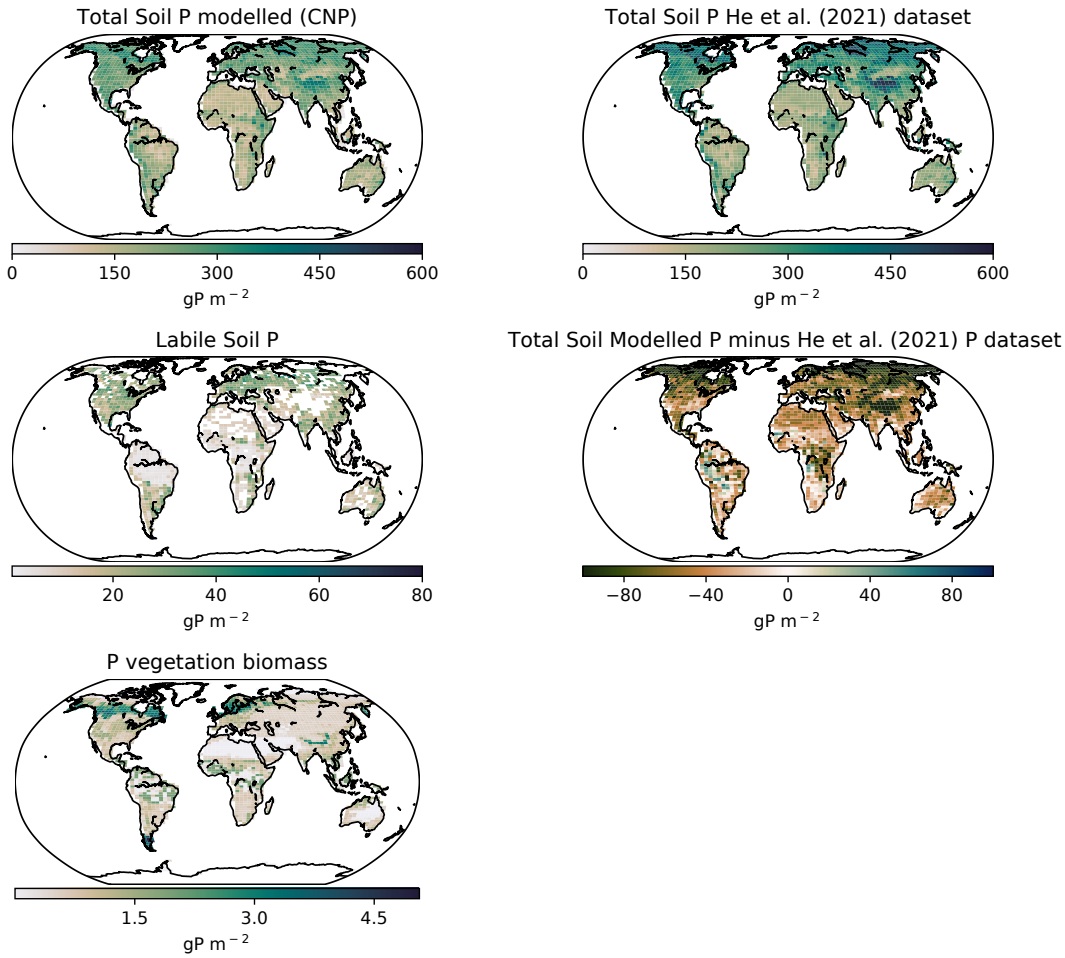

Figure 3.11: Soil and vegetation P global distribution. Modelled total P in soil, total P in soil as in He et al. 2021, soil P, labile P, vegetation biomass and the difference between modelled and observational P from He et al. (2021).

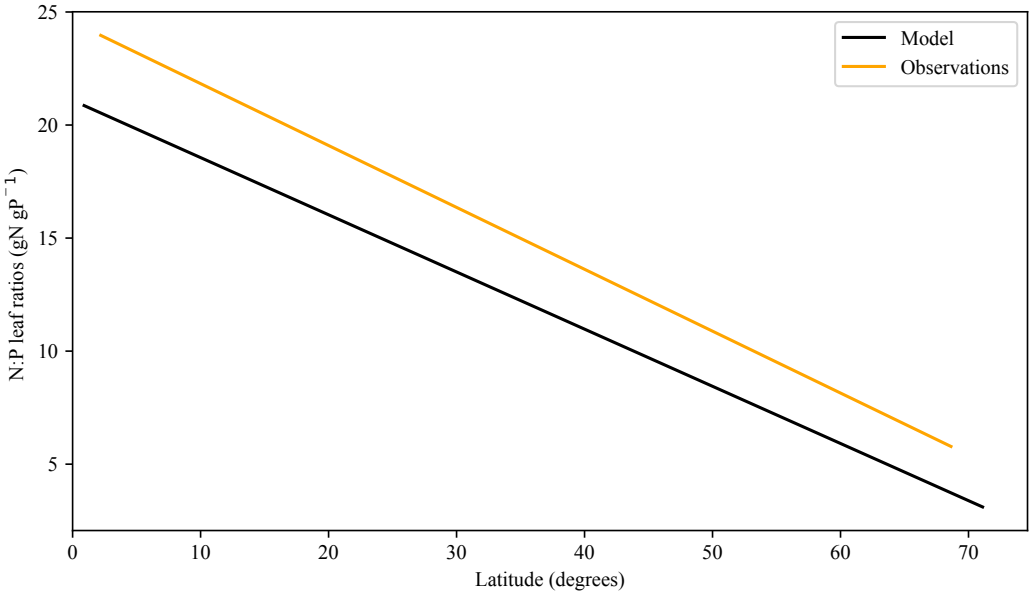

Figure 3.12: Modelled N:P leaf ratios trend vs an empirical relationship derived from Reich and Oleksyn (2004).

3.6 Conclusion

The N and P cycles simulated here fit the range of uncertainty shown in datasets and other modelling efforts. Generally, the simulated values fall into the lower range of the spectrum. N limits mainly high latitudes, especially in northern regions, but do show some limitation in tropical Africa and Asia. P limitations are greater in tropical regions and reduced vegetation biomass compared to the carbon-only version of the model bringing the model closer in line with observation (Mengis et al. (2020)).

The two nutrient limitations have improved the representation of the atmospheric carbon concentration in simulations forced with CO_2 emissions, using the Keeling curve as benchmark data. The land-atmospheric flux fits other simulations datasets and has been reduced from Mengis et al. (2020) values. Overall N and P addition have improved the carbon cycle feedbacks simulated in historical simulations. The GPP is lowered especially in the tropics mainly due to the reduction of woody vegetation biomass.

Many improvements remain to be made in the UVic ESCM structure. In regards to N cycle denitrification processes that need to be improved, N_2O fluxes while in the same magnitude as observations lack the trend showed in other benchmark datasets. The complexity of the P cycle could be improved especially the input and sorption processes. Finally, both N and P cycles could gain accuracy from adding dynamics leaf re-absorption rates that have been shown to change when nutrient limitation is present in the ecosystem and that can be used as in Du et al (2020) to clearly map the limitation pattern. Despite these limitations, the improved model has shown higher fidelity to observations and is expected to improve projections of the future of key carbon cycle feedbacks.

Chapter 4

Effect of terrestrial nutrient limitation on the estimation of the remaining carbon budget

Preface.

A version of this chapter is under review in the Journal Biogeosciences. I am the primary author. Along with my Co-author, Andrew MacDougall. I have carried out the simulations and validations of the model outputs. I have prepared the first draft of the manuscript and subsequently revised the manuscript, based on the feedback from my Co-author and also peer review process. As co-author, Andrew MacDougall assisted in the development of the concept and provided supervisory feedback by reviewing and revising the manuscript. The pre-print article can be access using the following link https://bg.copernicus.org/preprints/bg-2023-96/.

4.1 Abstract

The carbon cycle plays a foundational role in the estimation of the remaining carbon budget. It is intrinsic for the determination of the transient climate response to cumulative CO_2 emissions and the zero-emissions commitment. For the terrestrial carbon cycle, nutrient limitation has a core regulation on the amount of carbon fixed by terrestrial vegetation. Hence, the addition of nutrients such as nitrogen and phosphorus in land model structures in Earth system models is essential for an accurate representation of the carbon cycle feedback in future climate projections. Thereby, the estimation of the remaining carbon budget is impacted by the representation of nutrient limitation in modelled terrestrial ecosystems, yet it is rarely accounted for. Here, I estimate the carbon budget and remaining carbon budget of a nutrient-limited Earth system model, using nitrogen and phosphorus cycles to limit vegetation productivity and biomass. I use eight Shared Socioeconomic Pathways scenarios and idealized experiments on three distinct model structures: 1) carbon cycle without nutrient limitation, 2) carbon cycle with terrestrial nitrogen limitation and 3) carbon cycle with terrestrial nitrogen and phosphorus limitation. To capture the uncertainty of the remaining carbon budget, three different climate sensitives were tuned for each model version. The results of this study show that overall the nutrient limitation reduced the remaining carbon budget for all simulations in comparison with the carbon cycle without nutrient limitation. Between the nitrogen and nitrogen-phosphorus limitation, the latter had the lowest remaining carbon budget. The mean remaining carbon budget from the Shared Socioeconomic Pathways scenarios simulations for the 1.5 °C target in the no nutrient limitation, nitrogen-limited and nitrogen-phosphorus limited models obtained were 228, 185 and 175 Pg C respectively, relative to the year 2020. For the 2 °C target the mean remaining carbon budget was 471, 373 and 351

Pg C for the no-nutrient limitation, nitrogen-limited and nitrogen-phosphorus limited models respectively, relative to the year 2020. This represents a reduction of 19 and 24 % for the 1.5 °C target and 21 and 26 % for the 2 °C target in the nitrogen and nitrogen-phosphorus limited simulations compared to the no nutrient limitation model. These results show that terrestrial nutrient limitations constitute an important factor to be considered when estimating or interpreting remaining carbon budgets and are an essential uncertainty of remaining carbon budgets from Earth system model simulations.

4.2 Introduction

Future climate projections have only rarely accounted for nutrient limitation of the land carbon sink (Wang and Goll , 2021). For the sixth phase of the Coupled Model Intercomparison Project (CMIP6) this weakness was partially overcome with more Earth system models (ESMs) embracing nitrogen limitation as a standard for terrestrial system structures. However, the inclusion of phosphorus remains rare and representation of micro-nutrients remains a distant ambition (Arora et al. , 2020; Spafford and MacDougall , 2021). Thus, the future of the land carbon sink remains uncertain as projecting the interactions between the terrestrial system and atmosphere is a challenge without fully accounting for nutrient limitations (Achad et al. , 2016). Since year 1850, the cumulative CO_2 land sink has been estimated to be 210±45 PgC, which represents 31% of all anthropogenic carbon emissions. The terrestrial carbon sink has increased historically with increasing CO_2 emission rate, such that the proportion of carbon taken up by land has remained close to constant (Friedlingstein et al. , 2022). Nutrient availability constrains the capacity and rate at which terrestrial plants assimilate carbon (Goll et al. , 2012). Nitrogen and phosphorus are the nutrients that most commonly limit vegetation growth (Filipelli , 2002; Fowler et al. , 2013; Wang et al. , 2010; Du et al , 2020) and hence have been the subject of most research and large-scale modelling efforts. Globally, this effect varies. Most of the terrestrial biosphere is co-limited by both N and P, with N being the dominant nutrient limitation in higher latitudes while phosphorus predominates in lower latitudes (Du et al , 2020). Earth system models are designed to account for land use change, and biological productivity when estimating the carbon sink on land (Kiwamiya , 2020). The change of nutrient concentration in terrestrial systems in future simulations is an uncertainty for determining the land carbon sink over the next decades

(Shibata et al. , 2010, 2015; Menge et al. , 2012). Complicating this problem further, a large portion of nutrients on land is derived from anthropogenic sources, including agricultural fertilization (artificial, compost and manure), atmospheric deposition of N-bearing pollutants, and urban wastewaters (Lu and Tian , 2017; van Puijenbroek et al. , 2019).

It is likely that the first generation of ESMs simulations overestimated how much terrestrial ecosystems would respond to an increase in atmospheric carbon dioxide concentrations based on carbon-only schemes (Wieder et al. , 2015). A large amount of terrestrial carbon uptake was predicted by those simulations, which would result in unrealistic nutrient requirements. For example, in a study by Wieder et al. (2015) ESMs with nitrogen and nitrogen–phosphorus limitation were projected to decrease net primary productivity by 19% and 25%. Hence, the implementation of nutrient limitation in ESMs has been shown to improve the representation of carbon uptake in land (Wang et al. , 2007, 2010; Goll et al. , 2017; De Sisto et al. , 2023), and thus will affect the carbon budget.

The carbon budgets can be seen from two perspectives, the first describes pools and fluxes of carbon within the Earth system (Friedlingstein et al. , 2022). This perspective serves to understand how natural sinks respond to changes in climate, CO_2 and CH_4. The second is the remaining carbon budget, which describes the allowable future CO_2 emissions to reach a temperature target, commonly 1.5 and 2 °C, which is derived from another metric, the transient climate response to cumulative CO_2 emission (TCRE), which quantifies how global surface temperatures are nearly proportional to cumulative CO_2 emissions (Matthews et al. , 2009; MacDougall , 2016; Spafford and MacDougall , 2020). As TCRE represents the proportionality of cumulative CO_2 emission to its accompanying temperature change, its inverse can be used

to estimate the remaining carbon budget for temperature targets (Matthews et al. , 2020). The TCRE has been shown to be a good metric for predicting the response of temperature to cumulative CO_2 emissions. However, the TCRE only represented warming from CO_2 emissions, excluding the impacts of non-CO_2 forcing agents. A method to account for this issue is to use simulations with all anthropogenic forcing and plot the total anthropogenic warming as a function of cumulative CO_2 emissions, also known as effective TCRE (Tokarska et al. , 2018). There is a large uncertainty in the TCRE estimates, with a likely range from 1.0 to 2.3 K EgC^{-1} (IPCC , 2021). For idealized experiments, the Transient Climate Response (TCR) can be used to quantify the physical uncertainty in TCRE. TCR is the change of temperature at the time of doubling atmospheric CO_2 concentrations (year 70 in a 1pctCO_2 experiment). However, unlike TCRE, the TCR is dependent on the scenario used to compute it (e.g. MacDougall (2017)). The other important source of variability among TCRE estimates comes from uncertainties in carbon uptake by the ocean and terrestrial biosphere.

Terrestrial system nutrient limitation plays a vital role in the estimations of remaining carbon budgets due to their effect on the carbon cycle. Accounting for phosphorus limitation in carbon budget estimations is desirable due to its limiting effect at low latitudes (Du et al , 2020). Hence, P impact on terrestrial vegetation biomass and limitation of carbon sink almost certainly affect the remaining carbon budget estimates. The remaining carbon budget framework used in this study follows Rojeli et al. (2018), and assesses how nutrient limitation affects several uncertainties in remaining carbon budgets estimates, such as the TCRE, the estimated contribution of non-CO_2 climate forcings to future warming, the correction for the feedback processes presently unrepresented by Earth System Models, and response of temperature after emission have ceased, called the zero emissions commitment (ZEC) (Rojeli et al. , 2018). In

addition to these four factors knowledge of the human-induced warming to date is needed to compute the remaining carbon budget. This value is well estimated from historical records (Arias et al. , 2021). Nutrient limitation can be used to improve historical warming accuracy in emission-forced ESMs simulations (De Sisto et al. , 2023). The TCRE represents the response of temperatures to CO_2 emissions, hence different models can represent different remaining carbon budgets based on different carbon-climate sensitivities. The non-CO_2 emissions affect the change of temperatures and need to be understood to maintain desired temperature targets. Moreover, the change in temperature after emission cessation is an important dynamic that should be understood and considered in remaining carbon budget estimations. In future projections non-CO_2 climate forcings are likely affected by the introduction of nutrient limitation in ESMs. The main impacts include feedback changes due to land carbon sink and land use change emissions variation (including albedo changes), either by photosynthesis limitation or the reduction of terrestrial vegetation biomass. These changes might also impact the expected warming contribution after CO_2 emissions are ceased. Lastly, within this remaining carbon budget framework, N and P constitute an unrepresented sources of Earth system feedbacks that now is accounted in the present simulations.

A good representation of the carbon cycle response to CO_2 increase is vital for an accurate estimations of the remaining carbon budget for climate policies and management. The remaining carbon budget estimates need to account for feedback not usually represented in ESMs. As such, isolating the effects of N and P terrestrial limitation give a novel insight into how these underrepresented process in terrestrial systems have contributed to remaining carbon budget uncertainties. It is therefore important to understand ESMs carbon cycle sensitivity to nutrient limitation constrain of the land carbon sink in future simulations. Hence, I explore the effect of

terrestrial nitrogen and phosphorus limitation in the remaining carbon budget in an intermediate complexity Earth system and climate model under historical, idealized, and Shared Socioeconomic Pathways projections.

4.3 Methodology

4.3.1 Model description

Simulations to quantify the remaining carbon budgets were carried out with the University of Victoria Earth System Climate Model (UVic ESCM). The UVic ESCM version 2.10, is a global intermediate complexity model (Weaver et al. , 2001; Mengis et al. , 2020). The model is comprised of a 3D dynamic ocean circulation model (Pacanowski , 1995), along with a simplified moisture-energy balance atmosphere (Fanning and Weaver , 1996), a dynamic-thermodynamic sea ice model (Bitz et al. , 2001) and a land surface model (Meissner et al. , 2003).

In the model, the terrestrial and oceanic carbon cycles are represented. The ocean comprises 19 vertical levels that become thicker with depth (50 m near the surface to 500 m in the deep ocean). Ocean biogeochemistry is based on a simple nutrient-phytoplankton-zooplankton-detritus model (Keller et al., 2012; Schmittner et al., 2005), with the representation of ocean carbonate chemistry and sediments (Mengis et al. , 2020).

In the 2.10 version of the model, the soil is represented by 14 subsurface layers with their thickness increasing exponentially with depth, with the surface layer measuring 0.1 m, the bottom layer measuring 104.4 m, and the total layer measuring 250 m. Hydrological processes are active in the first eight soil layers (top 10m), while the layers below have granitic characteristics. The soil carbon cycle is active up to a depth of 3.35 m (6 layers) (Avis , 2012; MacDougall et al. , 2012). TRIFFID (top-down representation of interactive foliage and flora including dynamics) represents vegetation interaction between 5 functional plant types within the terrestrial vegetation. Based on the Lotka-Volterra equations (Cox , 2001), broadleaf trees, needleleaf

trees, shrubs, C3 grasses, and C4 grasses compete for space in the grid. Through photosynthesis, carbon is uptaken and allocated to growth and respiration, whereas the vegetation carbon is transferred to the soil through litter fall and allocated to the soil in a decreasing function of depth. Permafrost carbon is prognostically generated within the model using a diffusion-based scheme meant to approximate the process of cryoturbation (MacDougall and Knutti , 2016).

The UVic ESCM prescribes anthropogenic land-use changes based on standardized CMIP6 land-use forcing (Ma et al., 2020) regridded to the UVic ESCM grids. Land-use data products have been modified for UVic ESCM use by aggregating cropland and grazing land into one crop type, representing any of the five functional types of crops, and one grazing variable, representing pastures and rangelands. By using this forcing, the model determines the fraction of grid cells that contain crops and grazing areas, and these fractions are assigned to C3 and C4 grasses and excluded from the vegetation competition routine of TRIFFID. A full description of the model can be found in Mengis et al. (2020).

A terrestrial nitrogen and phosphorous model has recently been developed for the UVic ESCM (De Sisto et al. , 2023). The nitrogen cycle module consists of three organic pools (litter, soil organic matter, and vegetation) and two inorganic pools (NH_4^+ and NO_3^-). Biological nitrogen fixation and mineralization of organic nitrogen produce NH_4^+, which can be absorbed by plants (vegetation), leached, or transformed into NO_3^- via nitrification. NO_3^- is produced through nitrification, can be taken up by plants, leached or denitrified into NO, N_2O or N_2. Inorganic N is distributed between leaf, root, and wood, with wood having a fixed stoichiometric ratio and leaf and root pools having a variable ratio. Organic N leaves the living pools via litter-fall into the litter pool, which is either mineralized or transferred to the organic soil pool, part of

this N can be mineralized into the inorganic N pools. At the same time, N can flow from the inorganic to the soil organic pool via immobilization. A complete description of the nitrogen cycle can be found in Wania et al. (2012) and De Sisto et al. (2023).

The phosphorus module included three inorganic (labile, sorbed and strongly sorbed) and three organic P pools: Vegetation (leaf, root and wood), litter and soil organic P. The P input is driven by a fixed estimates of P release per global soil type as in Wang et al. (2010). Inorganic P (P_{soil}) in soil follows the dynamics described in Goll et al. (2017). After uptake, P is distributed in three vegetation compartments: leaf, root and wood. Leaf and root have a dynamic value that varies between a minimum and a maximum, while wood has a fix C:P ratio. The vegetation P biomass dynamics is determined from the difference between the amount of uptake and the loss from litterfall. The soil litter decomposed is transferred to the soil organic P pool. The dynamics of P organic matter are adapted from Wang et al. (2007). A complete description of the P cycle can be found in De Sisto et al. (2023). Nitrogen and phosphorus limit terrestrial vegetation growth in the model in two different ways: 1) Nitrogen limits the photosynthetical activity (by regulating the maximum carboxilation rate of RuBISCO) and directly by reducing biomass. This reduction is controlled by the maximum C:N leaf ratio, where reducing this value corresponds to a larger reduction of vegetation biomass. 2) Phosphorus only limits vegetation biomass based on maximum C:P leaf ratios.

4.3.2 Experimental set-up

The effects of nitrogen and phosphorus were analyzed from the perspective of the sources of uncertainty in the remaining carbon budget estimates. Here, the framework includes how nitrogen and phosphorus impact the representation of: 1) Model fidelity

of human warming to date, 2) the TCRE, 3) the unrealized warming from past CO_2 emissions (zero emissions commitment) and, 4) the estimated contribution of non-CO_2 climate forcings to future warming. I run three different versions of the UVic ESCM version 2.10: 1) Carbon only (C-only), 2) Carbon Nitrogen (CN) and Carbon Nitrogen and Phosphorus (CNP). Furthermore, to capture the uncertainty of the carbon budget estimates the climate sensitivity was tuned using an equilibrium climate sensitivity parameter designed by Zickfeld et al. (2009) to alter climate sensitivity in the UVic ESCM by altering the flow of long-wave radiation back to space. Model variants were tuned to have Equilibrium Climate Sensitivities (ECSs) per doubling of CO_2 of 2.0°C, 4.5°C to represent the "likely bounds" (IPCC , 2021), as well as using the emergent climate sensitivity of the model (3.4°C) as the central estimate.

Historical human-induced warming to date

I conducted three historical simulations to assess the historical climate response differences between the C-only and CN and CNP. Each model structure was calibrated using aerosol scaling so that historical temperatures matches observations. Three-dimensional aerosol optical depth can be scaled by a fraction in the UVic ESCM and was used in version 2.10 to calibrate aerosol forcing to fit current values (Mengis et al. , 2020). Thus the historical warming to date is similar for all model variants but the estimated historical emissions vary, allowing model validation.

Transient climate response to cumulative emissions

To diagnose the TCR and the TCRE, I run simulations starting with a 1% yr^{-1} increase in CO_2 concentrations until a doubling and quadrupling(2x and 4xCO_2) were reached after which the concentration was kept constant (Eyring et al. , 2016). Both

TCR and TCRE are computed at year 70 of this 1pctCO_2 experiment, when atmospheric CO_2 concentration has doubled. To account for non-CO_2 forcing effect on climate sensitivity, I applied Tokarska et al. (2018) approach to compute effective-TCRE. Using a SSP 5-8.5 a high emission scenario I determined the response of temperature to cumulative emissions including all forcing accounted in the SSP scenario.

Zero emissions commitment

To explore the effects of nutrient limitation on zero emission commitment, an experiment following the Zero Emission Commitment Model Intercomparison Project (ZECMIP) protocol was conducted (Jones et al. , 2019) for C-only, CN and CNP. For these experiments the 1pctCO_2 experiment is followed until diagnosed cumulative emissions of CO_2 reaches 1000 PgC thereafter emissions are set to zero further CO_2 emissions. I diagnosed three emissions pathways corresponding to C-only, CN and CNP simulations. I used two metrics to assess the nutrient limitation effect on ZEC. The first is the temperature at the 50th year after emissions have ceased relative to the global average temperature when emissions ceased, averaged from year 40 to year 59 after emissions cease (ZEC_{50}) as in MacDougall et al. (2020). The second is the mean ZEC for 100 years after emissions have ceased.

Estimated contribution of non-CO_2 climate forcings to future warming

To estimate the impact of nutrient limitation on the contribution of non-CO_2 climate forcings to future warming, eight SSPs scenarios for the C-only, CN and CNP version of the UVic ESCM version 2.10 were run. I included the CMIP6 SSPs array scenarios representing each distinct future (1-5) narrative. The following scenarios were run: SSP1-1.9, SSP1-2.6, SSP2-4.5, SSP3-7.0, SSP4-3.4, SSP4-6.0, SSP5-3.4-OS

and SSP5-8.5. SSP1 represents a low challenge scenario for mitigation and adaptation, where both social and energy aspects evolve so that the anthropogenic climate impact decrease in the future. SSP2 described a future of medium challenges where the change of society and technology is not remarkably different from the historical baseline. SSP3 and SSP5 describe a high challenge to mitigation, the difference between the two being that SSP3 described high challenge for adaptation while SSP5 does not. SSP4 describes a scenario where there a low challenges for mitigation but there are high challenges for adaptation.

The carbon budget follows temperature anomalies normalized to 1850-1900 mean for 1.5, 2, 2.5 and 3 °C targets. For the four overshoot scenarios (SSP1-1.9, SSP1-2.6, SSP4-3.4, and SSP5-3.4-OS) the remaining carbon budget is computed for the time when the target is first breached. To estimate the effect of nutrient limitation in land use change emissions and terrestrial albedo an extra set of three simulations for C-only, CN and CNP and the same eight SSP scenario simulations were conducted. In these simulations land use change forcing was set to the pre-industrial year 1850 value. The model adjusts its diagnosed CO_2 emissions to account for the missing forcing. Hence, the diagnosed emission difference between the simulations with land use change forcing and without forcing corresponds to the estimated amount of land use change emissions (Mengis et al. , 2018) These values also carry the effect of albedo change due to land use change. Hence, the UVic ESCM model values show the total land use change emission + albedo effect simulated in the model.

4.4 Results

4.4.1 Historical human-induced warming to date

For each model structure, the historical temperature was calibrated to match historical observations by altering the efficacy of aerosol forcing. Figure 4.1 shows the resulting near-surface air temperature anomalies for UVic ESCM C-only, CN, and CNP configurations after calibration relative to 1951-1980 climate normal. The temperature anomalies were plotted against GISS near-surface air temperature anomalies relative to 1951-1980 (GISTEMP Team , 2023). For the three different versions of the model, the resulting calibrated simulations reproduced well the historical temperature trend when compared to GISS observations. As shown in De Sisto et al. (2023) without calibration the UVic ESCM CN and CNP have higher temperatures when compared to C-only, given that nutrients limit the capacity of the terrestrial system to uptake atmospheric CO_2. That is, atmospheric CO_2 is higher given the same total emissions of CO_2. Between CN and CNP, CNP results in higher temperature response mainly as a result of tropical terrestrial nutrient limitation and extra phosphorus limitation in higher latitudes.

Figure 4.2 shows the historical global carbon cycle from 1850-2021 for C-only, CN and CNP. There are two main impacts of nutrient limitation on terrestrial systems: 1) reduction of the land carbon sink and 2) reduction of the land use change emissions. The reduction of the land carbon sink is related to the decrease of the photosynthetic capacity and the regulation of terrestrial vegetation biomass. This biomass reduction leads to the reduction of land use change emissions, especially as N and P affect woody biomass greatly. The global reduction of carbon uptake increases the concentration of CO_2 in emission-driven simulations. Following this logic and given that

concentration-driven simulations have a set atmospheric CO_2 concentrations, the diagnosed emissions estimated in the UVic ESCm simulations were reduced in CN and CNP compared to C-only. The model estimates less emissions to be necessary to keep the CO_2 concentration on track as less carbon is uptake from land. In order to be comparable to the latest carbon budget report, the estimation of the historical carbon cycle follows carbon fluxes from 1850-2021 while the estimation of the remaining carbon budgets starts from the year 2020 following different future SSPs scenarios pathways. From 1850-2021 (Figure 4.2) the range of reduction in the CN and CNP nutrient-limited simulations for the cumulative land carbon sink was 75 to 106 Pg C compared to C-only. The range of reduction for cumulative land use change emission was 60 to 93 Pg C. Finally, the range of reduction of the cumulative carbon emissions diagnosed by the concentration-driven simulations was 11 to 29 Pg C. The CNP cumulative fossil fuel CO_2 emissions of 483 PgC is within the value of 465±25 PgC given by Friedlingstein et al. (2022) while C-only and CN are slightly over the estimate with 501 and 512 PgC (Figure 4.2).

4.4.2 Transient climate response to cumulative CO_2 emissions

The TCR for doubling CO_2 concentrations was 1.78, 1.79 and 1.79 °C in C-only, CN and CNP. Corresponding to a small difference, driven by albedo changes. Between CNP and CN, the albedo change has a small increase effect of 0.004 °C in CNP compared to CN (note the UVic ESCM lacks internal variability, so this very small difference is computable). The TCRE for C-only resulted in 1.74 K EgC^{-1} compared to CN 1.94 K EgC^{-1} and CNP 2.07 K EgC^{-1}. The TCRE values for all the simulations are within the range of 1 - 2.3 K EgC^{-1} given by the IPCC AR6 Summary for Policy Makers (IPCC, 2021). Under a 1% atmospheric CO_2 increase per year experiment, nutrient limitation has a heavy restriction on terrestrial vegetation uptake due to much

faster rise in CO_2 relative to the historical trajectory (MacDougall et al. , 2019). If vegetation were free to uptake carbon, in such a steep increase scenario terrestrial plants are expected to increase biomass as a corresponding response. However, the limit of uptake given by the concentration and availability of nutrients regulate the rate at which vegetation metabolizes carbon. Hence, despite the high concentration of CO_2 in the atmosphere, terrestrial vegetation is constrain nutrient limitation. The effective TCRE estimated from SSP5-8.5 resulted in 1.97, 2.27 and 2.36 K EgC $^{-1}$ for C-only, CN and CNP. Overall the TCRE and effective TCRE were increased in the nutrient-limited simulations. The range of increase for TCRE was: 0.2 to 0.3 K EgC $^{-1}$. The range of increase of the effective TCRE was: 0.3 to 0.4 K EgC $^{-1}$. Figure 4.2 shows how terrestrial carbon cycle fluxes change in historical simulations. Due to these changes the diagnosed CO_2 emissions are reduced, hence, for any temperature target less CO_2 emissions need to be emitted in the nutrient-limited simulations. This translates into a more sensitive models, where for 1000Pg C emitted, the nutrient limiting simulations are going to result in higher temperatures.

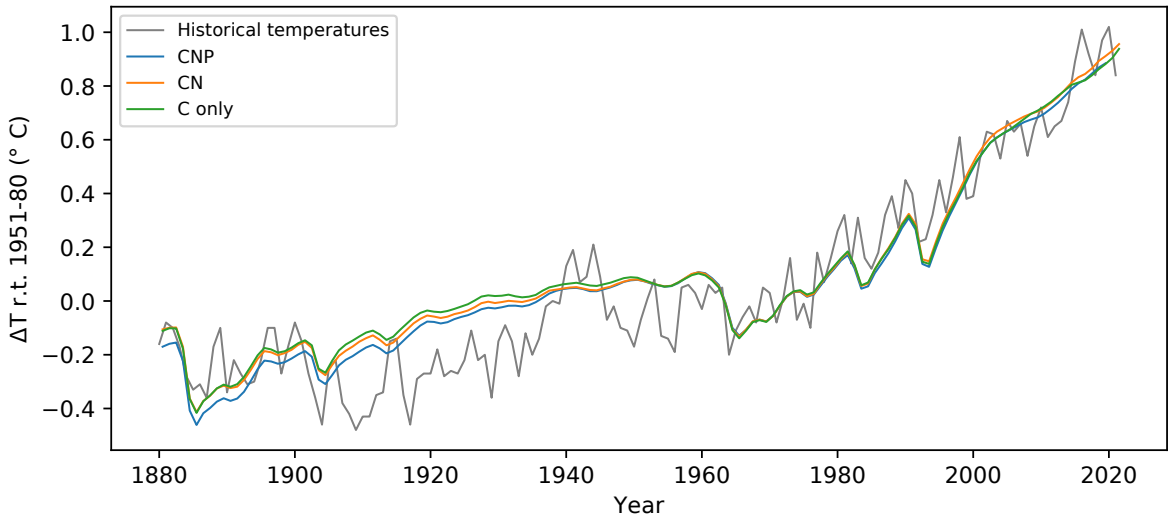

Figure 4.1: Historical temperature relative to 1951-1980 of C-only, CN and CNP compared to GISS historical temperature dataset (GISTEMP Team , 2023).

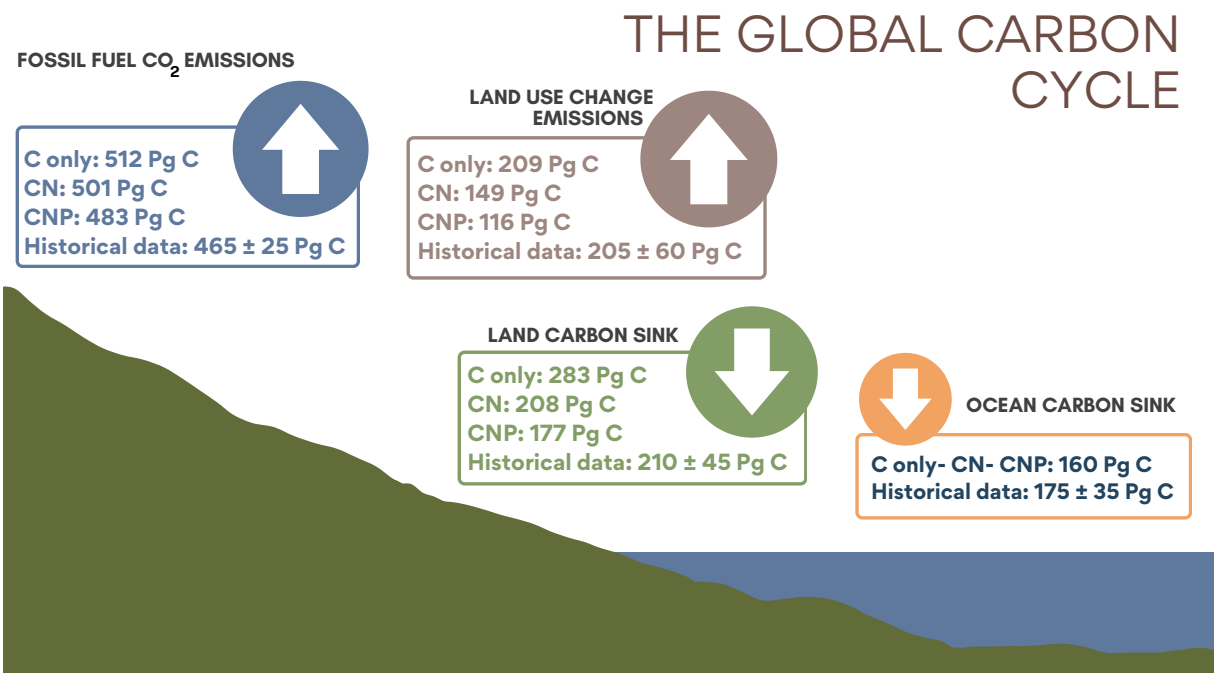

Figure 4.2: Historical 1850-2021 cumulative land carbon sink, ocean sink, land use change emissions and diagnosed CO_2 emissions simulated compared to Friedlingstein et al. (2022).

4.4.3 Zero Emission Commitment

To analyze the impact of nutrient limitation in zero-emission scenarios, ZECMIP type experiments were conducted in C-only, CN and CNP. Figure 4.3 show the temperature anomaly relative to the estimated temperature at the year of cessation. The temperature pattern in the 100 years following cessation is similar for all the model structures. There is an initial rise of temperature around the 20th year and a quick decline on the 35-40th year, followed by an increase around the 70-80th year. A difference between C-only and CN and CNP is that the C-only simulation increase is lower than the nutrient-limited simulations. The overall ZEC value is higher in CNP and CN than in C-only. For CN and CNP the ZEC_{50} value resulted in 0.07 and 0.09 °C compared to 0.02 °C in C-only. These values are similar to the ZEC_{50} of 0.03 °C shown in MacDougall et al. (2020) for the same model. The ZEC across 100 years of simulation after emission has ceased show a larger difference in temperature change after emission has ceased. C-only resulted in 0.05 °C compared to 0.17 °C in CN and 0.21 °C in CNP. This represents a relevant increase of temperature after emissions have ceased in the nutrient-limited simulations.

4.4.4 Estimated contribution of non-CO_2 climate forcing to future warming

In this section, I assessed the remaining carbon budget variability between different nutrient limitation model structures in the eight SSPs used in CMIP6. Furthermore, the emphasis was to show the role of N and P representation in remaining carbon budget estimates from different future scenarios. Figures 4.3, 4.4, 4.5, 4,6, 4.7 and 4.8 show the resulting remaining carbon budgets for SSP 1-1.9, 1-2.6, 2-4.5, 3-7.0, 4-3.4, 4-6.0, 5-3.4 and 5-8.5. Among these projections, not all reached the 1.5, 2,

2.5 and 3 °C targets. SSP1-1.9 and SSP1-2.6 only reached the 1.5 °C target, SSP 4-3.4 and SSP 5-3.4 only reached the 2 °C target, SSP 2-4.5 reached the 2.5 °C target and SSP 3-7.0, SSP 4-6.0 and SSP 5-8.5 reached the 3 °C target. The remaining carbon budget estimates and the SSP temperature anomalies can be seen in more detailed in Appendix A1, A2, A3, B1, B2 and B3. Overall, the application of nutrient limitation increased the TCRE and hence, decrease the carbon budget for all set targets. As expected, among CN and CNP simulations phosphorus limitation reduced the remaining carbon budgets. The mean remaining carbon budgets estimated among the SSPs simulations for ECS 3.4 [ECS 4.5 to ECS 2] in the C-only, CN and CNP for 1.5 °C target were: 228[31 to 291], 185[25 to 259] and 175[9 to 223] Pg C respectively. For the 2 °C target the mean remaining carbon budget were 471[205 to 554], 373[154 to 479] and 351[137 to 402] Pg C for the C, CN and CNP configurations respectively. The remaining carbon budgets for the 2.5 °C target were 719[378 to 869], 591[321 to 725] and 596[315 to 673] Pg C. Finally, the remaining carbon budgets for the 3 °C target were 974.4[546 to 1174], 798[460 to 986] and 796[467 to 920] Pg C. This represents a reduction of 19 and 24 % for the 1.5 °C target, 21 and 26 % for the 2 °C target, 18 and 17% for the 2.5 °C target and finally 18 and 19 % for the 3 °C target in CN and CNP compared to C-only.

One of the impacts of nutrient limitation is in the change of land use change emissions corresponding to the reduction and change of vegetation. I found that the mean land use change emission budget among SSPs simulation from year 2020 to the 1.5 °C target in the ECS 3.4[ECS 4.5 to ECS 2] were: 31[2 to 39], 20[2 to 40] and 13[1 to 23] Pg C for C-only, CN and CNP respectively (Figure 4.9). Corresponding to a reduction of 11.2 and 18.4 Pg C in CN and CNP compared to C-only. These results demonstrate that the remaining carbon budgets is clearly sensitive to the availability of nutrients represented in SSPs model simulations. As shown in figures 4.2,4.3,4.4,4.5,4.6,4.7

and 4.8 the remaining carbon budgets vary between the SSPs scenarios as temperature rises are affected by non-CO_2 forcings, corresponding to socioeconomic global uncertainties. Furthermore, the land carbon cycle in this case nutrient limitation, represents an implicit uncertainty under these different socioeconomic projections.

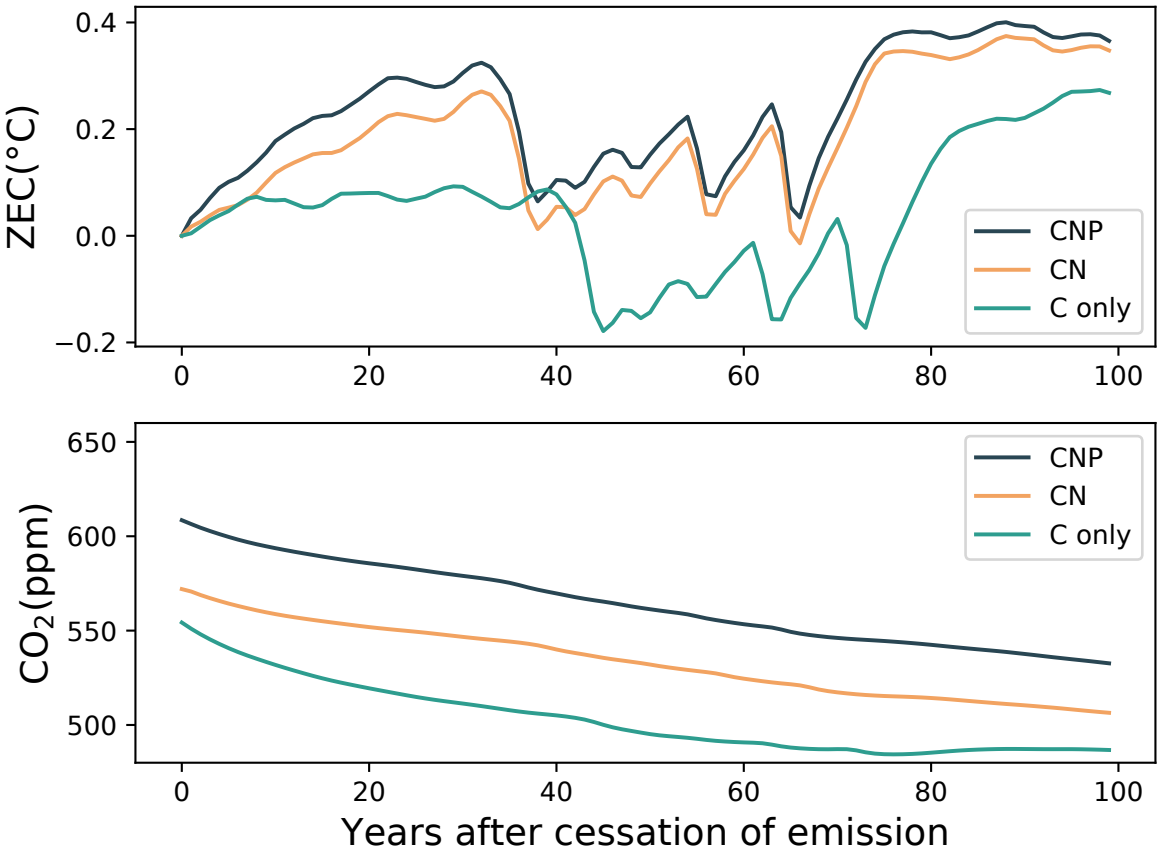

Figure 4.3: Zero Emissions Commitment following the cessation of emissions during the experiment wherein 1000 PgC was emitted following the 1pctCO2 experiment. ZEC is the temperature anomaly relative to the estimated temperature at the year of cessation. Note the UVic ESCM lacks internal variability. The rapid changes in global temperature seen in the top panel are due to disruptions to the ocean meridional overturning circulation (Mengis et al. , 2020)

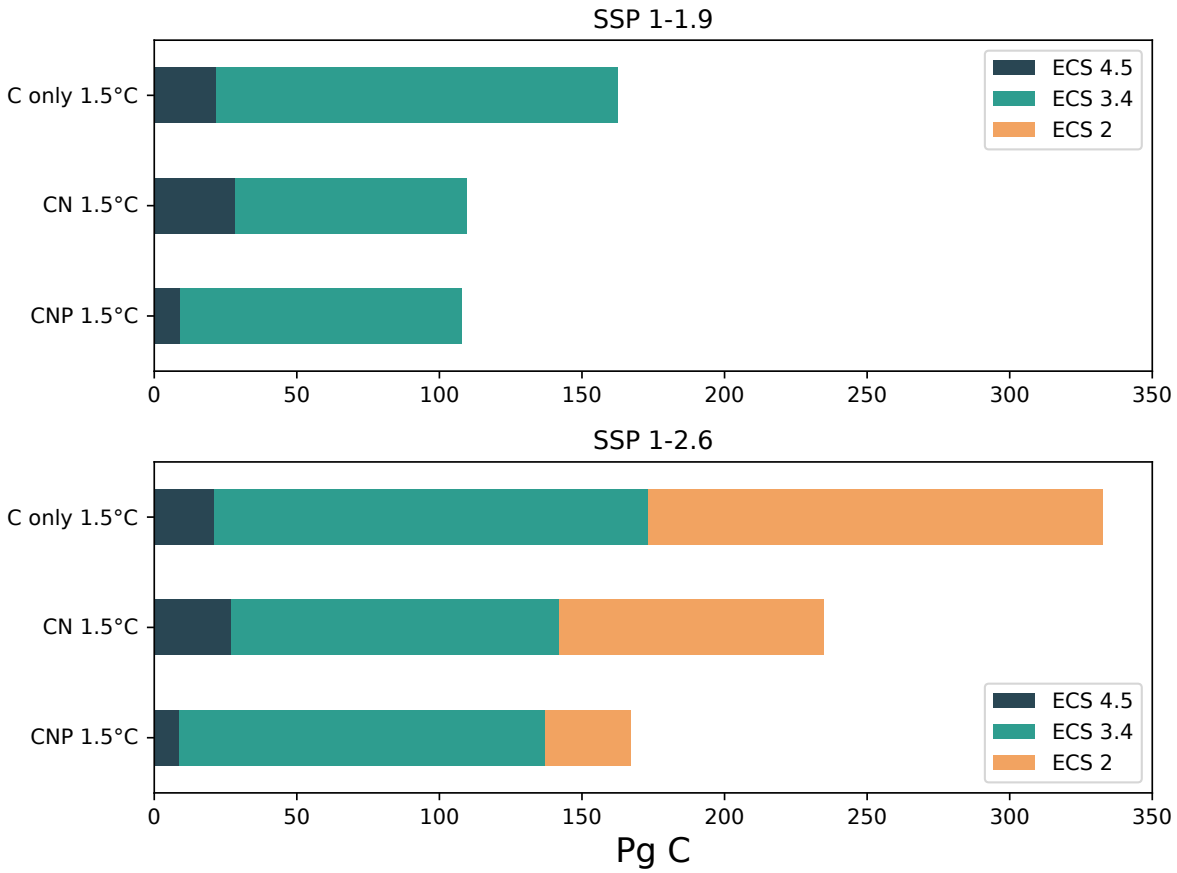

Figure 4.4: Carbon budgets for the 1.5 °C target for SSP 1-1.9 and 1-2.6. Three model sensitivities are shown as: ECS 4.5 dark blue, ECS 3.4 green and ECS 2 orange.

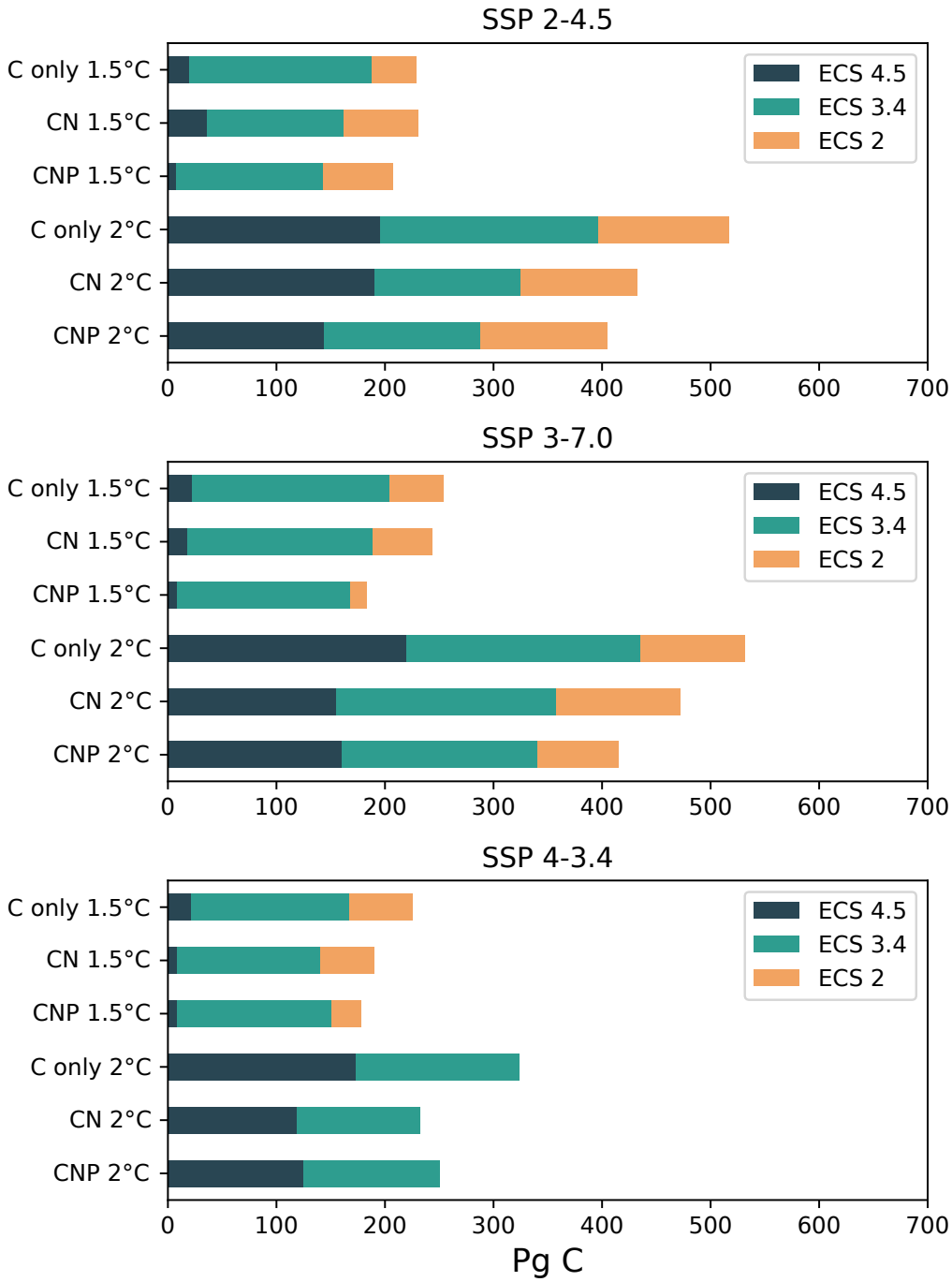

Figure 4.5: Carbon budgets for the 1.5 and 2 °C targets for SSP 2-4.5, 3-7.0 and 4-3.4. Three model sensitivities are shown as: ECS 4.5 dark blue, ECS 3.4 green and ECS 2 orange.

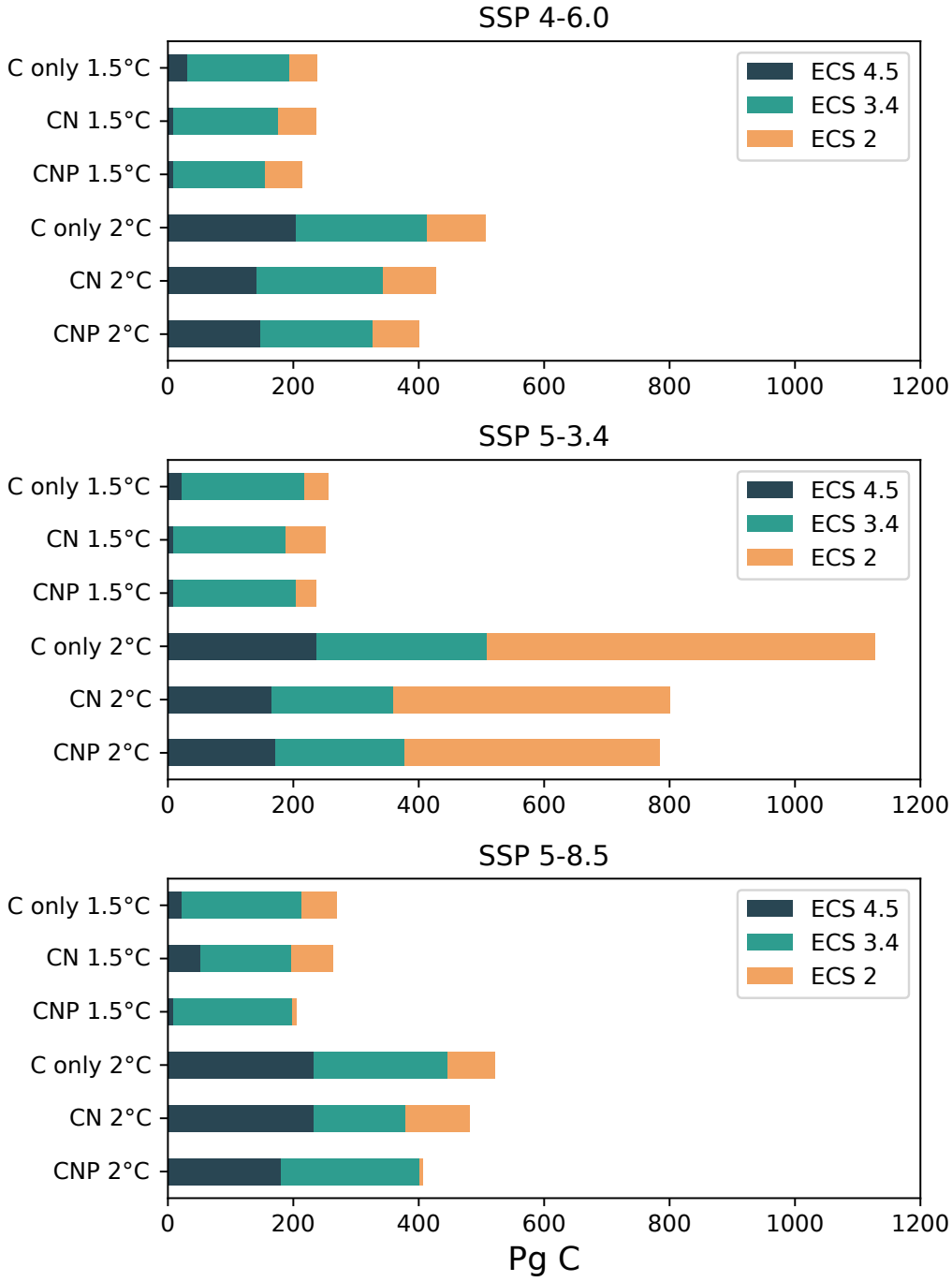

Figure 4.6: Carbon budgets for the 1.5 and 2 °C targets for SSP 4-6.0, 5-3.4 and 5-8.5. Three model sensitivities are shown as: ECS 4.5 dark blue, ECS 3.4 green and ECS 2 orange.

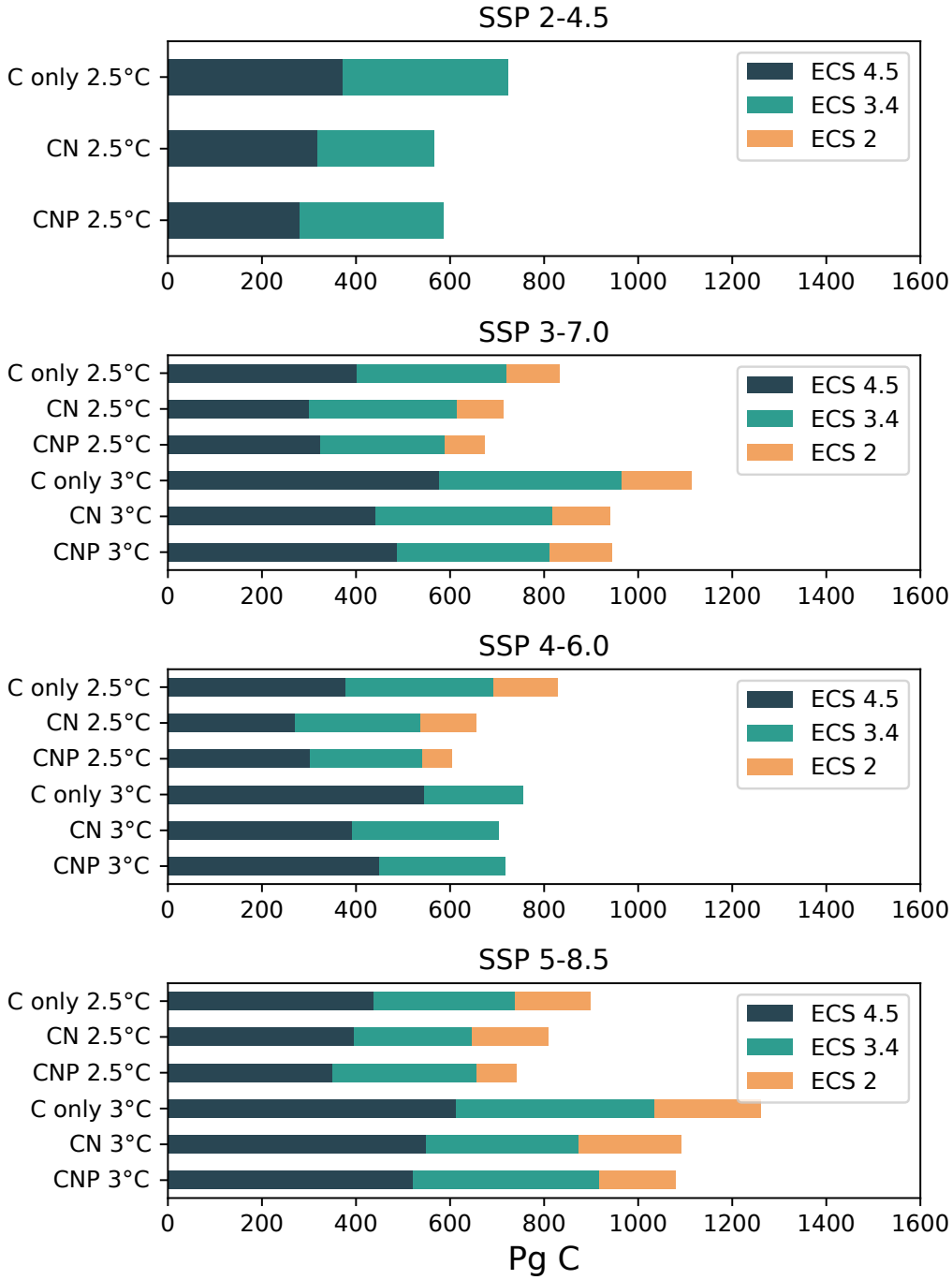

Figure 4.7: Carbon budgets for the 2.5, 3 °C targets for SSP 3-7.0, 4-6.0 and 5-8.5. These were the only scenarios that reached the targets. Three model sensitivities are shown as: ECS 4.5 dark blue, ECS 3.4 green and ECS 2 orange.

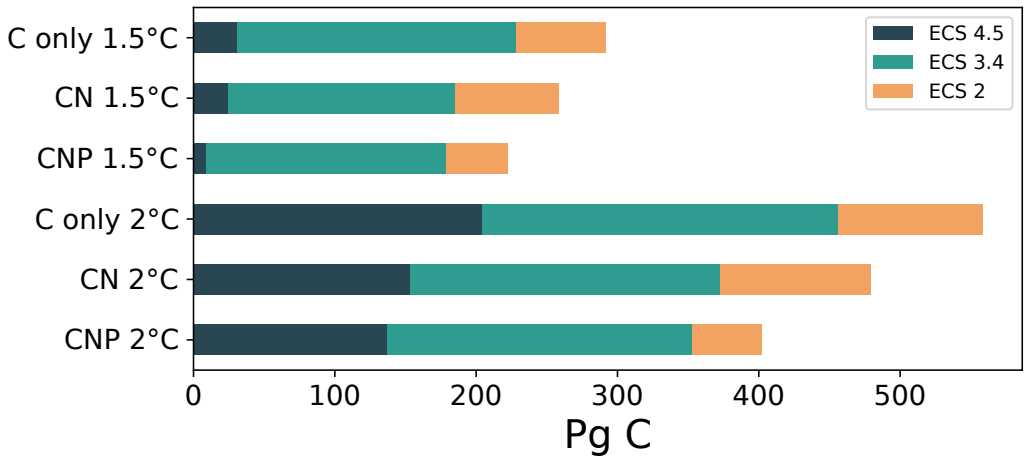

Figure 4.8: Mean SSP carbon budgets for the 1.5 and 2 °C temperature targets.

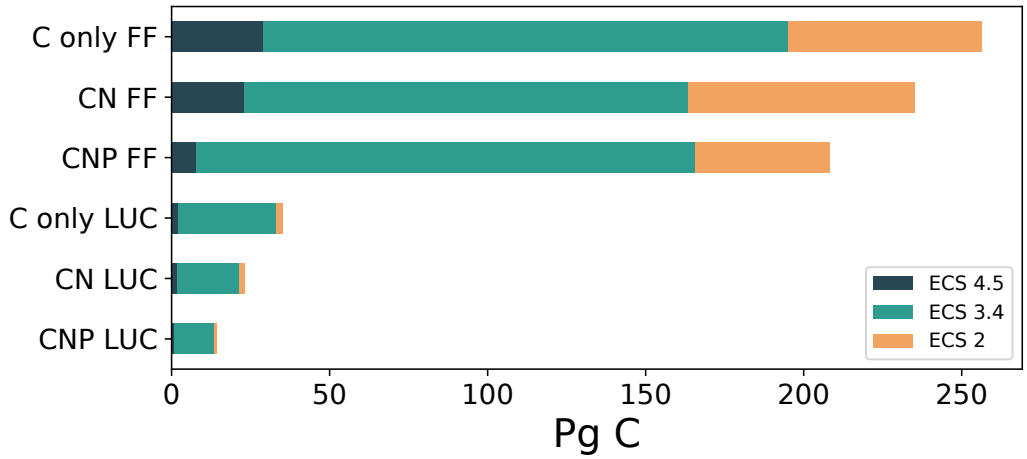

Figure 4.9: Mean SSP carbon budgets for Fossil Fuel (FF) and LUC emissions for the 1.5 °C temperature target.

4.5 Discussion

In nature, N and P limitation or co-limitation has a core regulation on vegetation productivity. Hence, it is expected that the inclusion of both in ESMs improves the presentation of vegetation productivity and biomass representation. Being core regulators of terrestrial vegetation, adding N and P in model structures influences the

carbon dynamics in terrestrial systems. These changes include: 1) vegetation biomass, 2) vegetation distribution, 3) primary productivity, 4) land use change emissions and, 5) terrestrial albedo. In the UVic ESCM version 2.10, the vegetation biomass, distribution and productivity were addressed in (De Sisto et al. , 2023), while land use change emission and albedo remained unexplored. In this study, land use change emission accounts for albedo changes due to plant functional types changes in model simulations. As the model reduces vegetation due to nutrient limitation and trees are replaced by grassed, the land surface albedo is increased. Hence, CNP and CN has a larger albedo value than C-only for land. I have identified that a terrestrial system stressed with nutrient limitation reduces the land use change emissions budget and increases land surface albedo.

The terrestrial carbon cycle in nutrient-limiting model structures is usually suppressed by the capacity of primary producers to uptake carbon, either by controlling the photosynthesis or reducing the biomass directly by setting maximum nutrient ratios boundaries. In this case the terrestrial nitrogen and phosphorus act as a limiting factor for terrestrial vegetation by restricting the photosynthesis (N) and by reducing the biomass given a set ratio value (N and P). N and P control biomass directly by the maximum C:N or C:P leaf ratio threshold. The lower the set ratio is the higher impact will the nutrients have. When the diagnosed C:N or C:P leaf ratios are higher than the set maximum leaf ratio, the vegetation biomass dies so that the leaf ratios decrease back to the maximum ratio threshold. The nutrient limitation is also different for plant functional types and hence, the change in vegetation biomass is dependent on differences among the limitation applied to each PFTs. Therefore, the application of multiple nutrient-limiting stressors such as nitrogen and phosphorus should be applied carefully as a high limitation of phosphorus can easily underestimate the land sink capacity of tropical vegetation.

It is clear then that the representation of the carbon cycle in model structures affects the estimation of the remaining carbon budgets. Permafrost thawing for example has been studied for its carbon budget reduction effect in ESMs (MacDougall and Knutti , 2016; MacDougall et al. , 2021). In this study, the effect of the terrestrial carbon dynamics has a direct impact on the reduction of the remaining carbon budgets. The impact of nitrogen and phosphorus limitation due to the reduction of the land carbon sink should be explicitly considered as a variable that can reduce the remaining carbon budgets for any temperature target. Furthermore, a significant number of socioeconomic uncertainties exist in the remaining carbon budget estimates, including the inability to predict future levels of carbon dioxide emissions based on sociopolitical system dynamics and technological advancements, such as the one represented in the different Shared Socioeconomic Pathways. Hence the carbon budgets are ultimately linked to the rate of emissions and the measures taken to mitigate carbon emissions in the future (Matthews et al. , 2020).

The IPCC AR6 (IPCC , 2021) reports remaining carbon budget estimates from 2020 of 245, 177, 136, 108 and 82 PgC for the 1.5 °C target with a probability of 17, 33, 50, 67 and 83% respectively. Compared to the 50% of probability of 136 PgC, the UVic ESCM nutrient limited model simulations, CN 185 PgC and CNP 175 PgC estimated a closer value than the C-only 228 PgC. C-only tending more to the 17% probability value. Hence, nutrient-limited simulations bring the estimate from the UVic ESCM closer to the multi-model mean.

As shown in this study the representation of carbon processes can affect the estimation of remaining carbon budgets in ESMs. As unrepresented processes in other models nitrogen and phosphorus limitation reduced the estimated remaining carbon budget in CN and CNP by 43 and 53 PgC for the 1.5 °C target and 98 and 120 PgC for the 2 °C

target when compared to the C-only simulation. These estimations are larger than the roughly estimate of 27 PgC reduction of carbon budgets due to unrepresented carbon feedbacks (Rojeli et al. , 2018), suggesting that this value may have been underestimated in the IPCC 1.5°C report.

The TCRE shows that nitrogen and phosphorus limitation had a direct effect on the temperature-to-carbon emission proportionality. The nutrient limitation on biomass and photosynthesis has a direct impact on the temperature-to-carbon emission proportionality. Mainly impacting the carbon fluxes, reducing the land carbon sink and increasing the ocean carbon sink, leading ultimately to a net decrease of the carbon uptake from land and ocean. In emission-driven simulations, this will lead to a high buildup of atmospheric CO_2. Although, it is clear that more understanding of nutrient distribution is necessary to build even more reliable nutrient-limited models. The effort should be directed towards the creation of reliable data including global nutrient distribution, global nutrient inputs and future fertilization projections encompassing agriculture and human waste load into terrestrial, riverine and aquatic systems.

The inclusion of P in ESMs and the benefits of CNP models have been shown to improve the accuracy of the terrestrial carbon cycle (Wang et al. , 2010; Goll et al. , 2017; De Sisto et al. , 2023). However, the necessity of models of including P in their structures is debatable. If the objective is to improve the carbon cycle accuracy the inclusion of P is advisable for its limiting role in tropical regions. From a carbon budget estimations view, I observed similar results for CN and CNP. Overall, the results of this study show that the remaining carbon budgets estimated in CNP simulations were lower than CN. In SSPs were this was not the case, a medium or high land use regulation was implicit in the scenario. Hence, one of the main differences between CN and CNP models is how the model responds to land use

change management in different future projections scenarios. The inclusion of P in ESMs has been shown to improve the terrestrial model performance and hence, I believe that the addition of P limitation should be thought in the development plans of different model working groups.

4.6 Conclusion

The remaining carbon budgets are crucial for climate policy and management. As the remaining carbon budgets are intrinsically linked to the TCRE and the dynamics of the global carbon budget, it is important to consider the uncertainties that nutrient limitation has on model terrestrial model structures. In this study, I found that nutrient limitation, in this case N and P had a considerable effect on the remaining carbon budget estimates. Historically, N and P limitations reduced the land carbon sink and land use change emission. The range of reduction of land carbon sink was: 75 to 106 Pg C and the range of reduction for the land use change emission was: 60 to 93 Pg C. Overall under the Shared Socioeconomic Pathways, N and P reduced the remaining carbon budgets estimates for 1.5, 2, 2.5 and 3 °C targets. CN and CNP showed a reduction of 43 and 53 Pg C for the 1.5 C target and 98 and 120 Pg C for the 2 C target, respectively when compared to C-only. Theses values represent a reduction of 19 and 24 % for the 1.5 °C target, 21 and 26 % for the 2 °C target. After emission has ceased N and P had a relevant impact on the temperature change, the ZEC across 100 years of simulations after emission have ceased showed an increase in temperature for the nutrient-limited simulations CN and CNP of 0.12 and 0.16 °C when compared to C-only. The uncertainty of the magnitude of the reduction in the remaining carbon budget from nutrient limitation will be more clear if a multimodel assessment is conducted. Overall I assess that accounting for nutrient limitations will

lead to a substantial reduction in the estimated remaining carbon budget.

Chapter 5

Projecting atmospheric N_2O rise until the end of the 21st century

Preface.

A version of this chapter has been submitted for publication in Environmental Research Letters. I am the primary author. Along with Co-authors, Andrew MacDougall, Christopher Somes and Angela Landolfi. I developed the model code for the terrestrial N_2O dynamics and coupled the existing ocean N_2O module into the current model structure. I have carried out the simulations and validations of the model outputs. I have prepared the first draft of the manuscript and subsequently revised the manuscript, based on the feedback from Co-authors. As Co-author, Andrew MacDougall assisted in the development of the concept and provided supervisory feedback by reviewing and revising the manuscript. Christopher Somes contributed in the calibration of the model and provided feedbacks to the manuscript. Angela Landolfi developed the ocean N_2O module and contributed by providing feedbacks to the manuscript.

5.1 Abstract

Nitrous Oxide (N_2O) is a potent greenhouse gas with a centennial-scale lifetime that contributes significantly to global warming. It is emitted from natural and anthropogenic sources. In nature, N_2O is released mainly from nitrification and denitrification from the ocean and terrestrial systems. The use of agricultural fertilizers has significantly increased the emission of N_2O in the past century. Here I present, to my knowledge, the first coupled ocean and terrestrial N_2O modules within an Earth System Model. The coupled modules were used to simulate the six Shared Socioeconomic Pathways scenarios with available nitrogen fertilizer inputs. The results of this study are compared to projections of atmospheric N_2O concentrations used for SSPs scenario experiments. Further simulations were prescribed with this available N_2O concentrations. I report three main drivers for terrestrial N_2O uncertainties: atmospheric temperature, agricultural fertilizers input and wetland extent. I project an atmospheric N_2O concentration range from 401 to 418 ppb in six SSPs simulations with a robust lack of sensitivity to equilibrium climate sensitivity. I found a large difference between the results of the low emission scenarios N_2O concentrations by 2100 in this study compared to the concentration provided for SSPs experiments. This gap is likely explained by strong mitigation assumptions that were not accounted for in this study, which would require a substantial decrease of agricultural N_2O emissions, and the lack of atmospheric N_2O dynamics. The coupled model and the simulations prescribed with N_2O concentrations showed a difference between -0.02 and 0.09 °C by 2100. The UVic ESCM simulation shows a lack of sensitivity to climate mitigation efforts projecting similar N_2O concentration in low and high mitigation scenarios. Further improvements in Earth system models should focus on the impact of oxygen decline on N_2O dynamics in the ocean and the representation of anaerobic soils and

agricultural dynamics on land, including mitigation methods on nitrogen fertilizers.

5.2 Introduction

Despite carbon dioxide being the largest contributor to anthropogenic climate warming, other naturally occurring but anthropogenically produced greenhouse gasses, such as methane and nitrous oxide (N_2O), also contribute substantially to warming (Montzka et al. , 2011; Tian et al. , 2016; IPCC , 2022). N_2O is a powerful greenhouse gas with a lengthy lifetime and a strong global warming potential. It is removed from the atmosphere slowly with a lifetime of about 120 years (Prather et al. , 2015), an order of magnitude longer than the lifetime of CH_4 but far shorter than CO_2 (IPCC , 2022). In nature, N_2O is released as an intermediate product during nitrification and denitrification in terrestrial and aquatic ecosystems, both of which are mediated by microorganisms (Fowler et al. , 2013). Total N_2O emissions are enhanced by anthropogenic activities including agriculture, industry (chemical processing), wastewater management and fossil fuel combustion (Tian et al. , 2016; IPCC , 2022).

The release of N_2O during nitrification occurs as a product of the intermediate compound HNO during oxidation of NH_2OH to NO_2. NH_4 is oxidized to NO_2^- via NH_2OH, followed by a the oxidation of NO_2^- to NO_3^- (Caranto and Lancaster , 2017). During denitrification NO_3^- is converted into gaseous nitrogen compounds such as N_2O, NO, and N_2. NO_3^- is reduced to NO_2^-, followed by NO, N_2O, and N_2 (Scheer et al. , 2020). Nitrogen oxides serve as electron acceptor during the process, similar to the electron transport chain involved in aerobic respiration. There are four stages involved in denitrification: reducing nitrates, reducing nitrites, reducing nitric oxides, and reducing nitrous oxides. They are catalyzed by a specific reductase enzyme. An incomplete process results in the emission of NO and N_2O (Chen and Storus , 2012).

The emission of intermediates is caused when electron fluxes are unbalanced over the four subsequent steps of denitrification or when incomplete pathways are expressed or present in denitrifying organisms (Ward , 2012). Multiple promoters regulate gene expression during the induction of the denitrification pathway after oxygen depletion. Despite of the fact that many types of bacteria have similar promoters, the exact mechanism of regulation varies from one species to another. Specific environmental factors such as oxygen and nitrogen oxide concentrations, as well as metal ions, affect gene expression (Carreira et al. , 2018).

A large portion of atmospheric N_2O is photolyzed at ultraviolet wavelengths around 200 nm, in the stratosphere. The photodissociation of N_2O is important for the photochemical balance of ozone and is the major contributor to NO_x species in the stratosphere (Nishida et al. , 2004). The lifetime of N_2O is therefore associated to the photolysis rate of N_2O in the stratopshere. Considering the Brewer-Dobson circulation that describes tropospheric air ascending in tropical stratopshere, where photochemical reaction takes place and later distribution across latitudes with descent in mid-high latitudes, the increase of N_2O abundances are expected to reach higher stratospheric altitudes leading to increase photochemical destruction (Prather et al. , 2023). Consequently, the lifetime of N_2O is expected to decrease with higher N_2O abundances.

In the oceans, N_2O production can occur both in the water column and marine sediments (Landolfi et al. , 2017) and is sensitive to the rate of remineralization of organic matter. The reduction of oxygen and expansion of oxygen minimum zones are expected to increase the oceanic N_2O production (Landolfi et al. , 2017; Yang et al , 2020). Conversely, N_2O is consumed in oxygen depleted waters, which could compensate the aformentioned increased production, albeit likely to a small extent

given the small volume of oxygen deficient waters. Marine N_2O is released into the atmosphere where N_2O rich waters resurface and diffuse to the atmosphere (Yang et al , 2020). Other variables such as irrandiance, temperature, and substrate supply also affect the rate of N_2O production in marine systems (Martinez et al. , 2015; Battliaga and Joos , 2018). The main locations for N_2O production in the ocean has been identified to be low oxygen waters in the eastern upwelling systems (Battliaga and Joos , 2018). On land, denitrification has been identified as the main pathways of nitrogen loss for agricultural soils and natural ecosystems. Combined global marine and terrestrial denitrification estimates range from 220 to 570 Tg N yr^{-1} (Scheer et al. , 2020). In terrestrial systems, denitrification estimates range from 100 to 250 Tg N yr^{-1} most of which occurs in soils and half of it on agricultural land followed by lakes, rivers and groundwater (Groffman , 2012; Scheer et al. , 2020). Denitrification is usually found in the interface of aquatic and soil ecosystems.

Based on NOAA atmospheric measurements, N_2O concentrations reached 336 ppb in 2023 with a tropospheric growth rate of 0.71 ppb yr^{-1} (Lan et al. , 2023). This represents an increase of 24% over preindustrial concentrations (270 ppb). Emissions from agricultural activities are a major source of atmospheric N_2O (Tian et al. , 2020). Agricultural fertilizers are the primary contributor to N_2O emissions in agricultural systems. Fertilizer application increases the release of N_2O by increasing nitrogen concentration in soils leading to an increase of nitrification and denitrification processes. Tian et al. (2020) estimated an increase of 31 ppb of atmospheric N_2O from 1980-2019 due to synthetic fertilizers and manure, nitrogen deposition from agriculture and fossil fuel burning. Various strategies have been proposed to mitigate N_2O emissions from agricultural sources. These include improving fertilizer management practices, developing best management practices for animal manure management, and utilizing cover crops and crop rotations (Hassan et al. , 2022). Additionally, a

number of technologies have been developed to reduce N_2O emissions from agricultural sources, such as nitrification inhibitors, nitrification-denitrification inhibitors, and nitrification-denitrification reactors (Norton et al. , 2019; Saud et al. , 2022). Non-agricultural sources of N_2O include industry (chemical processing), wastewater and fossil fuel combustions. Industrial emission are mainly due to nitric and adipic acid production (Berstein et al. , 2007). Sewage from domestic and industrial sources are estimated to emit from 0.2 to 0.5 TgN yr^{-1} from 1980 and 2016 (Tian et al. , 2020). Terrestrial biomass burning (crop residue, grassland, savannahs, forests) also emit around 0.6 TgN yr^{-1} of N_2O.

In the ocean, climate projections have suggested that N_2O emissions are likely to decline during the current century. Mainly due to warming induced ocean stratification that decreases nutrient supply to the surface ocean, lowering productivity and organic matter export (Steinacher et al. , 2010; Bopp et al. , 2013; Landolfi et al. , 2017). Although, the reduction of nutrient supply might be offset by the increase of metabolic rates in nitrogen fixers. The warming induced changes in nutrient distribution and marine production is an uncertainty that affects the representation of deoxygenation and denitrification, and hence, the oceanic N_2O production and emission.

The total N_2O emissions from 2007 to 2016 were estimated to be 17.0 (12.2 to 23.5) TgN yr^{-1} (Tian et al. , 2020). These estimations are a result of a combination of multiple approaches and not a single model that combines both terrestrial and oceanic, natural and anthropogenic N_2O sources. The terrestrial sources contribute to a total of 11.3 (10.2 to 13.2) TgN yr^{-1} and the ocean 5.7 (3.4 to 7.2) TgN yr^{-1}. Anthropogenic emission of N_2O are estimated to be around 40% of the total. From a modelling perspective, oceanic and terrestrial N_2O emission have been represented separately in Earth system models previously (Manizza et al. , 2012; Suntharalingam

et al. , 2012; Davidson and Kanter , 2014; Martinez-Rey et al. , 2015; Landolfi et al. , 2017; Buitenhuis et al. , 2018; Tian et al. , 2020). The model estimates are usually constrained by the effectiveness of the model to represent denitrification and nitrification processes. The challenges include the definition of the dynamics of inland waters, estuaries, oxygen in soil and column of water. The multimodel ocean and land (no agriculture) estimate N_2O emission to be 3.4 (2.5 to 4.3) and 6.7 (5.3 to 8.1) TgN yr^{-1} (IPCC , 2022).

The total anthropogenic radiative forcing of greenhouse gasses between 1960-2019 was 63% for CO_2, 11% for CH_4, 6% for N_2O, and 17% for the halogenated species (Canadel et al. , 2021). The future N_2O in highly uncertain given that is highly dependent on anthropogenic sources (e.g. agriculture fertilization). Martinez-Rey et al. (2015) projected oceanic N_2O emissions from 2005 to 2100 and found a decrease from 4.03 to 3.54 TgN yr^1 similar to (Landolfi et al. , 2017) and (Battliaga and Joos , 2018). A larger decline is projected in Landolfi et al. (2017), which also considers the atmospheric N_2O increase relative to a fixed preindustrial value. Davidson and Kanter (2014) found an almost 50% increase of total global N_2O emissions in high emission scenarios, while only 22% increase in low emission scenarios when compared to 2005. In this novel study, I couple terrestrial and oceanic N_2O emissions modules of an Earth system model and assess long term impacts and forcing of atmospheric N_2O concentrations on different future emission scenarios.

5.3 Methodology

5.3.1 Model description

The University of Victoria Earth system climate model (UVic ESCM version 2.10), is a global intermediate complexity climate model (Weaver et al. (2001); Mengis et al. (2020)). It has a three dimensional ocean general circulation represented by the Modular Ocean Model version 2 (MOM2), coupled to a simple atmosphere represented by a simplified moisture-energy balance structure (Fanning and Weaver , 1996). The ocean is coupled to a thermodynamic-dynamic sea-ice model (Bitz et al. , 2001).

The ocean module contains ocean biogeochemistry (Keller et al. , 2012; Somes and Oschlies , 2015; Landolfi et al. , 2017). The ocean biogeochemistry module includes two phytoplankton classes, N_2-fixing diazotrophs and other phytoplankton, zooplankton, particulate detritus, nitrate, phosphate, dissolved oxygen, dissolved organic nitrogen, dissolved organic phosphorus, dissolved inorganic carbon, and N_2O. The prognostic global nitrogen budget includes atmospheric N deposition, N_2 fixation, water column denitrification, and benthic denitrification (Somes and Oschlies , 2015; Somes et al. , 2016). The oceanic subsurface N_2O production is a function of O_2 consumption with a linear O_2 dependency, including both nitrification and denitrification (Zamora et al. , 2012; Zamora and Oschlies , 2014; Landolfi et al. , 2017). In O_2-deficient waters (<4 mmol m^3), denitrification becomes a sink of N_2O in the UVic ESCM, that is consumed at a constant rate. The gradient driving the air-sea N_2O gas exchange, computed based on the departure of the surface ocean concentration from the saturation value using the solubility coefficients of Weiss and Price (1980) and varying prescribed atmospheric N_2O concentrations. A detailed description of the N_2O module can be found in Landolfi et al. (2017).

The terrestrial module represents vegetation dynamics via TRIFFID (top-down representation of interactive foliage and flora including dynamics). Plants are classified into five functional types that interact with each other. Broadleaf trees, needleleaf trees, shrubs, C3 grasses, and C4 grasses compete for space within the grid following Lotka-Volterra equations (Cox , 2001). As a result of photosynthesis, carbon is captured and allocated to growth and respiration, whereas vegetation provides carbon to the soil in the form of litter fall. The soil is divided in 14 subsurface layers that grow exponentially in thickness with depth. Hydrological procesess occurs in the first eight soil layers (top 10 m), while the layers below have granitic characteristics. The carbon cycle is active until a depth of 3.35 m (Avis , 2012; MacDougall et al. , 2012). The model contains crops and grazing lands that were adapted by aggregating croplands and grazing lands into a single "crop" type. The crops are represented as a fraction of each grid cell and are assigned to C3 and C4 grasses (Mengis et al. , 2020).

The model has recently been upgraded to include a terrestrial nitrogen and phosphorus cycle. In this variant called UVic ESCM-CNP. The terrestrial nitrogen cycle module represents the flow of nitrogen among three organic pools (litter, soil organic matter, and vegetation) and two inorganic pools (NH_4^+ and NO_3^-). Inorganic nitrogen inputs consists of Biological Nitrogen Fixation (BNF), atmopsheric deposition and agricultural fertilization. NH_4 can be absorbed by plants, leached, or transformed into $NO3^-$ via nitrification. NO_3^- is produced through nitrification, can be taken up by plants, leached or denitrified into NO, N_2O or N_2. Inorganic N is taken up by plants and allocated among leaf, root, and wood. Wood has a fixed stoichiometric ratio, while leaf and root pools have variable ratio. Organic nitrogen from vegetation compartments is transported to soil via litterfall. This pool is either mineralized or transferred to the organic soil pool. A portion of the organic N can be then mineralized into the inorganic N pools. Conversely, immobilization moves N from the

inorganic to the soil organic pool.

In the UVic ESCM-CNP (De Sisto et al. , 2023), the wetland module determines anoxic fractions for each soil layer, based on the wetland scheme of Gedney and Cox (2003). Nzotungicimpaye et al. (2021) implemented the determination of inundated soils and saturated layer fraction in the UVic ESCM. In here the hydrology is combined with a prescribed topographic index to determine the presence of wetlands at the sub-grid scale. The model assumes a wetland in an area with a topographic index (λ) that satisfies:

$$\lambda_{min} \leq \lambda \leq \lambda_{max}, \tag{5.1}$$

where λ_{min} is a lower threshold representing under-saturation and λ_{max} represents is an upper threshold or over-saturation.

The anoxic fraction, is taken to be the saturated fraction of the soil layer that is shielded from O_2. Denitrification is only allowed to be estimated in soils with anoxic fractions and is calculated as in equation 5.2:

$$R_{an} = K_{rNO_3} f_t f_m C_s A_f \ \frac{[NO_3(av)]}{[NO_3(av)] + K_n}, \tag{5.2}$$

where R_{an} is the anaerobic respiration, K_{rNO3} is the ideal respiration rate via NO_3 reduction, f_t and f_m are temperature and moisture functions, C_s is the concentration of organic carbon, Af is the anaerobic fraction of the soil layer, K_n is the half-saturation of N-oxides (Li et al. , 2000).

As N_2O and NO are intermediate products of denitrification and nitrification the

complex modelling representation is handled as a 'leaky-pipe' conceptualization of soil-nitrogen processes as in Firestone and Davidson (1989). In this conceptual model N_2O and NO leak out of reactions of one species of nitrogen into another, during nitrification (NH_4 to NO_3) and denitrification (NO_3 to N_2). The size of the holes is determined by the soil processes. In the UVic ESCM version 2.10 the size of the holes controlling the amount of gas that can be leaked is fixed. Using Davidson et al. (2000) equation the partitioning ratio between NO and N_2O changes based on water filled pore space of the soil layer. The ratio is estimated as in equation 5.3:

$$\frac{N_2O}{NO} = 10^{2.6S_U - 1.66}, \tag{5.3}$$

where S_U is the waterfilled pore space. Thus, the model produces a total flux of both NO and N_2O for nitrification and denitrification, which is partitioned between the two species based on the above relationship. The NO flux is added to the atmosphere and redeposited as part of the nitrogen deposition flux. The N_2O has a constant lifetime of 100 years. Decayed N_2O is assumed to become part of the atmospheric N_2 pool. The implementation of terrestrial N_2O in the UVic ESCM version 2.10 was shown in (De Sisto et al., 2023).

Experimental design and forcing data

The CNP version of the UVic ESCM version 2.10 (Mengis et al. , 2020; De Sisto et al. , 2023) was coupled to the ocean N_2O module developed by Landolfi et al. (2017). The new coupled terrestrial and ocean N_2O modules were used to run all the simulations in this study. The model was spun up for 6000 years with boundary conditions as outlined in the CMIP6 protocol (Eyring et al. , 2016) and fixed atmospheric N_2O concentration of 270 ppb. Historical N_2O emissions were tuned to match historical

observations by adjusting the denitrification N_2O 'leakage' hole size from NO_3 to N_2. Historical temperatures were calibrated using aerosol scaling to match historical observations. Three-dimensional aerosol optical depth can be scaled by a fraction in the UVic ESCM and was used in version 2.10 to calibrate aerosol forcing to fit current values (Mengis et al. , 2020).

Given that N_2O is closely linked to anthropogenic inputs and socioeconomically factors, the simulations of this study project emission using Shared Socioeconomic Pathways (SSPs) to represent different future scenarios (Gidden et al. , 2019). Six SSPs scenarios were run, I included the following: SSP1-1.9, SSP2-4.6, SSP2-4.5, SSP3-7.0, SSP5-3.4-OS and SSP5-8.5 ext. SSP4-3.4 and SSP4-6.0 were excluded from the study due to lack of nitrogen fertilizers inputs for these scenarios. These scenarios are the same used in the Coupled Model Intercomparison Project phase 6 (CMIP6) (Eyring et al. , 2016). Artificial and manure fertilizers data were used in the model simulations. The historical and SPPs fertilizer data were obtained from the publicly available CMIP6 data (Tachirii et al. , 2019). The datasets represent N fertilization from 1850-2100.

I have compared the atmospheric N_2O concentration simulated in this study with the projected by Meinhaussen et al. (2020). In their study Meinhaussen et al. (2020) provided atmospheric N_2O concentrations for long-term climate analysis using the reduced-complexity climate–carbon-cycle model MAGICC 7. Meinhaussen et al. (2020) used Prather et al. (2012) model to set N_2O assumptions and lifetimes to calibrate MAGICC 7. To assess the response of the temperature to N_2O concentrations between the UVic ESCM structure and Meinhaussen et al. (2020) results, I have prescribed N_2O concentrations using Meinhaussen et al. (2020) projected atmospheric

N_2O into the UVic ESCM N_2O module and compared the resulting temperature response to the UVic ESCM- CNP with N_2O dynamics. As temperature response varies depending on model climate sensitivity I have set three different model variants tuned to have Equilibrium Climate Sensitivities (ECSs) per doubling of CO_2 of 2.0°C, 4.5°C to represent the 'likely bounds' (IPCC , 2021), as well as using the emergent climate sensitivity of the model (3.4°C) as the central estimate. The climate sensitivity was tuned using an equilibrium climate sensitivity parameter designed by Zickfeld et al. (2009) to alter climate sensitivity in the UVic ESCM by altering the flow of longwave radiation back to space. Furthermore, the model sensitivity variants serve to assess the impact of climate sensitivity on the UVic ESCM N_2O emissions and hence, atmospheric N_2O concentrations.

5.4 Results & Discussion

5.4.1 Historical and projected N_2O atmospheric concentrations and emissions

The coupled terrestrial and ocean N_2O dynamics from De Sisto et al. (2023) and Landolfi et al. (2017) were tuned to match historical atmospheric N_2O concentrations. Figure 1 shows the N_2O concentration simulated with the UVic ESCM compared to Machida et al. (2015), Lan et al. (2023) and Prinn et al. (2023). The model outputs follow observations closely. The preindustrial atmospheric N_2O concentration captures the ice cores observations from Machida et al. (2015) with high fidelity. After 1945 I observed a gap between the Uvic ESCM increase of N_2O concentrations and atmospheric measurements. This gap is likely a consequence of a simplified representation of agriculture, where in both natural and agricultural fractions of grid cells

feed into the same subsurface soil column in the UVic ESCM. Despite this limitation the model fairly represents the historical trends and magnitudes. For the year 2023 I estimate a N_2O concentration of 335 ppb, close to the NOAA (Lan et al. , 2023) measurement of 336 ppb locating the UVic ESCM results close to historical atmospheric N_2O concentrations. From 2000-2005 I simulated an atmospheric N_2O growth rate between 0.86 to 0.89 ppb yr^{-1} similar to the value of 0.73 reported by NOAA (Hall et al. , 2007). However, the UVic ESCM lacks the annual variability of atmospheric growth rate shown in Tian et al. (2020). This lack of variability can be attributed to the lack of internal variability in the UVic ESCM and a constant N_2O decay prescribed in the UVic ESCM rather than a dynamic change as shown in Prather et al. (2023). Prather et al. (2023) simulated a reduction of N_2O lifetime over the period of 2005-2100 that indicates that the accumulation of N_2O could be slowed down as N_2O is reduced more rapidly photochemically from the atmosphere. The lack of decay dynamics in the UVic ESCM can lead to overestimation in the UVic ESCM simulations results by the end of the 21st century.

Oceanic N_2O emissions

Both terrestrial and oceanic N_2O modules simulate fluxes within the range of uncertainty of other studies. The ocean N_2O is similar to Landolfi et al. (2017) oceanic N_2O emissions. The UVic ESCM simulations represents a decline in ocean N_2O emissions from 3.6 to 3.0 Tg N yr^{-1} from 1850 to 2020 and to 2.7 [2.6 to 2.8] Tg N yr^{-1} by 2100. The historical results are consistent with the IPCC range of 1.8 to 9.45 Tg N yr^{-1} and other studies such as Martinez-Rey et al. (2015) estimating a range of 3.71 to 4.03 Tg N yr^{-1} (2005), Landolfi et al. (2017) with a value of around 3.2 Tg N yr^{-1} and Yang et al (2020) with a value of 4.2 1.0 TgN yr^{-1}. For the end of the 21st century, I simulate a reduction of 0.9 TgN yr^{-1} [0.8 to 1 TgN yr^{-1}] . This

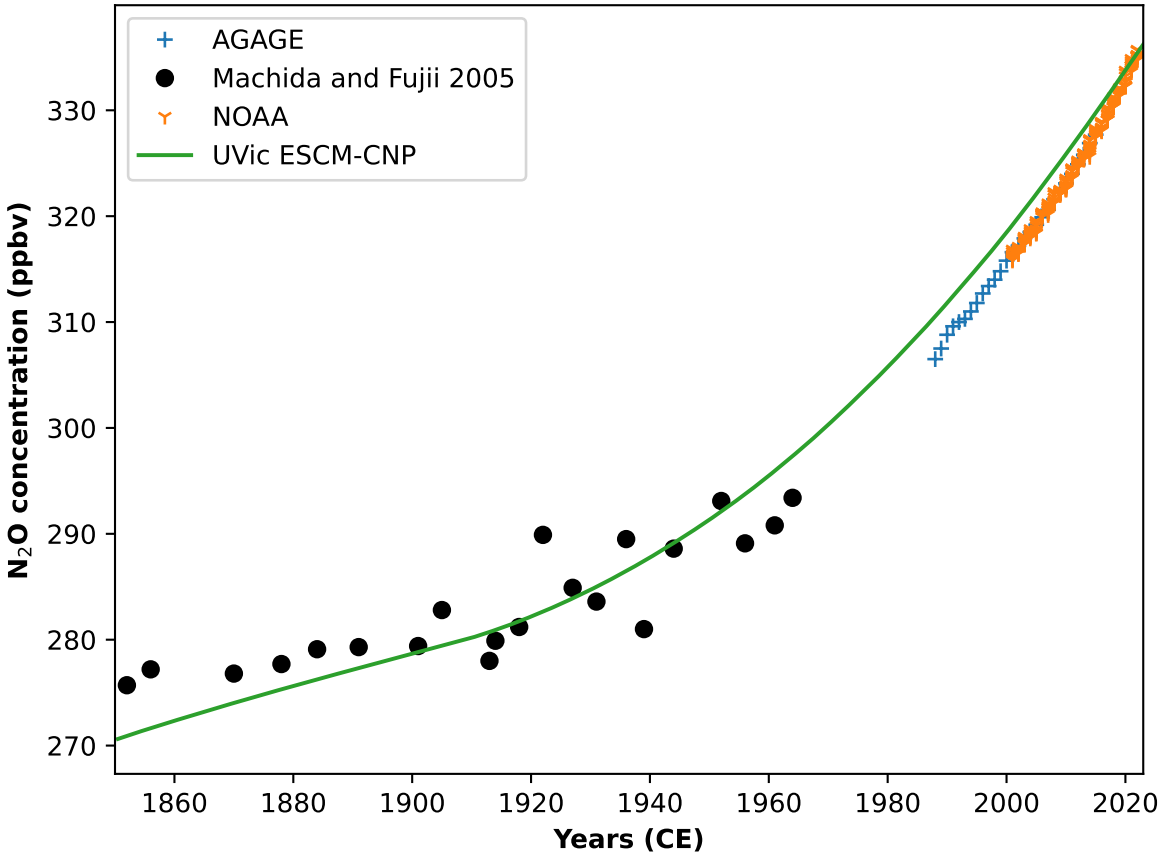

Figure 5.1: Historical atmospheric N_2O concentrations, estimated using a terrestrial and ocean N_2O modules in the UVic ESCM version 2.10. Machida et al. 2015 measured the concentration of N_2O from Antarctic ice cores, the N_2O measurement covers 1735 to 1965. AGAGE (Prinn et al. , 2023) and NOAA (Lan et al. , 2023) show monthly atmospheric N_2O measurements.

decline is also shown by Landolfi et al. (2017) where by 2100 ocean N_2O emissions decline by around 1.1 TgN yr $^{-1}$ for most simulations from 1850 to 2100 mainly due to reduced temperature-dependent surface solubility and transport to greater depths. Furthermore, Martinez-Rey et al. (2015) reports a decline between 0.15 to 0.49 TgN yr $^{-1}$ from 2005 to 2100. These values are comparable to the UVic ESCM value of 0.3 TgN yr $^{-1}$[0.2 to 0.4 TgN yr $^{-1}$] decline simulated from 2020 to 2100.

As in Landolfi et al. (2017), the warming-induced mean reduction of the mixed

layer depth of -5% [-9% to 1%] from 1850 to 2100, increases the nutrient limitation by declining the supply of nutrients to primary producers in tropical latitudes. The reduced supply increases nitrogen and phosphorus limitation to phytoplankton and hence, reduces ocean productivity. On the other hand, the ocean oxygen concentration declines overall from 197 to 188 mmol m^{-3} [186 to 190] between 1850 to 2100. Consequently, this leads to an increase in the size of oxygen deficient zones where water column denitrification and N_2O consumption occur. This increase is overcompensated by the decline in export production and consequently, the decline of N_2O production in water with high oxygen concentrations via nitrification. However, in the high emissions scenario with highest levels of oxygen decline, marine N_2O production reaches an inflection point where marine N_2O emissions begin increasing before the year 2100. This indicates that severe ocean oxygen decline can eventually drive increased ocean N_2O emissions on long time scales. The reduction of fluxes reduces the growth rate of N_2O concentration in the atmosphere, but it is rapidly overcome by the terrestrial increase of N_2O due to fertilizer inputs.

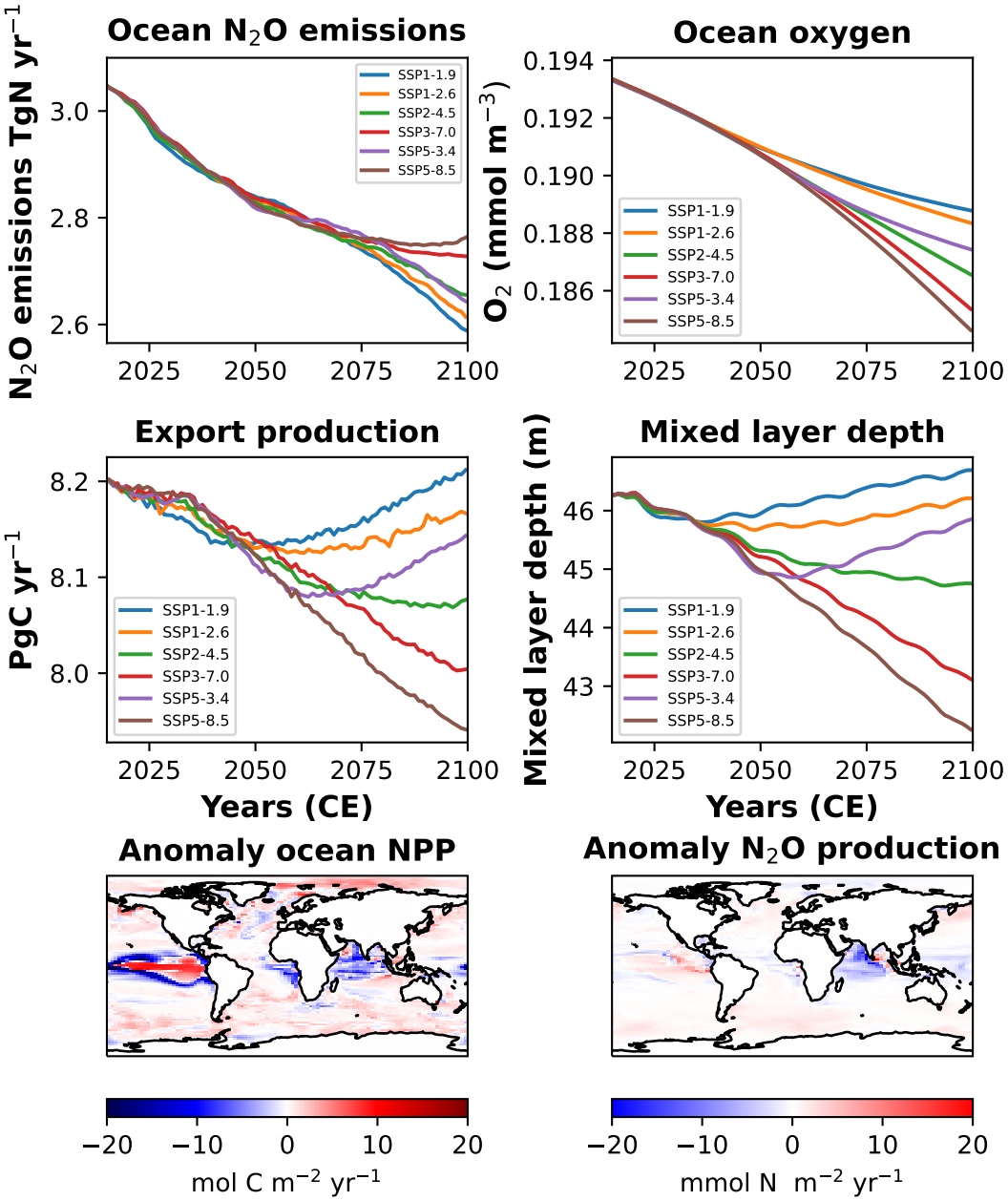

Figure 5.2: Ocean N_2O relevant variables: ocean N_2O emissions, oxygen concentration, NPP and mixed layer depth for each SSPs simulations. The final two maps show the mean ocean NPP and ocean N_2O production from 2090 to 2100 relative to 1850-1860 in SSPs simulations.

Terrestrial N_2O emissions

The terrestrial N_2O emissions in 2020 was estimated to be 11 TgN yr yr^{-1}. This value is within the range of 8-12 TgN yr^{-1} reported in Tian et al. (2020) and Crippa et al. (2021). In preindustrial years, the UVic ESCM fluxes underestimate the value of around 6 TgN yr^{-1} reported in Tian et al. (2020) by 2 TgN yr^{-1}. However, as shown in figure 1, this magnitude of emissions seems to represent the preindustrial atmospheric N_2O concentrations along with the marine N_2O emissions with high fidelity. After 1945 the increasing nitrogen fertilizers led to the rise of N_2O emissions and are a key factor for the rise of N_2O concentrations in the atmosphere. The UVic ESCM model shows a good fit with concentration measurements, as shown in Figure 1. With decreasing ocean emission rates, the terrestrial system is primarily responsible for the future rise of N_2O concentrations. I found a historical rise of 6 TgN yr^{-1} between 1850 and 2020. The total oceanic and terrestrial N_2O emissions for the year 2020 was simulated to be 13 TgN yr^{-1}. This value falls within the range of uncertainty presented by the IPCC AR6 report and Tian et al. (2020).

The UVic ESCM model estimates different terrestrial N_2O emissions for six SSP simulations. There are three main reasons behind this difference: 1) the change of temperature that determines the rate of biological processes, 2) the rate of N fertilizers input, projected differently based on each scenario narrative, and 3) the reduction of wetland areas that determines the anaerobic fractions in the UVic ESCM. Among these, the wetland area reduction is by far the most important (Figure 3). For the year 2050 the UVic ESCM simulates a mean terrestrial N_2O emission of 13 TgN yr^{-1} [12 to 14 TgN yr^{-1}]. By 2100 I simulated a mean terrestrial N_2O emission of 14 TgN yr^{-1} [12 to 16 TgN yr^{-1}]. The differences between terrestrial N_2O emissions among SSPs simulations coincide with the rate of increase or decrease of wetlands

areas and consequently the anaerobic fractions in soils estimated by the model. In the UVic ESCM-CNP the anaerobic fraction is estimated from grid inundations given by a wetland scheme. These terrestrial aquatic interfaces simulated by the model peak from around 2030 in low-emission scenarios and continue to increase in high-emission scenarios. This feedback gives a clear hint of a possible reduction of N_2O increase in natural systems in the future due to the reductions of terrestrial-aquatic interphases. As the UVic ESCM does not have a dedicated agricultural subsurface module, the reduction of N_2O emission is likely overestimated as agricultural irrigation is not accounted for in this simulation and hence, the anaerobic fractions estimated here are uncertain. However, it is possible that the anaerobic respiration in natural systems will reduce the rate of increase of N_2O emissions as aquatic systems dry.

Our simulations show that in Earth system models the simulation of N_2O emissions in terrestrial systems is sensitive to the representation of anaerobic respiration processes, as the utilization of increasing nitrogen concentrations in soil due to agricultural input can only be utilized by microbes when the right abiotic conditions are met. With the reduction of atmospheric N_2O lifetime and the limitation from anaerobic respiration, the accelerated increase rate of N_2O concentrations can be expected to slow. Nonetheless, if agricultural factors not included in this model simulations maintain the increase of anaerobic conditions, the nitrogen utilization by microbes will maintain the rise of N_2O in the future. Conversely, the assumption of targeted N_2O management schemes over the SSPs scenarios could imply a reduction of N_2O emission that is not represented in this model.

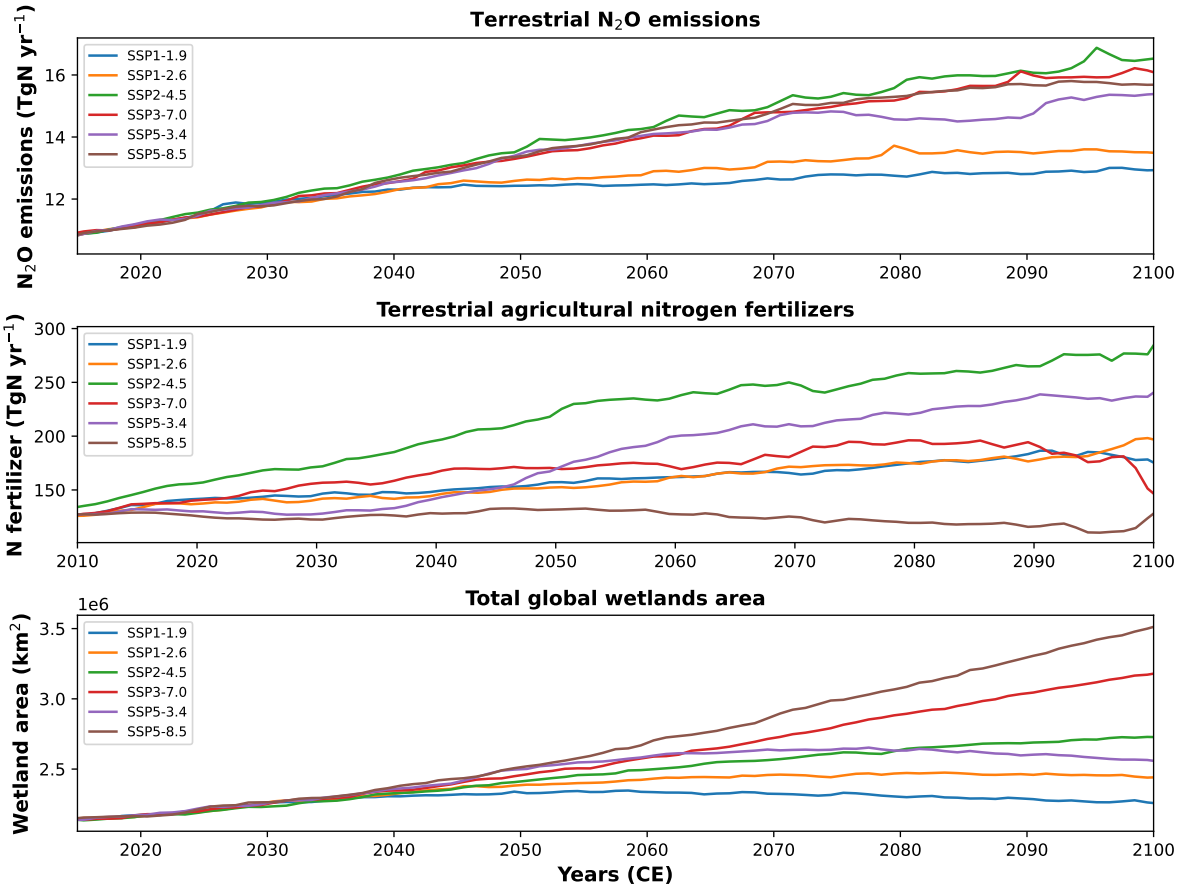

Figure 5.3: Terrestrial N_2O emissions, N_2 emissions and wetland area for each SSPs simulations from 2010 to 2100.

Predicted N_2O concentration for 2100

Terrestrial N_2O emissions are the most important source of N_2O to atmospheric concentrations. Given that atmospheric temperature, N fertilizers, and anaerobic fractions vary among SSP narratives the UVic ESCM simulated different atmospheric N_2O concentrations by the 21st century (Figure 4). This array of results is more similar among each other than that projected by Meinhaussen et al. (2020), where in year 2100 SSP1-1.9 N_2O concentration is projected to have a value of 351 ppb and SSP3-7.0 N_2O concentration of 421 ppb, representing the lowest and the highest concentrations. For 2100 the UVic ESCM projects SSP1-1.9 N_2O concentration of 401 ppb and SSP2-4.5 N_2O concentration of 418 ppb representing the lowest and the highest concentrations. These results show that the difference between the low to the high range of atmospheric N_2O concentration is 67 ppb in Meinhaussen et al. (2020) and 17 ppb for the UVic ESCM-CNP simulations. Furthermore, our lowest estimate for future N_2O concentration by 2100 is higher than the value projected by Meinhaussen et al. (2020). This lowest estimate corresponds to low-emission SSPs scenarios.

Atmospheric N_2O concentration from different equilibrium climate sensitivities variants of the models (ECS 2, 3.4 and 4.5 °C) did not show a large difference between lower a high climate sensitivities as shown in Figure 5. The mean difference between the lower has higher sensitivity among SSP simulations was 2.5 ppbv [1.5 to 2.9 ppbv]. These small changes demonstrate a robust lack of sensitivity of N_2O projections to different climate sensitivities.

These results and differences reflect important dynamics in N_2O systems and uncertainties of Earth system models when simulating N_2O emissions. The first observable

dynamic is that N_2O concentration will keep rising until it peaks beyond the 21st-century timeline, even in low emission scenarios where terrestrial N_2O emission peaks around the year 2030. The second dynamic is that in the UVic ESCM, wetland areas slow the accumulation of atmospheric N_2O concentrations by constraining the terrestrial N_2O emitted. The wetland constraint is due to how anaerobic soils are determined in the model structure. This means that the representation of anaerobic soil dynamics in Earth system model is of utmost importance for accurately estimating N_2O concentration in future simulations. Furthermore, the difference in the lower range of Meinhaussen et al. (2020) and our results may indicate that low emission scenarios in Meinhaussen et al. (2020) have idealistic assumptions for atmospheric N_2O concentration projection that would require a substantial decrease of terrestrial N_2O emissions in the UVic ESCM. The equation determining N_2O emission input used in Meinhaussen et al. (2020) is determined by the emissions of the specific pollutant per country, the absence of any emission control measures, the reduction efficiency and the actual implementation rate of the considered abatement. Hence, the variables that determine the N_2O emission in Meinhaussen et al. (2020) account for mitigation efforts per SSPs. Furthermore, Meinhaussen et al. (2020) account for dynamic changes of N_2O lifetimes. Both N_2O mitigations and dynamic lifetime are not accounted for in the UVic ESCMling structure. Consequently, the reduction of atmospheric N_2O concentration would likely come from intensive management practices to reduce agricultural N_2O emissions and a slower increase of atmospheric N_2O concentration due to the projected decrease of N_2O lifetime.

The difference between our simulated atmospheric N_2O with a dynamic N_2O structure and simulations with Meinhaussen et al. (2020) N_2O concentrations forcing resulted in contrasting global temperatures among the SSPs scenarios (Figure 6). I report a range of -0.02 to 0.09 °C difference between the dynamic atmospheric N_2O simulated

and the prescribed simulations with Meinhaussen et al. (2020) data. In scenarios where our atmospheric N_2O concentrations were close to Meinhaussen et al. (2020) concentrations, the temperature difference was the lowest. Conversely, where large gaps of N_2O concentrations were observed, the temperature difference was larger as a result. For negative temperature differences, the UVic ESCM simulates lower atmospheric N_2O concentrations than Meinhaussen et al. (2020) while the opposite corresponds to positive temperature differences. Our simulations for low emission SSP scenarios have higher atmospheric N_2O concentration than Meinhaussen et al. (2020), while our high emission scenarios simulations tend to have lower N_2O concentrations than Meinhaussen et al. (2020). The temperature difference between the N_2O dynamic and prescribed simulations impacted the years where the 1.5 and 2 °C targets are reached. The temperature targets were established as threshold goals, where global efforts were agreed to be carried to maintain the global temperature increase under a limit by the end of the 21st century (IPCC , 2018). As forcing are different within the SSPs scenarios, some may reach the 1.5 °C target but not the 2 °C target, while others may reach both targets and beyond. The dynamic structure decreased the time for our simulations to reach 1.5 and 2 °C among the SSP scenarios by one to two years.

One of the most remarkable results of this study is that N_2O is shown to be relatively insensitive to mitigation efforts among the SSP simulations. Compared to CO_2 and methane, which are projected to decrease with mitigation efforts, N_2O projections seem to increase at a similar rate regardless of the scenario. Our simulations show a lack of sensitivity to mitigation in SSPs scenarios. I have identified the lack of agricultural N_2O mitigation and a constant lifetime as responsible for this lack of sensitivity in the UVic ESCM simulations. Currently, I are unable to quantify the individual impact of each. However, a takeaway message from our simulations is

that mitigation efforts directed at carbon emissions, which ideally have a significant effect on atmospheric temperature, have only a slight effect on the projected N_2O emissions. The little effect is reflected in the gap between Meinhaussen et al. (2020) and our low emission scenarios. Under idealistic scenarios, the mitigation of N_2O should be targeted directly with proper management schemes. Future coupled N_2O models should in theory take into account N_2O management practices to avoid this lack of sensitivity. However, global estimates of mitigation efficiency and deployment feasibility needs to be assessed before such mitigation could be part of N_2O dynamic models.

5.4.2 Model uncertainties

There are many model uncertainties around the estimation of N_2O emission and the atmospheric chemistry of N_2O. In the ocean, N_2O production representation is sensitive to estimations of productivity, oxygen concentration and oxygen minimum zones. Consequently, the marine biogeochemical uncertainties over these variables are crucial for a more accurate estimation of marine N_2O emissions. On land, the representation of anaerobic dynamics limits the capacity of the utilization of nitrogen agricultural fertilizers. Thereby, the anaerobic fractions limit the increase of terrestrial N_2O emissions and can impact the accuracy of projections. In the UVic ESCM, the lack of agricultural dynamics lead to low sensitivity to N fertilizers. Furthermore, the lack of N_2O mitigation is a source of uncertainty in future N_2O projections as our simulations show low sensitivity to the mitigation efforts represented in the SSPs scenarios. Among the possible N_2O mitigation efforts that could be included are slow-release fertilizers, nitrification inhibitors, appropriate crop rotations and schemes, tillage and irrigation practices and the use of biochar and lime. The plausibility of the global application of terrestrial N_2O mitigation strategies needs to be addressed in future

studies to assess the effectiveness and, consequently, reassess if these mitigation efforts can be realistically deployed and added to the SSP mitigation efforts for N_2O projections. Finally, the UVic ESCM lacks dynamic N_2O atmospheric chemistry dynamics. Hence, N_2O lifetimes remain to be constant in the UVic ESCM simulation, underestimating the sensitivity of atmospheric N_2O accumulation to changes if N_2O lifetimes.

5.5 Conclusions

To my knowledge, this study is the first to successfully couple an ocean and terrestrial N_2O modules and the resulting model to project atmospheric N_2O concentrations to the end of the 21st century. In the ocean, I project a decline of N_2O emissions from 3.7 to around 2.6 TgN yr^{-1} by 2100. On land, I simulated N_2O emission from 4 TgN yr^{-1} in preindustrial times to between 12 to 16 TgN yr^{-1} depending on SSP scenario in the year 2100. In the atmosphere, I project an atmospheric N_2O concentration between 401 and 418 ppb in six SSPs scenarios. I report at least 49 ppb more atmospheric N_2O concentrations than Meinhaussen et al. (2020) by 2100 corresponding to low-emission scenarios projections. The UVic ESCM simulations showed a robust lack of sensitivity to equilibrium climate sensitivity. Finally, I found that the estimation of wetland areas and resultant anoxic soils is the most important factor controlling N_2O emissions in the future. Therefore improving representations of wetlands be prioritized to improve the accuracy of terrestrial N_2O emissions and atmospheric N_2O concentration representation in simulations. Overall I assess that N_2O will remain an important greenhouse gas for the remainder of the 21st century, with a potential for larger impacts further into the future.

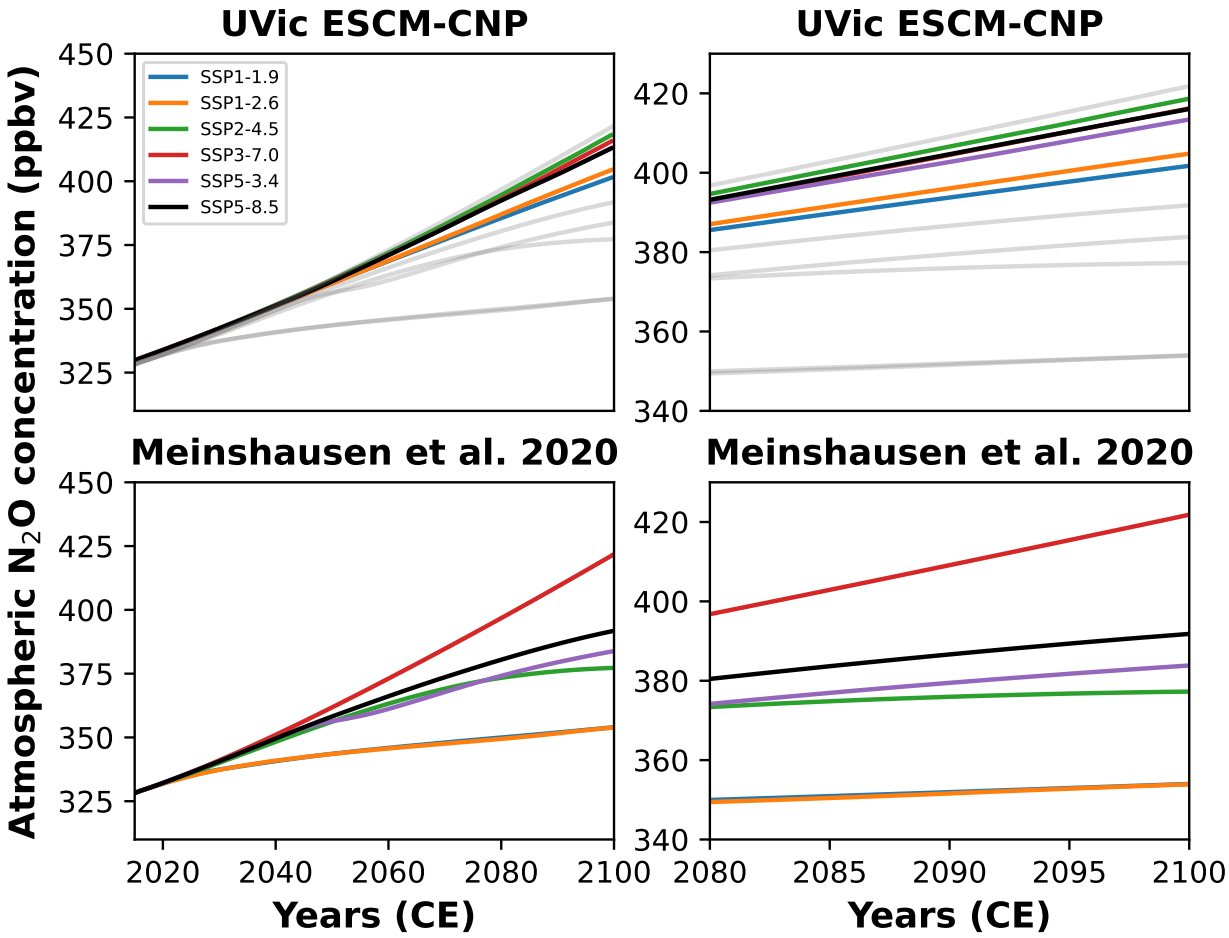

Figure 5.4: Top left: atmospheric N_2O projection from year 2015 until 2100 for each SSP simulation in the UVic ESCM-CNP. Top right: atmospheric N_2O projection from year 2080 until 2100 for each SSP simulation in the UVic ESCM-CNP. The background grey lines in the top panels represent Meinhaussen et al. (2020) projections. Bottom left: atmospheric N_2O projection from year 2015 until 2100 projected by Meinhaussen et al. (2020). Bottom right: atmospheric N_2O projection from year 2080 until 2100 projected by Meinhaussen et al. (2020).

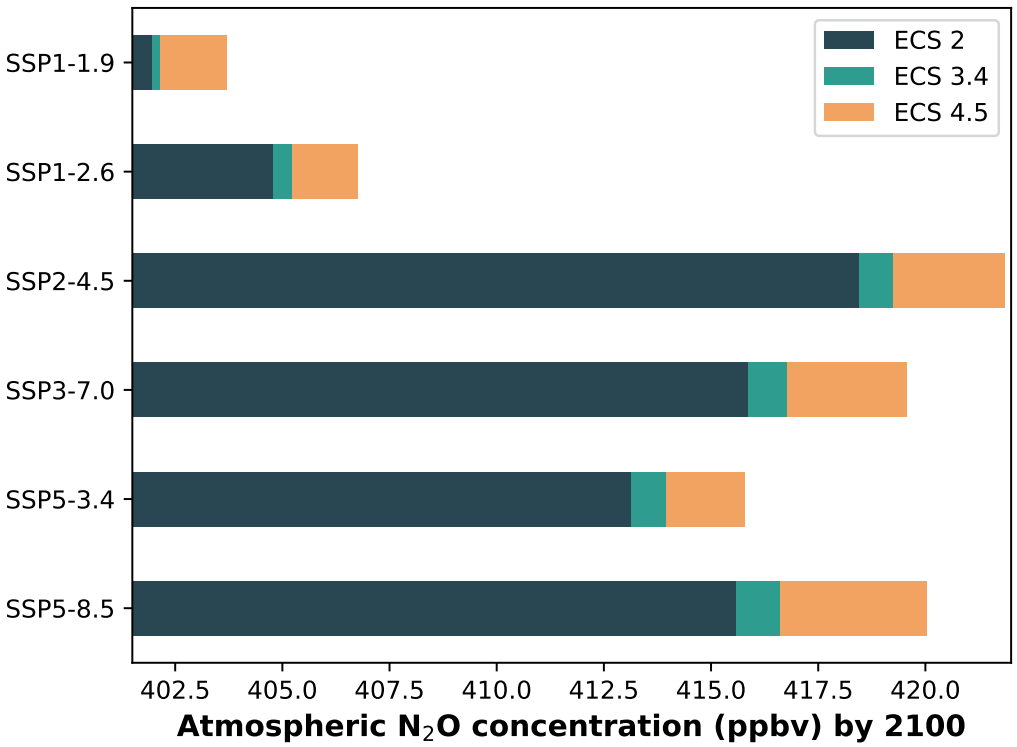

Figure 5.5: Atmospheric N_2O concentration sensitivity to equilibrium climate sensitivity (ECS). Three sensitivities were simulated for each SSP scenario: ECS 2, 3.4 and 4.5 °C.

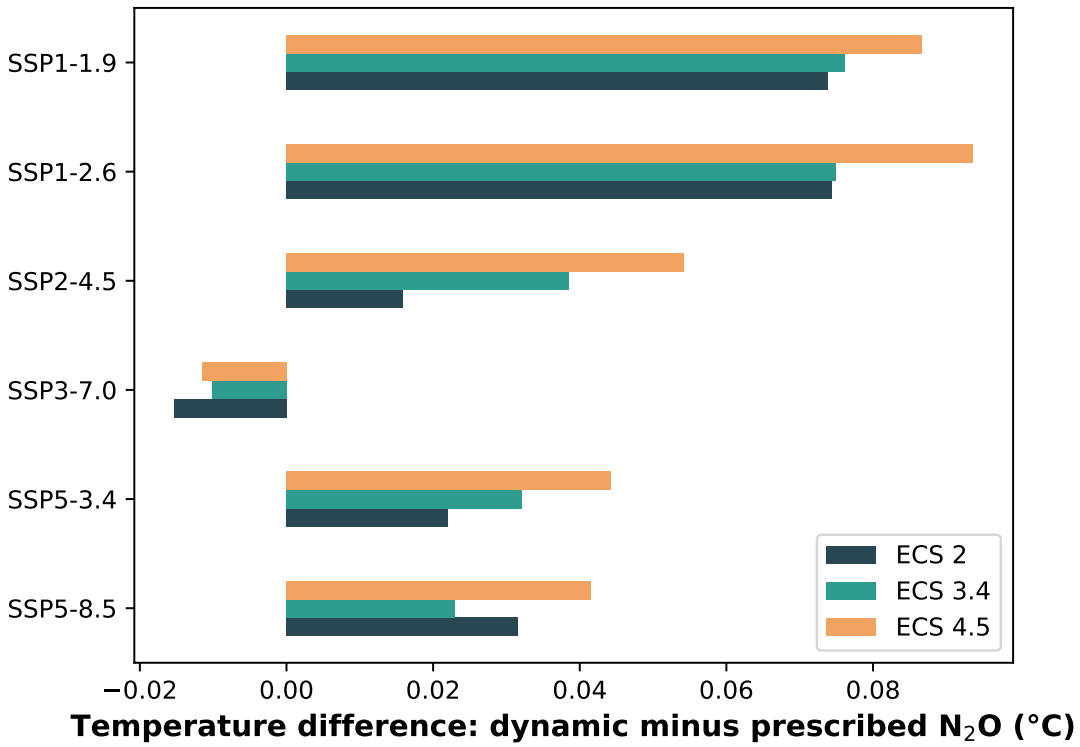

Figure 5.6: N_2O forcing effect on atmospheric temperature in a dynamic (current UVic ESCM-CNP simulations) and prescribed (Meinhaussen et al. , 2020) N_2O concentrations projections averaged over year 2080 to 2100. Lower temperature differences reflect scenarios were the UVic ESCM-CNP and Meinhaussen et al. (2020) N_2O concentrations are more similar. ECS is Equilibrium Climate Sensitivity.

Chapter 6

Summary and future work

6.1 Summary

The availability of terrestrial nitrogen and phosphorus in soils constrains the uptake capacity of vegetation. Hence, in Earth system models, the representation of terrestrial nitrogen and phosphorus cycles is imperative to improve the accuracy of their carbon cycle representation. In this thesis, a terrestrial nitrogen and phosphorus cycle has been successfully developed and implemented in an intermediate complexity Earth system climate model. The nutrient concentration in soils represented by the new models is within the range of uncertainty of observations and modelling studies. The resulting global pattern is similar to current studies and follows biogeochemical logic. Nitrogen is a limitation in high latitudes, while phosphorus is the limiting nutrient in low latitudes. The addition of phosphorus reduced tropical forests biomass and extend, and has improved an overestimation in the previous UVic ESCM state. The overall reduction of terrestrial vegetation leads to the decrease of atmosphere-land carbon flux as well as a decrease in simulated land use change emissions.

The implementation of terrestrial nitrogen and phosphorus limitation reduced the gross primary productivity by 13 PgC yr^{-1} in CN and 16 PgC yr^{-1} in CNP, resulting in a better match for observations. This implies that the model efficiently represents a nutrient limitation over the CO_2 fertilization effect. Using nutrient limitation, the model seemed to represent historical temperature with higher accuracy than the base state of the model. The representation of nitrogen and phosphorus resulted in a critical tool to improve terrestrial vegetation biomass and distribution.

The remaining carbon budget estimations were affected by the implementation of terrestrial nitrogen and phosphorus limitation. The nutrient limitation reduced the carbon budgets estimated in eight SSPs scenarios. Consequently, being an integral part of the carbon cycle uncertainties that affect carbon budget estimates. Among nitrogen and nitrogen-phosphorus structures, nitrogen-phosphorus results in lower carbon budgets overall in different SSPs scenarios. Furthermore, the nutrient limitation increases the response of temperature after cessation of emissions in Zero Emissions Commitment experiments.

The range of reduction of land carbon sink for the nutrient limited simulations was 75 to 106 Pg C and the reduction for the land use change emission was 60 to 93 Pg C. Under the Shared Socioeconomic Pathways, CN and CNP showed a reduction of 43 and 53 Pg C for the 1.5 °C target and 98 and 120 Pg C for the 2 °C target respectively when compared to the simulation with no nutrient limitation. Theses values represent a reduction of 19 and 24 % for the 1.5 °C target, 21 and 26 % for the 2 °C target. The ZEC across 100 years of simulations after emission have ceased showed an increase in temperature for the nutrient limited simulations CN and CNP of 0.12 and 0.16 °C when compared to C-only.

Allowing for the estimation of terrestrial N_2O emission, this thesis documents the

first successful attempt to project N_2O emission using dynamic coupled ocean and terrestrial N_2O emission modules in an Earth system model. These results show an estimated atmospheric N_2O concentration that ranges from 401 to 418 ppb. These results are similar to other non-dynamic N_2O projections with a range of 350 to 420 ppb by the end of the 21st century. I found a significant difference in the atmospheric N_2O projection in low emissions scenarios and the projected by the available N_2O concentrations in SSPs scenarios. A possible explanation for this difference is the lack of a dynamic N_2O atmospheric decay and a lack of representation of N_2O mitigation assumptions in agricultural technologies. However, given that the projection shown in other non-dynamic atmospheric studies, in theory, would require a significant reduction of terrestrial N_2O emissions, such projections have idealistic expectations of mitigation efforts that are yet to be tested to be plausible and effective in a global scale. In this study, even with strong mitigation scenarios N_2O rise will continue until the end of the 21st century, similar to the expected in higher emission-less mitigated scenarios.

6.2 Future work

Future work should be directed to improve the terrestrial nitrogen and phosphorus cycles. There are many uncertainties that can be improved by the availability of global observations. Certainly, over time more global datasets will be available as the use of machine learning techniques will likely provide reasonably accurate datasets. Hence, there is a need for observations and machine learning studies to provide reliable datasets for model improvement. In Earth system models, changing parameters to dynamic structures could improve the terrestrial nitrogen and phosphorus cycles. Examples of this are the resorption of nitrogen and phosphorus in leaves, microbial

processes and soil sorption-resorption dynamics. Furthermore, limitations to the vegetation uptake capacity, including carbon costs and mycorrhizal, could help to improve the representation of both nutrient cycles. For the UVic ESCM, the next step should be the connection between the land-ocean coastal continuum of nutrient flux. Moreover, the implementation of dedicated agricultural dynamics could help to improve the representation of N_2O emissions, especially in low mitigation scenarios. The irrigation in agricultural fields should be revisited as anaerobic fractions plays a crucial role in terrestrial N_2O emissions.

This thesis has shown a successful development and implementation of terrestrial nitrogen and phosphorus cycles. The implementation has improved the land productivity estimates in comparison with the no-nutrient base version of the model. The change in land by nutrient limitation reduced the estimation of remaining carbon budgets, showing that it is integral in the uncertainties of the carbon cycle. Finally, the first coupled ocean-land N_2O dynamics show that N_2O emission is relatively insensitive to mitigation efforts, projecting similar values among different future scenarios.

Appendix A

Table 6.1: Remaining carbon budgets from the Shared Socioeconomic Pathways: SSP 2- 4.5, 3- 7.0 and 4- 3.4 simulations for 1.5, 2°C targets relative to a warming from 1850-1900.

SSP scenarios	Target	Climate sensitivity	C-only(PgC)	CN(PgC)	CNP(PgC)
1- 1.9	1.5 °C	4.5	20	22	8
1- 1.9	1.5 °C	3.4	163	110	108
1- 1.9	1.5 °C	2	Not reached	Not reached	Not reached
1- 2.6	1.5 °C	4.5	21	27	9
1- 2.6	1.5 °C	3.4	173	142	137
1- 2.6	1.5 °C	2	332	235	167
2- 4.5	1.5 °C	4.5	21	37	9
2- 4.5	1.5 °C	3.4	189	161	144
2- 4.5	1.5 °C	2	231	231	208
2- 4.5	2 °C	4.5	197	191	144
2- 4.5	2 °C	3.4	397	325	288
2- 4.5	2 °C	2	516	433	406
3- 7.0	1.5 °C	4.5	23	19	9
3- 7.0	1.5 °C	3.4	204	189	170
3- 7.0	1.5 °C	2	255	244	184
3- 7.0	2 °C	4.5	220	155	161
3- 7.0	2 °C	3.4	435	359	343
3- 7.0	2 °C	2	532	473	416
4- 3.4	1.5 °C	4.5	22	9	- 9
4- 3.4	1.5 °C	3.4	168	141	150
4- 3.4	1.5 °C	2	226	190	178
4- 3.4	2 °C	4.5	174	119	125
4- 3.4	2 °C	3.4	324	233	250
4- 3.4	2 °C	2	Not reached	Not reached	Not reached

Table 6.2: Remaining carbon budgets from the Shared Socioeconomic Pathways simulations: SSP 4- 6.0, 5- 3.4 and 5- 8.5 for 1.5, 2°C targets relative to a warming from 1850-1900.

SSP scenarios	Target	Climate sensitivity	C-only(PgC)	CN(PgC)	CNP(PgC)
4- 6.0	1.5 °C	4.5	32	8	10
4- 6.0	1.5 °C	3.4	194	177	157
4- 6.0	1.5 °C	2	238	236	215
4- 6.0	2 °C	4.5	174	119	125
4- 6.0	2 °C	3.4	324	233	250
4- 6.0	2 °C	2	Not reached	Not reached	Not reached
5- 3.4	1.5 °C	4.5	25	12	10
5- 3.4	1.5 °C	3.4	219	189	204
5- 3.4	1.5 °C	2	255	251	236
5- 3.4	2 °C	4.5	238	169	174
5- 3.4	2 °C	3.4	509	359	378
5- 3.4	2 °C	2	1129	800	785
5- 8.5	1.5 °C	4.5	22	52	12
5- 8.5	1.5 °C	3.4	211	199	198
5- 8.5	1.5 °C	2	270	264	210
5- 8.5	2 °C	4.5	233	232	183
5- 8.5	2 °C	3.4	446	380	403
5- 8.5	2 °C	2	570	504	446

Table 6.3: Remaining carbon budgets from the Shared Socioeconomic Pathways simulations: SSP-2.45, SSP 3-7.0, 4-6.0 and 5-8.5 for 2.5, 3°C targets relative to a warming from 1850-1900.

SSP scenarios	Target	Climate sensitivity	C-only(PgC)	CN(PgC)	CNP(PgC)
2- 4.5	2.5 °C	4.5	373	321	282
2- 4.5	2.5 °C	3.4	721	567	584
2- 4.5	2.5 °C	2	Not reached	Not reached	Not reached
3- 7.0	2.5 °C	4.5	405	303	325
3- 7.0	2.5 °C	3.4	722	616	591
3- 7.0	2.5 °C	2	830	714	676
3- 7.0	3 °C	4.5	580	444	490
3- 7.0	3 °C	3.4	967	820	816
3- 7.0	3 °C	2	1118	939	942
4- 6.0	2.5 °C	4.5	380	271	303
4- 6.0	2.5 °C	3.4	670	528	542
4- 6.0	2.5 °C	2	830	658	601
4- 6.0	3 °C	4.5	545	391	454
4- 6.0	3 °C	3.4	756	703	717
4- 6.0	3 °C	2	Not reached	Not reached	Not reached
5- 8.5	2.5 °C	3.4	437	398	356
5- 8.5	2.5 °C	3.4	742	648	658
5- 8.5	2.5 °C	2	900	809	742
5- 8.5	3 °C	4.5	615	552	521
5- 8.5	3 °C	3.4	1037	875	918
5- 8.5	3 °C	2	1260	1093	1080

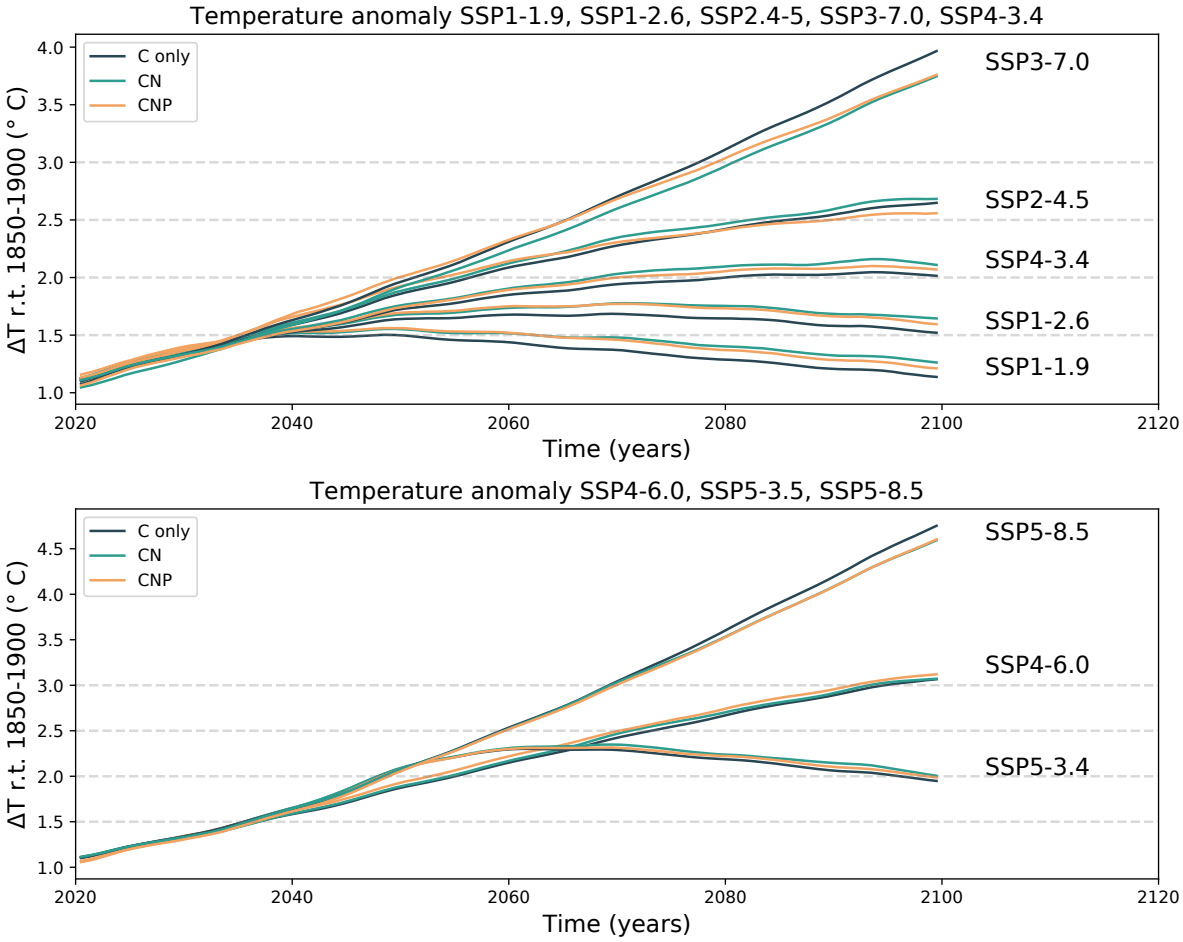

Figure 6.1: SSP temperature anomaly relative to 1850-1900 of C-only, CN and CNP simulations.

Bibliography

Achat, D., Gallet-Budynek, A. and Loustau, D. (2016). Future challenges in coupled C–N–P cycle models for terrestrial ecosystems under global change: a review. Biogeochemistry, 131. 10.1007/s10533-016-0274-9.

Anas, M., Liao, F., Verma, K.K. et al. (2020). Fate of nitrogen in agriculture and environment: agronomic, eco-physiological and molecular approaches to improve nitrogen use efficiency. Biol Res 53, 47. https://doi.org/10.1186/s40659-020-00312-4.

Archer, D. (1996). A data-driven model of the global calcite lysocline. Global Biogeochem. Cy., 10, 511–526, https://doi.org/10.1029/96GB01521, 1996.

Arias, P.A., N. Bellouin, E. Coppola, R.G. Jones, G. Krinner, J. Marotzke, V. Naik, M.D. Palmer, G.-K. Plattner, J. Rogelj, M. Rojas, J. Sillmann, T. Storelvmo, P.W. Thorne, B. Trewin, K. Achuta Rao, B. Adhikary, R.P. Allan, K. Armour, G. Bala, R. Barimalala, S. Berger, J.G. Canadell, C. Cassou, A. Cherchi, W. Collins, W.D. Collins, S.L. Connors, S. Corti, F. Cruz, F.J. Dentener, C. Dereczynski, A. Di Luca, A. Diongue Niang, F.J. Doblas-Reyes, A. Dosio, H. Douville, F. Engelbrecht, V. Eyring, E. Fischer, P. Forster, B. Fox-Kemper, J.S. Fuglestvedt, J.C. Fyfe, N.P. Gillett, L. Goldfarb, I. Gorodetskaya, J.M. Gutierrez, R. Hamdi, E. Hawkins, H.T. Hewitt, P. Hope, A.S. Islam, C. Jones, D.S. Kaufman, R.E.

Kopp, Y. Kosaka, J. Kossin, S. Krakovska, J.-Y. Lee, J. Li, T. Mauritsen, T.K. Maycock, M. Meinshausen, S.-K. Min, P.M.S. Monteiro, T. Ngo-Duc, F. Otto, I. Pinto, A. Pirani, K. Raghavan, R. Ranasinghe, A.C. Ruane, L. Ruiz, J.-B. Sallée, B.H. Samset, S. Sathyendranath, S.I. Seneviratne, A.A. Sörensson, S. Szopa, I. Takayabu, A.-M. Tréguier, B. van den Hurk, R. Vautard, K. von Schuckmann, S. Zaehle, X. Zhang, and K. Zickfeld: Technical Summary. In Climate Change 2021: The Physical Science Basis. Contribution of Working Group I to the Sixth Assessment Report of the Intergovernmental Panel on Climate Change [Masson-Delmotte, V., P. Zhai, A. Pirani, S.L. Connors, C. Péan, S. Berger, N. Caud, Y. Chen, L. Goldfarb, M.I. Gomis, M. Huang, K. Leitzell, E. Lonnoy, J.B.R. Matthews, T.K. Maycock, T. Waterfield, O. Yelekçi, R. Yu, and B. Zhou (eds.)]. Cambridge University Press, Cambridge, United Kingdom and New York, NY, USA, pp. 33144. doi:10.1017/9781009157896.002. 2021.

Arora, V. K., Katavouta, A., Williams, R. G., Jones, C. D., Brovkin, V., Friedlingstein, P., Schwinger, J., Bopp, L., Boucher, O., Cadule, P., Chamberlain, M. A., Christian, J. R., Delire, C., Fisher, R. A., Hajima, T., Ilyina, T., Joetzjer, E., Kawamiya, M., Koven, C. D., Krasting, J. P., Law, R. M., Lawrence, D. M., Lenton, A., Lindsay, K., Pongratz, J., Raddatz, T., Séférian, R., Tachiiri, K., Tjiputra, J. F., Wiltshire, A., Wu, T., and Ziehn, T. (2020). Carbon–concentration and carbon–climate feedbacks in CMIP6 models and their comparison to CMIP5 models. Biogeosciences, 17, 4173–4222. https://doi.org/10.5194/bg-17-4173-2020.

Avis, C. A. (2012). Simulating the Present-Day and Future Distribution of Permafrost in the UVic Earth System Climate Model, PhD thesis, University of Victoria.

Atilio B., Causin, H. (1996). The central role of amino acids on nitrogen

utilization and plant growth, Journal of Plant Physiology, 149(3), 358-362. https://doi.org/10.1016/S0176-1617(96)80134-9.

Ator S. W., Brakebill J. W. and Blomquist J. D. (2011). Sources, Fate, and Transport of Nitrogen and Phosphorus in the Chesapeake Bay Watershed: An Empirical Model. U.S. Geological Survey Scientific Investigations Report, 2011–5167.

Davies-Barnard, T. and Friedlingstein, P. (2020). The global distribution of biological nitrogen fixation in terrestrial natural ecosystems. Global Biogeochemical Cycles, 34, e2019GB006387. https://doi.org/10.1029/2019GB006387.

Battaglia, G., and Joos, F. (2018). Marine N2O emissions from nitrification and denitrification constrained by modern observations and projected in multimillennial global warming simulations. Global Biogeochemical Cycles, 32, 92–121. https://doi.org/10.1002/2017GB00.

Bauer, N., Calvin, K., Emmerling, J., et al. (2017). Shared Socio-Economic Pathways of the Energy Sector – Quantifying the Narratives. Global Environmental Change, 42, 316-330. https://doi.org/10.1016/j.gloenvcha.2016.07.006.

Bernstein L, Roy J, Delhotal K C, et al. (2007). Industry. In Climate Change 2007: Mitigation. Contribution of Working Group III to the Fourth Assessment Report of the Intergovernmental Panel on Climate Change (ed B Metz et al.). Cambridge University Press.

Beusen, A., Slomp, C. P., and Bouwman, A. (2013). Global land-ocean linkage: Direct inputs of nitrogen to coastal waters via submarine groundwater discharge. Environmental Research Letters, 8, 034035. doi:10.1088/1748-9326/8/3/034035.

Bouwman, A. F., Beusen, A. H. W., and Billen, G. (2009). Human alteration of

the global nitrogen and phosphorus soil balances for the period 1970–2050. Global Biogeochemical Cycles, 23, GB0A04. doi:10.1029/2009GB003576.

Beusen, A. H. W., Bouwman, A. F., Van Beek, L. P. H., Mogollón, J. M., and Middelburg, J. J. (2016). Global riverine N and P transport to ocean increased during the 20th century despite increased retention along the aquatic continuum. Biogeosciences.

Beusen, A., Doelman, J., Van Beek, L., Van Puijenbroek, P., Mogollón, J., Van Grinsven, H., Stehfest, E., Van Vuuren, D., and Bouwman, A. (2022). Exploring river nitrogen and phosphorus loading and export to global coastal waters in the Shared Socio-economic pathways. Global Environmental Change, 72. https://doi.org/10.1016/j.gloenvcha.2021.102426.

Bengtson, P., and Bengtsson, G. (2005). Bacterial immobilization and remineralization of N at different growth rates and N concentrations. FEMS Microbiology Ecology, 54(1), 13–19. https://doi.org/10.1016/j.femsec.2005.02.006.

Bitz, C. M., Holland, M. M., Weaver, A. J., and Eby, M. (2001). Simulating the ice-thickness distribution in a coupled. J. Geophys. Res., 106, 2441–2463. https://doi.org/10.1029/1999JC000113.

Bonan, G. B., and Levis, S. (2010). Quantifying carbon-nitrogen feedbacks in the Community Land Model (CLM4). Geophys. Res. Lett., 37, 2261–2282.

Bodirsky, B. L., Rolinski, S., Biewald, A., et al. (2015). Global Food Demand Scenarios for the 21st Century. PLOS ONE, 10(11), e0139201. https://doi.org/10.1371/journal.pone.0139201.

Bopp L, Resplandy L, Orr J C, et al. (2013) Multiple stressors of ocean ecosystems in the 21st century: projections with CMIP5 models, Biogeosciences, 10, 6225–6245.

Bouwman, A. F., Beusen, A. H. W., Lassaletta, L., Van Apeldoorn, D. F., Van Grinsven, H. J. M., Zhang, J., and Ittersum Van M. K. (2017). Lessons from temporal and spatial patterns in global use of N and P fertilizer on cropland. Sci. Rep., 7, 40366.

Bouwman, A. F., Goldewijk, K. K., Van Der Hoek, K. W., Beusen, A. H. W., Van Vuuren, D. P., Willems, J., Rufino, M. C., and Stehfest, E. (2013). Exploring global changes in nitrogen and phosphorus cycles in agriculture induced by livestock production over the 1900–2050 period. Proc. Natl Acad. Sci. USA, 110, 20882–7.

Buitenhuis, E. T., Suntharalingam, P., and Le Quéré, C. (2018). Constraints on global oceanic emissions of N2O from observations and models. Biogeosciences, 15, 2161–2175.

Braghiere, R. K., Fisher, J. B., Fisher, R. A., et al. (2021). Mycorrhizal distributions impact global patterns of carbon and nutrient cycling. Geophysical Research Letters, 48, e2021GL094514. https://doi.org/10.1029/2021GL094514.

Braghiere, R. K., Fisher, J. B., Allen, K., et al. (2022). Modeling global carbon costs of plant nitrogen and phosphorus acquisition. Journal of Advances in Modeling Earth Systems, 14, e2022MS003204. https://doi.org/10.1029/2022MS003204.

Bronson, K., Schepers, J. S., and Raun, W. (2008). Forms of Inorganic Nitrogen in Soil. In Agronomy Monograph 49. doi:10.2134/agronmonogr49.c2.

Canadell, J.G., Monteiro, P.M.S., Costa, M.H., Cotrim da Cunha, L., Cox, P.M., Eliseev, A.V., Henson, S., Ishii, M., Jaccard, S., Koven, C., Lohila, A., Patra, P.K., Piao, S., Rogelj, J., Syampungani, S., Zaehle, S., and Zickfeld, K. (2021). Global Carbon and other Biogeochemical Cycles and Feedbacks. In Climate Change 2021:

The Physical Science Basis. Contribution of Working Group I to the Sixth Assessment Report of the Intergovernmental Panel on Climate Change (pp. 673–816). Cambridge University Press. doi:10.1017/9781009157896.007.

Carreira, C., Mestre, O., Nunes, R.F., Moura, I., and Pauleta, S.R. (2018). Genomic organization, gene expression, and activity profile of Marinobacter hydrocarbonoclasticus denitrification enzymes. PeerJ, 6, e5603. doi:10.7717/peerj.5603.

Caranto, J., and Lancaster, K. (2017). Nitric oxide is an obligate bacterial nitrification intermediate produced by hydroxylamine oxidoreductase. Proceedings of the National Academy of Sciences, 114, 201704504. doi:10.1073/pnas.1704504114.

Carstensen, A., Herdean, A., Schmidt, S. B., Sharma, A., Spetea, C., Pribil, M., and Husted, S. (2018). The Impacts of Phosphorus Deficiency on the Photosynthetic Electron Transport Chain. Plant Physiology, 177(1), 271-284. doi: 10.1104/pp.17.01624.

Chen, X., Dunfield, K., Fraser, T.D., Wakelin, S., Richardson, A., and Condron, L.M. (2019). Soil biodiversity and biogeochemical function in managed ecosystems. Soil Research, 58. doi:10.1071/SR19067.

Chen, J. and Strous, M. (2012). Denitrification and aerobic respiration, hybrid electron transport chains and co-evolution. Biochimica et biophysica acta. 1827. 10.1016/j.bbabio.2012.10.002.

Chester, M., Underwood, B.S., Allenby, B., et al. (2021). Infrastructure resilience to navigate increasingly uncertain and complex conditions in the Anthropocene. npj Urban Sustainability, 1, 4. doi:10.1038/s42949-021-00016-y.

Clark, D.B., Mercado, L.M., Sitch, S., Jones, C.D., Gedney, N., Best, M.J., Pryor, M., Rooney, G.G., Essery, R.L.H., Blyth, E., Boucher, O., Harding, R.J., Huntingford,

C., and Cox, P.M. (2011). The Joint UK Land Environment Simulator (JULES), model description – Part 2: Carbon fluxes and vegetation dynamics. Geoscientific Model Development, 4, 701–722. doi:10.5194/gmd-4-701-2011.

Cox, P.M., Huntingford, C., and Harding, J. (1998). A canopy conductance and photosynthesis model for use in a GCM land surface scheme. Journal of Hydrology, Volumes 212–213. doi:10.1016/S0022-1694(98)00203-0.

Cox, P. M., Betts, R. A., Bunton, C. B., Essery, R. L. H., Rowntree, P. R., and Smith, J. (1999). The impact of new land surface physics on the GCM simulation of climate and climate sensitivity. Clim. Dynam., 15, 183–203.

Cox, P. M.: Description of the TRIFFID dynamic global vegetation model, Tech. Rep. 24, Hadley Centre, Met office, London Road, Bracknell, Berks, RG122SY, UK, 2001.

Collier, N., Hoffman, F.M., Lawrence, D.M., Keppel-Aleks, G., Koven, C.D., Riley, W.J., Mu, M., and Randerson, J.T. (2018). The International Land Model Benchmarking (ILAMB) System: Design, Theory, and Implementation. Journal of Advances in Modeling Earth Systems, 10(11), 2731–2754. doi:10.1029/2018MS001354.

Cotrufo, M.F., Wallenstein, M.D., Boot, C.M., Denef, K., and Paul, E. (2013). The Microbial Efficiency-Matrix Stabilization (MEMS) framework integrates plant litter decomposition with soil organic matter stabilization: do labile plant inputs form stable soil organic matter?. Global Change Biology, 19, 988-995. doi:10.1111/gcb.12113.

Crippa, M., Guizzardi, D., Muntean, M., Schaaf, E., Lo Vullo, E., Solazzo, E., Monforti-Ferrario, F., Olivier, J., and Vignati, E. (2021). EDGAR v6.0 Greenhouse

Gas Emissions. European Commission, Joint Research Centre (JRC). [Dataset] PID: http://data.europa.eu/89h/97a67d67-c62e-4826-b873-9d972c4f670b.

Crippa, M., Guizzardi, D., Solazzo, E., Muntean, M., Schaaf, E., Monforti-Ferrario, F., et al. (2021). GHG emissions of all world countries - 2021 Report. EUR 30831 EN, Publications Office of the European Union. doi:10.2760/173513.

Coskun D, Britto DT, Kronzucker HJ. (2016) Nutrient constraints on terrestrial carbon fixation: The role of nitrogen. J Plant Physiol., 203, 95-109. doi: 10.1016/j.jplph.2016.05.016.

Cross, A.F., and Schlesinger, W.H. (1995). A literature review and evaluation of the Hedley fractionation: applications to the biogeochemical cycle of soil phosphorus in natural ecosystems. Geoderma, 64, 197–214.

Davidson, E., and Kanter, D. (2014). Inventories and scenarios of nitrous oxide emissions. Environmental Research Letters, 9, 105012. doi:10.1088/1748-9326/9/10/105012.

Davidson, E., Keller, M., Erickson, H., Verchot, L., and Veldkamp, E. (2000). Testing a conceptual model of soil emissions of nitrous and nitric oxides: using two functions based on soil nitrogen availability and soil water content, the hole-in-the-pipe model characterizes a large fraction of the observed variation of nitric oxide and nitrous oxide emissions from soils. AIBS Bulletin, 50(8), 667–680.

DalCorso, G., Manara, A., Piasentin, S., and Furini, A. (2014) Nutrient metal elements in plants. Metallomics, 6(10), 1770–1788. doi: 10.1039/c4mt00173g.

de Bang, T.C., Husted, S., Laursen, K.H., Persson, D.P., and Schjoerring, J.K. (2021). The molecular–physiological functions of mineral macronutrients and their

consequences for deficiency symptoms in plants. New Phytol, 229, 2446-2469. doi: 10.1111/nph.17074.

De Sisto, M. L., MacDougall, A. H., Mengis, N., and Antoniello, S. (2023). Modelling the terrestrial nitrogen and phosphorus cycle in the UVic ESCM. Geoscientific Model Development, 16, 4113–4136. doi:10.5194/gmd-16-4113-2023.

Du, E., Terrer, C., Pellegrini, A., Ahlstrom, A., Van Lissa, C., Zhao, X., Xia, N., Wu, X., and Jackson, R. (2020). Global patterns of terrestrial nitrogen and phosphorus limitation. Nat. Geosci., 13, 221–226. doi:10.1038/s41561-019-0530-4.

Duncan, E. G., O'Sullivan, C. A., Roper, M. M., Biggs, J. S., and Peoples, M. B. (2018). Influence of co-application of nitrogen with phosphorus, potassium, and sulfur on the apparent efficiency of nitrogen fertilizer use, grain yield, and protein content of wheat: Review. Field Crops Research, 226, 56-65. doi:10.1016/j.fcr.2018.07.010.

Dynarski, K. A., Morford, S. L., Mitchell, S. A., and Houlton, B. Z. (2019). Bedrock nitrogen weathering stimulates biological nitrogen fixation. Ecology, 100(8), 1–10. doi:https://www.jstor.org/stable/26749507.

Eisele, K., Schimel, D., Kapustka, L., and Parton, W. (1989). Effects of available P and N:P ratios on non-symbiotic dinitrogen fixation in tall grass prairie soils. Oecologia, 79, 471–474.

Eby, M., Weaver, A. J., Alexander, K., Zickfeld, K., Abe-Ouchi, A., Cimatoribus, A. A., Crespin, E., Drijfhout, S. S., Edwards, N. R., Eliseev, A. V., Feulner, G., Fichefet, T., Forest, C. E., Goosse, H., Holden, P. B., Joos, F., Kawamiya, M., Kicklighter, D., Kienert, H., Matsumoto, K., Mokhov, I. I., Monier, E., Olsen, S. M., Pedersen, J. O. P., Perrette, M., Philippon-Berthier, G., Ridgwell, A., Schlosser,

A., Schneider von Deimling, T., Shaffer, G., Smith, R. S., Spahni, R., Sokolov, A. P., Steinacher, M., Tachiiri, K., Tokos, K., Yoshimori, M., Zeng, N., and Zhao, F. (2013). Historical and idealized climate model experiments: an intercomparison of Earth system models of intermediate complexity. Clim. Past, 9, 1111–1140. doi:10.5194/cp-9-1111-2013.

Eyring, V., Bony, S., Meehl, G. A., Senior, C. A., Stevens, B., Stouffer, R. J., and Taylor, K. E. (2016). Overview of the Coupled Model Intercomparison Project Phase 6 (CMIP6) experimental design and organization. Geosci. Model Dev., 9, 1937–1958. doi:10.5194/gmd-9-1937-2016.

Farzadfar, S., Knight, J. D., and Congreves, K. A. (2021). Soil organic nitrogen: an overlooked but potentially significant contribution to crop nutrition. Plant and Soil, 462, 7–23. https://doi.org/10.1007/s11104-021-04860-w.

Fanning, A. F., and Weaver, A. J. (1996). An atmospheric energy-moisture balance model: Climatology, interpentadal climate change, and coupling to an ocean general circulation model. Journal of Geophysical Research, 101, 15111.

Feng, E. Y., Keller, D. P., Koeve, W., and Oschlies, A. (2016). Could artificial ocean alkalinization protect tropical coral ecosystems from ocean acidification? Environmental Research Letters, 11(7), 074008. https://doi.org/10.1088/1748-9326/11/7/074008.

Fleischer, K., Dolman, A. J., van der Molen, M. K., Rebel, K. T., Erisman, J. W., Wassen, M. J., et al. (2019). Nitrogen deposition maintains a positive effect on terrestrial carbon sequestration in the 21st century despite growing phosphorus limitation at regional scales. Global Biogeochemical Cycles, 33, 810–824. doi:10.1029/2018GB005952.

Filippelli, G. (2002). The global phosphorus cycle, in phosphates: Geochemical, geobiological, and materials importance, Reviews in Mineralogy and Geochemistry, 391-425.

Firestone, M., and Davidson, E. (1989). Microbiological basis of NO and N2O production and consumption in soil. Exchange of trace gases between terrestrial ecosystems and the atmosphere, 47, 7–21.

Fisher, J., Badgley, G., and Blyth, E. (2012). Global nutrient limitation in terrestrial vegetation. Global Biogeochemical Cycles, 6. doi:10.1029/2011GB004252.

Fowler, D., Coyle, M., Skiba, U., Sutton, M. A., Cape, J. N., Reis, S., Sheppard, L. J., Jenkins, A., Grizzetti, B., Galloway, J. N., Vitousek, P., Leach, A., Bouwman, A. F., Butterbach-Bahl, K., Dentener, F., Stevenson, D., Amann, M., and Voss, M. (2013). The global nitrogen cycle in the twenty-first century. Philosophical transactions of the Royal Society of London. Series B, Biological sciences, 368(1621). doi:10.1098/rstb.2013.0164.

Friedlingstein, P., Jones, M. W., O'Sullivan, M., Andrew, R. M., Bakker, D. C. E., et al. (2022). Global Carbon Budget 2021. Earth Syst. Sci. Data, 14, 1917–2005. doi:10.5194/essd-14-1917-2022.

Gedney, N., and Cox, P. (2003). The sensitivity of global climate model simulations to the representation of soil moisture heterogeneity. Journal of Hydrometeorology, 4(6), 1265–1275.

Gerber, S., Hedin, L. O., Oppenheimer, M., Pacala, S. W., and Shevliakova, E. (2010). Nitrogen cycling and feedbacks in a global dynamic land model. Global Biogeochemical Cycles, 24, 121–149.

Gidden, M. J., et al. (2019). Global emissions pathways under different socioeconomic scenarios for use in CMIP6: A dataset of harmonized emissions trajectories through the end of the century. Geoscientific Model Development, 12, 1443–1475.

Giweta, M. (2020). Role of litter production and its decomposition, and factors affecting the processes in a tropical forest ecosystem: a review. Journal of Ecology and Environment, 44(1), 11.

Global Soil Data Task Group. (2000). Global gridded surfaces of selected soil characteristics (IGBP-DIS). Available online [http://daac.ornl.gov] from Oak Ridge National Laboratory Distributed Active Archive Center, Oak Ridge, Tennessee, U.S.A.

Global Soil Data Task Group. (2014). Global Soil Data Products CD-ROM Contents (IGBP-DIS). Data Set. Available online [http://daac.ornl.gov] from Oak Ridge National Laboratory Distributed Active Archive Center, Oak Ridge, Tennessee, U.S.A.

Goll, D., Brovkin, V., Parida, B., Reick, C., Kattge, J., Reich, P., van Bodegom, P., and Niinemets, Ü. (2012). Nutrient limitation reduces land carbon uptake in simulations with a model of combined carbon, nitrogen, and phosphorus cycling. Biogeosciences, 9, 3547–3569.

Goll, D., Vuichard, N., Maignan, F., Jornet-Puig, A., Sardans, J., Violette, A., et al. (2017). A representation of the phosphorus cycle for ORCHIDEE. Geoscientific Model Development, 10, 3745-3770.

Graeme, H. (2011). Future demographic change and its interactions with migration and climate change. Global Environmental Change, 21, S21–S33.

Gelbrecht, M., White, A., Bathiany, S., and Boers, N. (2023). Differentiable programming for Earth system modeling. Geoscientific Model Development, 16(6), 3123–3135.

GISTEMP Team. (2023). GISS Surface Temperature Analysis (GISTEMP), version 4. NASA Goddard Institute for Space Studies. Dataset accessed 20YY-MM-DD at https://data.giss.nasa.gov/gistemp/.

Groffman, P. M. (2012). Terrestrial denitrification: Challenges and opportunities. Ecological Processes, 1(11).

Grosso, S., Smith, W., Kraus, D., Massad, R. S., Vogeler, I., and Fuchs, K. (2020). Approaches and concepts of modeling denitrification: increased process understanding using observational data can reduce uncertainties. Current Opinion in Environmental Sustainability, 47, 37-45.

Gruber, N., and Galloway, J. (2008). An Earth-system perspective of the global nitrogen cycle. Nature, 451, 293–296.

Hall, B. D., Dutton, G. S., and Elkins, J. W. (2007). The NOAA nitrous oxide standard scale for atmospheric observations. J. Geophys. Res., 112, D09305. doi:10.1029/2006JD007954.

Harrison, J. A., Seitzinger, S. P., Bouwman, A. F., Caraco, N. F., Beusen, A. H. W., and Vorosmarty, C. J. (2005). Dissolved inorganic phosphorus export to the coastal zone: Results from a spatially explicit, global model. Global Biogeochemical Cycles, 19, GB4S03. doi:10.1029/2004GB002357.

Harrison, J. A., Bouwman, A. F., Mayorga, E., and Seitzinger, S. (2010). Magnitudes and sources of dissolved inorganic phosphorus inputs to surface freshwaters and the coastal zone: A new global model. Global Biogeochemical Cycles, 24. doi:10.1029/2009GB003590.

Harrison, J., Beusen, A., Fink, G., Tang, T., Strokal, M., Bouwman, A., Metson, G., and Vilmin, L. (2019). Modeling phosphorus in rivers at the global scale: recent

successes, remaining challenges, and near-term opportunities. Current Opinion in Environmental Sustainability, 36, 68-77. doi:10.1016/j.cosust.2018.10.010.

Halbleib, C. M., and Ludden, P. W. (2000). Regulation of Biological Nitrogen Fixation. The Journal of Nutrition, 130(5), 1081–1084.

Halsted, M., and Lynch, J. (1996). Phosphorus responses of C3 and C4 species. Journal of Experimental Botany, 47(4), 497–505.

Hassan, M. U., Aamer, M., Mahmood, A., Awan, M. I., Barbanti, L., Seleiman, M. F., Bakhsh, G., Alkharabsheh, H. M., Babur, E., Shao, J., Rasheed, A., and Huang, G. (2022). Management Strategies to Mitigate N2O Emissions in Agriculture. Life (Basel), 12(3), 439. doi:10.3390/life12030439.

Hartmann, J., and Moosdorf, N. (2012). The new global lithological map database GLiM: a representation of rock properties at the Earth surface. Geochemistry, Geophysics, Geosystems, 13, 1–37. doi:10.1029/2012GC004370.

Hartmann, J., Moosdorf, N., Lauerwald, R., Hinderer, M., and West, A. (2014). Global chemical weathering and associated P-release - The role of lithology, temperature, and soil properties. Chemical Geology, 363, 145–163. doi:10.1016/j.chemgeo.2013.10.025.

Haverd, V., Smith, B., Nieradzik, L., Briggs, P. R., Woodgate, W., Trudinger, C. M., et al. (2018). A new version of the CABLE land surface model (Subversion revision r4601) incorporating land use and land cover change, woody vegetation demography, and a novel optimization-based approach to plant coordination of photosynthesis. Geoscientific Model Development, 11, 2995–3026. doi:10.5194/gmd-11-2995-2018.

He, X., Augusto, L., Goll, D., Ringeval, B., Wang, Y., Helfenstein, J., et al. (2021).

Global patterns and drivers of soil total phosphorus concentration. Earth System Science Data, 13, 5831-5846. doi.org/10.5194/essd-13-5831-2021.

Hem, J. D. (1985). Study and Interpretation of the Chemical Characteristics of Natural Water. US Geological Survey Water Supply Paper 2254.

Hedley, M., and Stewart, J. (1982). Method to measure microbial phosphate in soils. Soil Biology and Biochemistry, 14, 377–385.

Hou, E., Luo, Y., Kuang, Y., et al. (2020). Global meta-analysis shows pervasive phosphorus limitation of aboveground plant production in natural terrestrial ecosystems. Nature Communications, 11, 637. doi:10.1038/s41467-020-14492-w.

Hungate, B., Dukes, J., Shaw, M., Luo, Y., and Field, C. (2003). Nitrogen and Climate Change. Science (New York, N.Y.), 302, 1512-3. doi:10.1126/science.1091390.

IPCC. (2018). Global Warming of 1.5C: An IPCC Special Report on the impacts of global warming of 1.5C above pre-industrial levels and related global greenhouse gas emission pathways, in the context of strengthening the global response to the threat of climate change, sustainable development, and efforts to eradicate poverty [Masson-Delmotte, V., P. Zhai, H.-O. Pörtner, D. Roberts, J. Skea, P.R. Shukla, A. Pirani, W. Moufouma-Okia, C. Péan, R. Pidcock, S. Connors, J.B.R. Matthews, Y. Chen, X. Zhou, M.I. Gomis, E. Lonnoy, T. Maycock, M. Tignor, and T. Waterfield (eds.)]. In Press.

IPCC. (2021). Summary for Policymakers. In: Climate Change 2021: The Physical Science Basis. Contribution of Working Group I to the Sixth Assessment Report of the Intergovernmental Panel on Climate Change [Masson-Delmotte, V., P. Zhai, A. Pirani, S.L. Connors, C. Péan, S. Berger, N. Caud, Y. Chen, L. Goldfarb, M.I.

Gomis, M. Huang, K. Leitzell, E. Lonnoy, J.B.R. Matthews, T.K. Maycock, T. Waterfield, O. Yelekçi, R. Yu, and B. Zhou (eds.)]. In Press.

IPCC. (2022). Climate Change 2022: Impacts, Adaptation, and Vulnerability. Contribution of Working Group II to the Sixth Assessment Report of the Intergovernmental Panel on Climate Change [H.-O. Pörtner, D.C. Roberts, M. Tignor, E.S. Poloczanska, K. Mintenbeck, A. Alegría, M. Craig, S. Langsdorf, S. Löschke, V. Möller, A. Okem, B. Rama (eds.)]. Cambridge University Press. In Press.

Isobe, K., and Ohte, N. (2014). Ecological Perspectives on Microbes Involved in N-Cycling. Microbes and environments / JSME. 29. 10.1264/jsme2.ME13159.

Jones, C. D., Frölicher, T. L., Koven, C., MacDougall, A. H., Matthews, H. D., Zickfeld, K., Rogelj, J., Tokarska, K. B., Gillett, N. P., Ilyina, T., Meinshausen, M., Mengis, N., Séférian, R., Eby, M., and Burger, F. A. (2019). The Zero Emissions Commitment Model Intercomparison Project (ZECMIP) contribution to C4MIP: quantifying committed climate changes following zero carbon emissions. Geosci. Model Dev., 12, 4375–4385. https://doi.org/10.5194/gmd-12-4375-2019.

Jung, M., Koirala, S., Weber, U., Ichii, K., Gans, F., Camps-Valls, G., Papale, D., Schwalm, C., Tramontana, G., and Reichstein, M. (2019). The FLUXCOM ensemble of global land-atmosphere energy fluxes. Scientific Data, in press, 6. https://doi.org/10.1038/s41597-019-0076-8.

Kanter, D. R., Winiwarter, W., Bodirsky, B. L., Bouwman, L., Boyer, E., Buckle, S., et al. (2020). Nitrogen futures in the shared socioeconomic pathways 4. Glob Environ Change, 61, 102029. https://doi.org/10.1016/j.gloenvcha.2019.102029.

Kawamiya, M., Hajima, T., Tachiiri, K., et al. (2020). Two decades of Earth system modeling with an emphasis on Model for Interdisciplinary Research on Climate

(MIROC). Prog Earth Planet Sci, 7, 64. https://doi.org/10.1186/s40645-020-00369-5.

Keller, D. P., Oschlies, A., and Eby, M. (2012). A new marine ecosystem model for the University of Victoria Earth System Climate Model. Geosci. Model Dev., 5(5), 1195–1220.

Keller, D. P., Feng, E. Y., and Oschlies, A. (2014). Potential climate engineering effectiveness and side effects during a high carbon dioxide-emission scenario. Nat. Commun., 5, 1–11. https://doi.org/10.1038/ncomms4304.

Kawamiya, M., Hajima, T., Tachiiri, K. et al. 2020. Two decades of Earth system modeling with an emphasis on Model for Interdisciplinary Research on Climate (MIROC). Prog Earth Planet Sci 7, 64. https://doi.org/10.1186/s40645-020-00369-5

Khatoon, H., Solanki, P., Narayan, M., Tewari, L., and Rai, J. (2017). Role of microbes in organic carbon decomposition and maintenance of soil ecosystem. 5, 1648-1656.

Kothawala, D., and Moore, T. (2009). Adsorption of dissolved nitrogen by forest mineral soils. Can. J. For. Res., 39, 2381–2390.

Kraut, J. (1988). How Do Enzymes Work?. Science, 242, 533-540. doi:10.1126/science.3051385.

Kvale, K., Prowe, A. E. F., Chien, C. T., et al. (2021). Zooplankton grazing of microplastic can accelerate the global loss of ocean oxygen. Nat Commun, 12, 2358. https://doi.org/10.1038/s41467-021-22554-w.

Lamarque, J.-F., et al. (2013). Multi-model mean nitrogen and sulfur deposition

from the Atmospheric Chemistry and Climate Model Intercomparison Project (ACCMIP): Evaluation of historical and projected future changes. Atmos. Chem. Phys., 13(16), 7997–8018. doi:10.5194/acp-13-7997-2013.

Lampitt, R., Achterberg, E., Anderson, R., Hughes, J., Iglesias, M., Kelly, B., Lucas, M., Popova, E., Sanders, R., Shepherd, J., Smythe, D., and Yool, A. (2008). Ocean fertilization: a potential means of geoengineering? Philosophical Transactions of the Royal Society A: Mathematical, Physical and Engineering Sciences, 366, 3919-3945. doi.org/10.1098/rsta.2008.0139.

Lan, X., Thoning, K. W., and Dlugokencky, E. J. (2023). Trends in globally-averaged CH4, N2O, and SF6 determined from NOAA Global Monitoring Laboratory measurements. Version 2023-07. https://doi.org/10.15138/P8XG-AA10.

Landolfi, A., Somes, C. J., Koeve, W., Zamora, L. M., and Oschlies, A. (2017). Oceanic nitrogen cycling and N2 flux perturbations in the Anthropocene. Global Biogeochemical Cycles, 31(8), 1236–1255. doi:10.1002/2017gb005633.

Lawrence, D. M., Fisher, R. A., Koven, C. D., Oleson, K. W., Swenson, S. C., Bonan, G., et al. (2019). The Community Land Model version 5: Description of new features, benchmarking, and impact of forcing uncertainty. Journal of Advances in Modeling Earth Systems, 11, 4245– 4287. https://doi.org/10.1029/2018MS001583.

Le Quéré, C., Andrew, R. M., Friedlingstein, P., Sitch, S., Hauck, J., Pongratz, J., Pickers, P. A., Korsbakken, J. I., Peters, G. P., Canadell, J. G., Arneth, A., Arora, V. K., Barbero, L., Bastos, A., Bopp, L., Chevallier, F., Chini, L. P., Ciais, P., Doney, S. C., Gkritzalis, T., Goll, D. S., Harris, I., Haverd, V., Hoffman, F. M., Hoppema, M., Houghton, R. A., Hurtt, G., Ilyina, T., Jain, A. K., Johannessen, T., Jones, C. D., Kato, E., Keeling, R. F., Goldewijk, K. K., Landschützer, P., Lefèvre,

N., Lienert, S., Liu, Z., Lombardozzi, D., Metzl, N., Munro, D. R., Nabel, J. E. M. S., Nakaoka, S., Neill, C., Olsen, A., Ono, T., Patra, P., Peregon, A., Peters, W., Peylin, P., Pfeil, B., Pierrot, D., Poulter, B., Rehder, G., Resplandy, L., Robertson, E., Rocher, M., Rödenbeck, C., Schuster, U., Schwinger, J., Séférian, R., Skjelvan, I., Steinhoff, T., Sutton, A., Tans, P. P., Tian, H., Tilbrook, B., Tubiello, F. N., van der Laan-Luijkx, I. T., van der Werf, G. R., Viovy, N., Walker, A. P., Wiltshire, A. J., Wright, R., Zaehle, S., and Zheng, B. (2018). Global Carbon Budget 2018, Earth Syst. Sci. Data, 10, 2141–2194, https://doi.org/10.5194/essd-10-2141-2018.

Leghari, S. J., Wahocho, N. A., Laghari, G. M., Hafeez Laghari, A., Mustafa Bhabhan, G., Hussain Talpur, K., and Lashari, A. A. (2016). Role of Nitrogen for Plant Growth and Development: A Review. Advances in Environmental Biology, 10, 209-219.

Li, C., Aber, J., Stange, F., Butterbach-Bahl, K., and Papen, H. (2000). A process-oriented model of N2O and NO emissions from forest soils: 1. model development. Journal of Geophysical Research: Atmospheres, 105(D4), 4369–4384.

Li, S., Lü, S., Liu, Y., et al. (2015). Variations and trends of terrestrial NPP and its relation to climate change in the 10 CMIP5 models. J Earth Syst Sci, 124, 395–403. https://doi.org/10.1007/s12040-015-0545-1.

López-Hernández, D., and Burnham, C. (2006). The effect of pH on phosphate adsorption in soils. Journal of Soil Science, 25, 207-216. doi:10.1111/j.1365-2389.1974.tb01117.x.

Lu, C., and Tian, H. (2017). Global nitrogen and phosphorus fertilizer use for agriculture production in the past half century: Shifted hot spots and nutrient imbalance. Earth System Science Data, 9, 181-192. doi:10.5194/essd-9-181-2017.

Maathuis, F. (2009). Physiological functions of mineral macronutrients. Current Opinion in Plant Biology, 12(3), 250-258. https://doi.org/10.1016/j.pbi.2009.04.003.

MacDougall, A. H. (2017). The oceanic origin of path-independent carbon budgets. Scientific Reports, 7, 10373. https://doi.org/10.1038/s41598-017-10557-x.

MacDougall, A. H., and Knutti, R. (2016). Projecting the release of carbon from permafrost soils using a perturbed parameter ensemble modeling approach. Biogeosciences, 13, 2123-2136. https://doi.org/10.5194/bg-13-2123-2016

MacDougall, A. H., Avis, C. A., and Weaver, A. J. (2012). Significant contribution to climate warming from the permafrost carbon feedback. Nature Geoscience, 5, 719-721.

MacDougall, A. H. (2016). The Transient Response to Cumulative CO2 Emissions: a Review. Current Climate Change Reports, 2, 39-47. https://doi.org/10.1007/s40641-015-0030-6

MacDougall, A. H., Swart, N. C., and Knutti, R. (2017). The Uncertainty in the Transient Climate Response to Cumulative CO2 Emissions Arising from the Uncertainty in Physical Climate Parameters. Journal of Climate, 30(2), 813-827.

MacDougall, A. H. (2019). Limitations of the 1% experiment as the benchmark idealized experiment for carbon cycle intercomparison in C4MIP. Geoscientific Model Development, 12, 597-611. https://doi.org/10.5194/gmd-12-597-2019.

MacDougall, A. H., Frölicher, T. L., Jones, C. D., Rogelj, J., Matthews, H. D., Zickfeld, K., et al. (2020). Is there warming in the pipeline? A multi-model analysis of the Zero Emissions Commitment from CO2. Biogeosciences, 17, 2987-3016. https://doi.org/10.5194/bg-17-2987-2020.

MacDougall, A. H. (2021). Estimated effect of the permafrost carbon feedback on the zero emissions commitment to climate change. Biogeosciences, 18, 4937-4952. https://doi.org/10.5194/bg-18-4937-2021

McDuffie, E. E., Smith, S. J., O'Rourke, P., Tibrewal, K., Venkataraman, C., Marais, E. A., et al. (2020). A global anthropogenic emission inventory of atmospheric pollutants from sector- and fuel-specific sources (1970–2017): an application of the Community Emissions Data System (CEDS). Earth System Science Data, 12, 3413-3442. https://doi.org/10.5194/essd-12-3413-2020

Machado, C., and Furlani, A. (2004). KINETICS OF PHOSPHORUS UPTAKE AND ROOT MORPHOLOGY OF LOCAL AND IMPROVED VARIETIES OF MAIZE. Sci. Agric. (Piracicaba, Braz.), 61, 69-76.

Machida, T., Nakazawa, T., Fujii, Y., Aoki, S., and Watanabe, O. (1995). Increase in the atmospheric nitrous oxide concentration during the last 250 years. Geophysical Research Letters, 22(23), 2921-2924. https://doi.org/10.1029/95GL02822

Mackenzie, F., Ver, L. M., and Lerman, A. (2002). Century-scale nitrogen and phosphorus controls of the carbon cycle. Chemical Geology, 190, 13-32.

Manizza, M., Keeling, R. F., and Nevison, C. D. (2012). On the processes controlling the seasonal cycles of the air–sea fluxes of O2 and N2O: A modeling study. Tellus B: Chemical and Physical Meteorology, 64(1), 18429. doi:10.3402/tellusb.v64i0.18429.

Malhotra, H., Vandana, and Sharma, S. (2018). Phosphorus Nutrition: Plant Growth in Response to Deficiency and Excess.

Malhi, Y., Baldocchi, D. D., and Jarvis, P. G. (1999). The carbon balance of tropical, temperate and boreal forests. Plant Cell and Environment, 22, 715-740.

Marcus, Y., Altman-Gueta, H., Wolff, Y., and Gurevitz, M. (2011). Rubisco mutagenesis provides new insight into limitations on photosynthesis and growth in Synechocystis PCC6803. Journal of Experimental Botany, 62(12), 4173-4182. doi:10.1093/jxb/err116

Martín, F., and D'Amelio, N. (2022). Biomembrane lipids: When physics and chemistry join to shape biological activity. Biochimie. https://doi.org/10.1016/j.biochi.2022.07.011

Martinez-Rey, J., Bopp, L., Gehlen, M., Tagliabue, A., and Gruber, N. (2015). Projections of oceanic N2O emissions in the 21st century using the IPSL Earth system model. Biogeosciences, 12(13), 4133–4148. doi:10.5194/bg-12-4133-2015.

Martius, C. (1992). Density, humidity, and nitrogen content of dominant wood species of floodplain forests (varzea) in Amazonia. Holz Roh Werkst., 50, 300–303.

Masclaux-Daubresse, C., Daniel-Vedele, F., Dechorgnat, J., Chardon, F., Gaufichon, L., and Suzuki, A. (2010). Nitrogen uptake, assimilation and remobilization in plants: Challenges for sustainable and productive agriculture. Annals of Botany, 105, 1141-1157. https://doi.org/10.1093/aob/mcq028.

Arévalo-Martínez, D. L., Kock, A., Löscher, C. R., Schmitz, R. A., and Bange, H. W. (2015). Massive nitrous oxide emissions from the tropical South Pacific Ocean. Nature Geoscience, 8, 530-533.

Matthews, H., Gillett, N., Stott, P., et al. (2009). The proportionality of global warming to cumulative carbon emissions. Nature, 459, 829–832. https://doi.org/10.1038/nature08047.

Matthews, H., and Weaver, A. (2010). Committed climate warming. Nature Geoscience, 3, 142–143. https://doi.org/10.1038/ngeo813

Matthews, H., and Caldeira, K. (2008). Stabilizing climate requires near-zero emissions. Geophysical Research Letters, 35. https://doi.org/10.1029/2007GL032388

Matthews, H. D., Tokarska, K. B., Nicholls, Z. R. J., et al. (2020). Opportunities and challenges in using remaining carbon budgets to guide climate policy. Nature Geoscience, 13, 769–779. https://doi.org/10.1038/s41561-020-00663-3

Mayorga, E., Seitzinger, S., Harrison, J., Dumont, E., Beusen, A., Bouwman, A., Fekete, B., Kroeze, C., and Van Drecht, G. (2010). Global Nutrient Export from Watersheds 2 (NEWS 2): Model development and implementation. Environmental Modelling and Software, 25, 837-853. https://doi.org/10.1016/j.envsoft.2010.01.007

McNeill, A., and Unkovich, M. (2007). The Nitrogen Cycle in Terrestrial Ecosystems. 10.1007/978-3-540-68027-7_2.

McGill, W., and Cole, C. (1981). Comparative aspects of cycling of organic C, N, S, and P through soil organic matter. Geoderma, 26, 267–286.

Meinshausen, M., Nicholls, Z. R. J., Lewis, J., Gidden, M. J., Vogel, E., Freund, M., Beyerle, U., Gessner, C., Nauels, A., Bauer, N., Canadell, J. G., Daniel, J. S., John, A., Krummel, P. B., Luderer, G., Meinshausen, N., Montzka, S. A., Rayner, P. J., Reimann, S., Smith, S. J., van den Berg, M., Velders, G. J. M., Vollmer, M. K., and Wang, R. H. J. (2020). The shared socio-economic pathway (SSP) greenhouse gas concentrations and their extensions to 2500. Geosci. Model Dev., 13, 3571–3605. https://doi.org/10.5194/gmd-13-3571-2020

Meissner, K. J., Weaver, A. J., Matthews, H. D., and Cox, P. M. (2003). The role of land surface dynamics in glacial inception: a study with the UVic Earth System Model. Climatic Dynamics, 21, 515–537. https://doi.org/10.1007/s00382-003-0352-2

Meissner, K. J., McNeil, B. I., Eby, M., and Wiebe, E. C. (2012). The importance of the terrestrial weathering feedback for multi-millennial coral reef habitat recovery. Global Biogeochemical Cycles, 26. https://doi.org/10.1029/2011GB004098

Menge D., Hedin, L., Pacala S. (2012). Nitrogen and Phosphorus Limitation over Long-Term Ecosystem Development in Terrestrial Ecosystems. PLOS ONE, 7(8). https://doi.org/10.1371/journal.pone.0042045

Menge D., Hedin, L., Pacala S. (2012). Nitrogen and Phosphorus Limitation over Long-Term Ecosystem Development in Terrestrial Ecosystems. PLOS ONE, 7(8). https://doi.org/10.1371/journal.pone.0042045.

Mengis, N., Partanen, A. I., Jalbert, J., et al. (2018). 1.5 C carbon budget dependent on carbon cycle uncertainty and future non-CO2 forcing. Scientific Reports, 8, 5831. https://doi.org/10.1038/s41598-018-24241-1

Mengis, N., Keller, D. P., MacDougall, A. H., Eby, M., Wright, N., Meissner, K. J., Oschlies, A., Schmittner, A., MacIsaac, A. J., Matthews, H. D., Zickfeld, K. (2020). Evaluation of the University of Victoria Earth System Climate Model version 2.10 (UVic ESCM 2.10). Geosci. Model Dev., 13, 4183–4204. https://doi.org/10.5194/gmd-13-4183-2020.

Modolo, G., Alkemade, R., Schipper, A. M., Benítez-López, A., Perring, M. P., and De Vries, W. (2019). Impacts of nitrogen addition on plant species richness and abundance: A global meta-analysis. Global Ecology and Biogeography, 28, 398–413. https://doi.org/10.1111/geb.12856.

Montzka, S., Dlugokencky, E., and Butler, J. (2011). Non-CO2 greenhouse gases and climate change. Nature, 476, 43–50. https://doi.org/10.1038/nature10322.

Montenegro, A., Brovkin, V., Eby, M., Archer, D., and Weaver, A. J. (2007). Long-term fate of anthropogenic carbon. Geophysical Research Letters, 34, L19707. doi:10.1029/2007GL030905

Muindi, E. (2019). Understanding Soil Phosphorus. International Journal of Plant and Soil Science. 1-18. https://doi.org/10.9734/ijpss/2019/v31i230208

Muratore, C., Espen, L., and Prinsi, B. (2021). Nitrogen Uptake in Plants: The Plasma Membrane Root Transport Systems from a Physiological and Proteomic Perspective. Plants, 10. https://doi.org/10.3390/plants10040681Muratore, C., Espen, L., Prinsi, B. (2021). Nitrogen Uptake in Plants: The Plasma Membrane Root Transport Systems from a Physiological and Proteomic Perspective. Plants, 10. https://doi.org/10.3390/plants10040681

Munawar, J., Bukhari, S. A. H., Zeng, J. B., Quan, X. Y., Ali, E., Muhammad, N., and Zhang, G. P. (2017). Nitrogen (N) metabolism related enzyme activities, cell ultrastructure, and nutrient contents as affected by N level and barley genotype. Journal of Integrative Agriculture, 16(1), 190-198. ISSN 2095-3119. https://doi.org/10.1016/S2095-3119(15)61308-9.

McGill, W., and Cole, C. (1981). Comparative aspects of cycling of organic C, N, S, and P through soil organic matter. Geoderma, 26, 267–286.

Myhre, G., Stocker, F., Qin, D., Plattner, G., Tignor, M., Allen, S., Boschung, J., Nauels, A., Xia, Y., Bex, V., and Midgley, P. (2013). Anthropogenic and natural radiative forcing. In Working Group I Contribution to the Intergovernmental Panel on Climate Change Fifth Assessment Report Climate Change 2013: The Physical Science Basis. Cambridge University Press.

Nakhavali, M., Mercado, L., Hartley, I., Sitch, S., Cunha, F., di Ponzio, R., et al.

(2021). Representation of phosphorus cycle in Joint UK Land Environment Simulator (vn5.5JULES-CNP). Geosci. Model Dev. Discuss, https://doi.org/10.5194/gmd-2021-403.

Neumann, B., Vafeidis, A. T., Zimmermann, J., and Nicholls, R. J. (2015). Future Coastal Population Growth and Exposure to Sea-Level Rise and Coastal Flooding - A Global Assessment. PLoS ONE, 10(3), e0118571, https://doi.org/10.1371/journal.pone.0118571.

Nishida, S., Takahashi, K., Matsumi, Y., Taniguchi, N., and Hayashida, S. (2004). The Journal of Physical Chemistry A 2004 108 (13), 2451-2456. DOI: 10.1021/jp037034o.

Norton, J.M. (2008). Nitrification in Agricultural Soils. In Nitrogen in Agricultural Systems (eds J.S. Schepers and W.R. Raun). https://doi.org/10.2134/agronmonogr49.c6.

Norton, J., and Ouyang, Y. (2019). Controls and Adaptive Management of Nitrification in Agricultural Soils. Front. Microbiol., 10, 1931, https://doi.org/10.3389/fmicb.2019.01931.

Nzotungicimpaye, C. M., Zickfeld, K., Macdougall, A. H., Melton, J., Treat, C., Eby, M., and Lesack, L. (2021). WETMETH 1.0: A new wetland methane model for implementation in Earth system models, Geoscientific Model Development, 14, 6215-6240, 2021 10.5194/gmd-14-6215-2021.

O'Neill, B. C., Kriegler, E., Ebi, K. L., Kemp-Benedict, E., Riahi, K., Rothman, D. S., et al. (2017). The roads ahead: Narratives for shared socioeconomic pathways describing world futures in the 21st century. Global Environmental Change, 42, 169-180, https://doi.org/10.1016/j.gloenvcha.2015.01.004.

Olander, L., and Vitousek, P. (2000). Regulation of soil phosphatase and chitinase activity by N and P availability. Biogeochemistry, 49, 175–190.

Oehl, F., Frossard, E., Fliessbach, A., Dubois, A., and Oberson, A. (2004). Basal organic phosphorus mineralization in soils under different farming systems. Soil Biology and Biochemistry, 36, 667-675. https://doi.org/10.1016/j.soilbio.2003.12.010.

Pacanowski, R. C. (1995). MOM 2 Documentation, users guide and reference manual, GFDL Ocean Group Technical Report 3, Geophys, Fluid Dyn. Lab., Princet. Univ. Princeton, NJ, 1995.

Plaxton, W. C., and Tran, H. T. (2011). Metabolic adaptations of phosphate-starved plants. Plant Physiology, 156(3), 1006-1015. doi: 10.1104/pp.111.175281.

Penn, C., and Camberato, J. (2019). A critical review on soil chemical processes that control how soil pH affects phosphorus availability to plants. Agriculture, 9. doi: 10.3390/agriculture9060120.

Pesce, M., Critto, A., Torresan, S., Giubilato, E., Santini, M., Zirino, A., Ouyang, W., and Marcomini, A. (2018). Modelling climate change impacts on nutrients and primary production in coastal waters. The Science of the total environment, 628-629, 919–937. https://doi.org/10.1016/j.scitotenv.2018.02.131.

Popp, J., Lakner, Z., Harangi-Rákos, M., and Fári, M. (2014). The effect of bioenergy expansion: Food, energy, and environment, Renewable and Sustainable Energy Reviews, 32, 559-578. 2014, https://doi.org/10.1016/j.rser.2014.01.056.

Poulter, B., MacBean, N., Hartley, A., et al. (2015). Plant functional type classification for earth system models: results from the European Space Agency's Land Cover Climate Change Initiative, Geosci. Model Dev., 8, 2315–2328, https://doi.org/10.5194/gmd-8-2315-2015, 2015.

Prather, M. J., Holmes, C. D., and Hsu, J. (2012). Reactive greenhouse gas scenarios: Systematic exploration of uncertainties and the role of atmospheric chemistry, Geophys. Res. Lett., 39, L09803, doi:10.1029/2012GL051440.

Prather, M., Hsu, J., DeLuca, N., Jackman, C., Oman, L., Douglass, A., Fleming, E., Strahan, S., Steenrod, S., Søvde, O., Isaksen, I., Froidevaux, L., and Funke, B. (2015). Measuring and modeling the lifetime of Nitrous Oxide including its variability: Nitrous Oxide and its Changing Lifetime. Journal of Geophysical Research: Atmospheres, 120, n/a-n/a. https://doi.org/10.1002/2015JD023267.

Prather, M. J., Froidevaux, L., and Livesey, N. J. (2023). Observed changes in stratospheric circulation: decreasing lifetime of N2O, 2005–2021, Atmos. Chem. Phys., 23, 843–849, https://doi.org/10.5194/acp-23-843-2023, 2023.

Prinn, R., Weiss, R., Arduini, J., Arnold, T., DeWitt, H., Fraser, P., Ganesan, A., Gasore, J., Harth, C., Hermansen, O., Kim, J., Krummel, P., Li, S., Loh, Z., Lunder, C., Maione, M., Manning, A., Miller, B., Mitrevski, B., Muhle, J., O'Doherty, S., Park, S., Reimann, S., Rigby, M., Saito, T., Salameh, P., Schmidt, R., Simmonds, P., Steele, L., Vollmer, M., Wang, H. J., Yao, B., Yokouchi, Y., Young, D., and Zhou, L. (2018). History of chemically and radiatively important atmospheric gases from the Advanced Global Atmospheric Gases Experiment (AGAGE). Carbon Dioxide Information Analysis Center (CDIAC), Oak Ridge National Laboratory (ORNL), Oak Ridge, TN (United States), ESS-DIVE repository. Dataset. doi:10.3334/CDIAC/ATG.DB1001. Retrieved from https://data.ess-dive.lbl.gov/datasets/doi:10.3334/CDIAC/ATG.DB1001.

Qiu, N., Jiang, D., WANG, X., WANG, B. and ZHOU, F.(2019). Advances in the members and biosynthesis of chlorophyll family. Photosynthetica. 57. 2019 10.32615/ps.2019.116.

Reed, S. C., Townsend, A. R., Davidson, E. A., and Cleveland, C. (2012). Stoichiometric patterns in foliar nutrient resorption across multiple scales. New Phytol., 196, 173–180. doi: 10.1111/j.1469-8137.2012.04249.

Reay, D., Davidson, E., Smith, K., Smith, P., Melillo, J., Dentener, F., and Crutzen, P. (2012). Global agriculture and nitrous oxide emissions. Nature Climate Change, 2, 410-416. doi: 10.1038/nclimate1458.

Reich, P. B., and Oleksyn, J. (2004). Global patterns of plant leaf N and P in relation to temperature and latitude. Proc. Natl Acad. Sci., 101, 11001–11006. doi:10.1073/pnas.0403588101.

Richter, J., Visioni, D., MacMartin, D., Bailey, D., Rosenbloom, N., Lee, W., Tye, M., and Lamarque, J.-F. (2022). Assessing Responses and Impacts of Solar climate intervention on the Earth system with stratospheric aerosol injection (ARISE-SAI). EGUsphere [preprint]. https://doi.org/10.5194/egusphere-2022-125.

Rockel, B. (2015). The Regional Downscaling Approach: a Brief History and Recent Advances. Curr Clim Change Rep 1, 22–29. https://doi.org/10.1007/s40641-014-0001-3

Rojeli, J., Shindell, D., Jiang, K., Fifita, S., Forster, P., Ginzburg, V., et al. (2018). Mitigation pathways compatible with 1.5C in the context of sustainable development. In Global warming of 1.5C. An IPCC Special Report on the impacts of global warming of 1.5C above pre-industrial levels and related global greenhouse gas emission pathways, in the context of strengthening the global response to the threat of climate change, sustainable development, and efforts to eradicate poverty (Eds. V. Masson-Delmotte et al.). In Press.

Rockström, J., Steffen, W., Noone, K., Persson, Å., Chapin III, F.S., Lambin, E.F.,

Lenton, T., Scheffer, M., Folke, C., Schellnhuber, H., Nykvist, B., de Wit, C.A., Hughes, T., van der Leeuw, S., Rodhe, H., Sörlin, S., Snyder, P.K., Costanza, R., Svedin, U., and Foley, J.A. (2009). A safe operating space for humanity. Nature, 461, 472-475.

Ryan, P.R., Dessaux, Y., Thomashow, L.S., and Weller, D.M. (2009). Rhizosphere engineering and management for sustainable agriculture. Plant and Soil 321(1–2), 363–383. doi:10.1007/s11104-009-0001-6.

Rychter, A. M., Rao, Idupulapati, and Cardoso, J. (2016). Role of phosphorus in photosynthetic carbon assimilation and partitioning.

Samal, D. P. K., Sukla, L., Pattanaik, A., and Pradhan, D. (2020). Mineralization of phosphorus by phosphate-solubilizing microbes affects soil fertility. 18,1-9.

Santoyo, G., Hernández-Pacheco, C., Hernandez-Salmeron, J., and Hernandez-León, R. (2017). The role of abiotic factors modulating the plant-microbe-soil interactions: Toward sustainable agriculture. A review. Spanish Journal of Agricultural Research, 15, e03R01. https://doi.org/10.5424/sjar/2017151-9990

Spanning, R., and Delgado, M. (2006). The nitrogen cycle: Denitrification and its relationship to N2 fixation. 10.1007/1-4020-3544-6_13.

Saud, S., Wang, D., and Fahad, S. (2022). Improved Nitrogen Use Efficiency and Greenhouse Gas Emissions in Agricultural Soils as Producers of Biological Nitrification Inhibitors. Frontiers in Plant Science, 13, 854195. https://doi.org/10.3389/fpls.2022.854195

Spafford, L., and MacDougall, A. H. (2020). Quantifying the probability distribution function of the transient climate response to cumulative CO2 emissions. Environmental Research Letters, 15. https://doi.org/10.1088/1748-9326/ab6d7b

Spafford, L., and MacDougall, A. H. (2021). Validation of terrestrial biogeochemistry in CMIP6 Earth system models: a review. Geoscientific Model Development, 14, 5863–5889. https://doi.org/10.5194/gmd-14-5863-2021

Selman, M., Greenhalgh, S., Diaz, R., and Sugg, Z. (2008). Eutrophication and hypoxia in coastal areas: a global assessment of the state of knowledge. WRI Policy Note, 1-6.

Seitzinger, S. P., Mayorga, E., Bouwman, A. F., Kroeze, C., Beusen, A. H. W., Billen, G., et al. (2010). Global river nutrient export: A scenario analysis of past and future trends. Global Biogeochemical Cycles, 24, GB0A08. https://doi.org/10.1029/2009GB003587.

Siahaan, A., Smith, R. S., Holland, P. R., Jenkins, A., Gregory, J. M., Lee, V., Mathiot, P., Payne, A. J., Ridley, J. K., and Jones, C. G. (2022). The Antarctic contribution to 21st-century sea-level rise predicted by the UK Earth System Model with an interactive ice sheet. The Cryosphere, 16, 4053–4086. https://doi.org/10.5194/tc-16-4053-2022.

Shi, M., Fisher, J. B., Brzostek, E. R., and Phillips, R. P. (2016). Carbon cost of plant nitrogen acquisition: Global carbon cycle impact from an improved plant nitrogen cycle in the Community Land Model. Global Change Biology, 22(3), 1299-1314.

Seitzinger, S. P., Mayorga, E., Bouwman, A. F., Kroeze, C., Beusen, A. H. W., Billen, G., Van Drecht, G., Dumont, E., Fekete, B. M., Garnier, J., and Harrison, J. A. (2010) Global river nutrient export: A scenario analysis of past and future trends. Global Biogeochem. Cy., 24, GB0A08, doi:10.1029/2009GB003587.

Shibata, H., Branquinho, C., McDowell, W. H., Mitchell, M. J., Monteith, D. T., Tang, J., et al. (2015). Consequence of altered nitrogen cycles in the coupled human and

ecological system under changing climate: The need for long-term and site-based research. Ambio, 44(3), 178–193. https://doi.org/10.1007/s13280-014-0545-4

Scheer, C., Fuchs, K., Pelster, D., and Butterbach-Bahl, K. (2020). Estimating global terrestrial denitrification from measured N2O:(N2O + N2) product ratios. Current Opinion in Environmental Sustainability, 47, 72-80. https://doi.org/10.1016/j.cosust.2020.07.005

Schlesinger, W.H.: Biogeochemistry: An Analysis of Global Change. San Diego, USA: Academic Press, 588pp. 1997.

Smil, V. (2000). Phosphorus in the environment: natural flows and human interferences, Annual Review of Energy and Environment, 25,53–88.

Smil, V. (2002). Nitrogen and food production: proteins for human diets. AMBIO, 31, 126–131.

Smith, S. V., et al. (2003). Humans, hydrology, and the distribution of inorganic nutrient loading to the ocean. BioScience, 53(3), 235– 245. https://doi.org/10.1641/0006-3568.

Somes, C. J., A. Landolfi, W. Koeve, and A. Oschlies (2016). Limited impact of atmospheric nitrogen deposition on marine productivity due to biogeochemical feedbacks in a global ocean model. Geophysical Research Letters, 43, 4500– 4509. https://doi.org/10.1002/2016GL068335.

Somes, C. J., and A. Oschlies (2015). On the influence of "non-Redfield" dissolved organic nutrient dynamics on the spatial distribution of N2 fixation and the size of the marine fixed nitrogen inventory. Global Biogeochemical Cycles, 29, 973– 993. https://doi.org/10.1002/2014GB005050.

Sorci, L., Kurnasov, O., Rodionov, D., and Osterman, A. (2010). Genomics and enzymology of NAD biosynthesis. In H. Liu and L. Mander (Eds.), Comprehensive Natural Products II (pp. 213-257). Elsevier. https://doi.org/10.1016/B978-008045382-8.00138-6.

Steinacher, M., Joos, F., Frölicher, T., Bopp, L., Cadule, P., Cocco, V., et al. (2010). Projected 21st century decrease in marine productivity: A multi-model analysis. Biogeosciences, 7, 979-1005. https://doi.org/10.5194/bg-7-979-2010.

Suntharalingam, P., et al. (2012). Quantifying the impact of anthropogenic nitrogen deposition on oceanic nitrous oxide. Geophysical Research Letters, 39(7), L07605. https://doi.org/10.1029/2011gl050778.

Tachiiri, K., Abe, M., Hajima, T., Arakawa, O., Suzuki, T., Komuro, Y., et al. (2019). MIROC MIROC-ES2L model output prepared for CMIP6 ScenarioMIP ssp585. Version YYYYMMDD[1]. Earth System Grid Federation.

Thorton, P., Lamarque, J., Rosenbloom, N., and Mahowald, N. (2007). Influence of carbon-nitrogen cycle coupling on land model response to CO_2 fertilization and climate variability. Global Biogeochemical Cycles, 21, doi:10.1029/2006GB002868.

Thum, T., Caldararu, S., Engel, J., Kern, M., Pallandt, M., Schnur, R., Yu, L., and Zaehle, S.: A new model of the coupled carbon, nitrogen, and phosphorus cycles in the terrestrial biosphere (QUINCY v1.0; revision 1996), Geosci. Model Dev., 12, 4781–4802, https://doi.org/10.5194/gmd-12-4781-2019, 2019.

Tian, H., Lu, C., Ciais, P., et al. (2016). The terrestrial biosphere as a net source of greenhouse gases to the atmosphere. Nature, 531, 225–228. https://doi.org/10.1038/nature16946

Tian, H., Xu, R., Canadell, J.G., et al. (2020). A comprehensive quantification of global nitrous oxide sources and sinks. Nature, 586, 248–256. https://doi.org/10.1038/s41586-020-2780-0.

Tilman, D., Cassman, K.G., Matson, P.A., Naylor, R., and Polasky, S. (2002). Agricultural sustainability and intensive production practices. Nature, 418, 671–677.

Tivig, Miriam, Keller, David, and Oschlies, Andreas. (2021). Riverine nitrogen supply to the global ocean and its limited impact on global marine primary production: a feedback study using an Earth System Model.

Tokarska, Katarzyna, Gillett, Nathan, Arora, Vivek, Lee, Warren, and Zickfeld, Kirsten. (2018). The influence of non-CO2 forcings on cumulative carbon emissions budgets. Environmental Research Letters, 13, doi:10.1088/1748-9326/aaafdd.

Tokarska, K. B., Zickfeld, K., and Rogelj, J. (2019). Path independence of carbon budgets when meeting a stringent global mean temperature target after an overshoot. Earth's Future, 7, 1283–1295. doi:10.1029/2019EF001312.

Travers, A., and Muskhelishvili, G. (2015). DNA structure and function. FEBS Journal, 282(12), 2279-2295. https://doi.org/10.1111/febs.13307.

Van Oijen, M., Barcza, Z., Confalonieri, R., Korhonen, P., Kroel-Dulay, G., Lellei-Kovács, E., Louarn, G., Louault, F., Martin, R., Moulin, T., Movedi, E., Picon-Cochard, C., Rolinski, S., Viovy, N., Wirth, S., and Bellocchi, G. (2020). Incorporating Biodiversity into Biogeochemistry Models to Improve Prediction of Ecosystem Services in Temperate Grasslands: Review and Roadmap. Agronomy. doi:10.3390/agronomy10020259.

Vitousek, P. M., Mooney, H. A., Lubchenco, J., and Melillo, J. M.: Human domination of Earth's ecosystems, Science, 277, 494– 499, 1997.

Vitousek, P.M., Cassman, K., Cleveland, C. et al. (2002) Towards an ecological understanding of biological nitrogen fixation. Biogeochemistry 57, 1–45 . https://doi.org/10.1023/A:1015798428743

Vitousek, P. M., Naylor, R., Crews, T., David, M. B., Drinkwater, L. E., Holland, E., Johnes, P. J., Katzenberger, J., Martinelli, L. A., Matson, P. A., and Nziguheba, G.: Nutrient imbalances in agricultural development, Science, 324, 1519–1520, 2009.

Vitousek, P.M., Porder, S., Houlton, B.Z. and Chadwick, O.A. (2010). Terrestrial phosphorus limitation: mechanisms, implications, and nitrogen–phosphorus interactions. Ecological Applications, 20: 5-15. https://doi.org/10.1890/08-0127.1.

Vitousek, P. M., Menge, D.N., Reed, S.C., and Cleveland, C.C. (2013). Biological nitrogen fixation: rates, patterns and ecological controls in terrestrial ecosystems. Philos Trans R Soc Lond B Biol Sci. 368(1621):20130119. doi: 10.1098/rstb.2013.0119.

Waithaisong, K., Robin, A., L'Huillery, V., Abadie, J., Sauvage, F. X., Chemardin, P., et al. (2022). Organic phosphorus immobilization in microbial biomass controls how N2-fixing trees affect phosphorus bioavailability in two tropical soils. Environmental Advances, 8, 100247. https://doi.org/10.1016/j.envadv.2022.100247.

Wagg, C., Bender, S., Widmer, F., Van der Heijden, M. (2014). Soil biodiversity and soil community composition determine ecosystem multifunctionality. Proceedings of the National Academy of Sciences 111(14), 5266–5270. doi:10.1073/pnas.1320054111.

Walker, T., and Syers, J. (1976). The fate of phosphorus during pedogenesis. Geoderma, 15, 1-19. doi.org/10.1016/0016-7061(76)90066-5.

Walker, A., Beckerman, A., Gu, L., Kattge, J., Cernusak, L., Domingues, T., et al. (2014). The relationship of leaf photosynthetic traits - Vcmax and Jmax - to leaf

nitrogen, leaf phosphorus, and specific leaf area: A meta-analysis and modeling study. Ecology and Evolution, 4. https://doi.org/10.1002/ece3.1042.

Wania, R., Meissner, K., Eby, M., Arora, V., Ross, I., and Weaver, A. (2012) Carbon-nitrogen feedbacks in the UVic ESCM, Geosci. Model Dev., 5, 1137–1160, https://doi.org/10.5194/gmd-5-1137-2012.

Wang, Y., Houlton, B., and Field, C. (2007). A model of biogeochemical cycles of carbon, nitrogen, and phosphorus including symbiotic nitrogen fixation and phosphatase production. Global Biogeochemical Cycles, 21. https://doi.org/10.1029/2006GB002797.

Wang, Y., Law, R., and Pak, B. (2010). A global model of carbon, nitrogen, and phosphorus cycles for the terrestrial biosphere. Biogeosciences, 7, 2261–2282. doi:10.5194/bg-7-2261-2010.

Wang, Y., and Goll, D. (2021). Modelling of land nutrient cycles: recent progress and future development. Faculty Reviews, 10. 10.12703/r/10-53.

Wang, Y. and Goll, D. (2021). Modelling of land nutrient cycles: recent progress and future development. Faculty Reviews. 10. 10.12703/r/10-53.

Wang, Y., Ciais, P., Goll, D., Huang, Y., Luo, Y., Wang, Y.-P., Bloom, A. A., Broquet, G., Hartmann, J., Peng, S., Penuelas, J., Piao, S., Sardans, J., Stocker, B. D., Wang, R., Zaehle, S., and Zechmeister-Boltenstern, S. (2018). GOLUM-CNP v1.0: a data-driven modeling of carbon, nitrogen and phosphorus cycles in major terrestrial biomes, Geosci. Model Dev., 11, 3903–3928, https://doi.org/10.5194/gmd-11-3903-2018.

Wang, Z., Tian, H., Yang, J., Shi, H., Pan, S., Yao, Y., et al. (2020). Coupling of phosphorus processes with carbon and nitrogen cycles in the dynamic land

ecosystem model: Model structure, parameterization, and evaluation in tropical forests. Journal of Advances in Modeling Earth Systems, 12, e2020MS002123. https://doi.org/10.1029/2020MS002123

Ward, B. (2008). Nitrification. In S. Erik Jørgensen, B. D. Fath (Eds.), Encyclopedia of Ecology (pp. 2511-2518). Academic Press. https://doi.org/10.1016/B978-008045405-4.00280-9.

Ward, B. (2012). The Global Nitrogen Cycle. In Fundamentals of Geobiology, First Edition. https://doi.org/10.1002/9781118280874.ch4.

Weaver, A. J., Eby, M., Wiebe, E. C., Bitz, C. M., Duffy, P. B., Ewen, T. L., et al. (2001). The UVic Earth System Climate Model: Model description, climatology, and applications to past, present and future climates. Atmosphere-Ocean, 39, 361–428.

Weber, S. (2010). The utility of Earth system Models of Intermediate Complexity (EMICs). Wiley Interdiscip Rev-Climate Change. 1. 10.1002/wcc.24.

Weiss, R. F., and Price, B. A. (1980). Nitrous oxide solubility in water and seawater. Marine Chemistry, 8, 347–359.

Wieder, W. R., Cleveland, C. C., Smith, W. K., and Todd, K. J. (2015). Future productivity and carbon storage limited by terrestrial nutrient availability. Nature Geoscience, 8, 441–444. https://doi.org/10.1038/ngeo2413.

Van Puijenbroek, P., Beusen, A., and Bouwman, A. (2019). Global nitrogen and phosphorus in urban wastewater based on the Shared Socioeconomic pathways. Journal of Environmental Management, 231, 446-456. https://doi.org/10.1016/j.jenvman.2018.10.048.

Xu-Ri, and Prentice, I. C. (2008). Terrestrial nitrogen cycle simulation with a dynamic global vegetation model. Global Change Biology, 14, 1745–1764.

Yang, X., Post, W., Thornton, P., and Jain, A. (2013). The distribution of soil phosphorus for global biogeochemical modeling. Biogeosciences, 10, 2525–2537. https://doi.org/10.5194/bg-10-2525-2013.

Yang, X. J., Wittig, V., Jain, A. K., and Post, W. (2009). Integration of nitrogen cycle dynamics into the Integrated Science Assessment Model for the study of terrestrial ecosystem responses to global change. Global Biogeochemical Cycles, 23, 121–149.

Yang, G., Wagg, C., Veresoglou, S. D., Hempel, S., and Rillig, M. C. (2018). How soil biota drive ecosystem stability. Trends in Plant Science, 23(12), 1057–1067. https://doi.org/10.1016/j.tplants.2018.09.007.

Yang, X., Ricciuto, D. M., Thornton, P. E., Shi, X., Xu, M., Hoffman, F., and Norby, R. J. (2019). The effects of phosphorus cycle dynamics on carbon sources and sinks in the Amazon region: a modeling study using ELM v1. Journal of Geophysical Research: Biogeosciences, 124, 3686–3698. https://doi.org/10.1029/2019JG005082.

Yang, S., Chang, B., Warner, M., Weber, T., Bourbonnais, A., Santoro, A., Kock, A., Sonnerup, R., Bullister, J., Wilson, S. and Bianchi, Daniele. (2020). Global reconstruction reduces the uncertainty of oceanic nitrous oxide emissions and reveals a vigorous seasonal cycle. Proceedings of the National Academy of Sciences. 117. 201921914. 10.1073/pnas.1921914117.

Zamora, L. M., A. Oschlies, H. W. Bange, K. B. Huebert, J. D. Craig, A. Kock, and C. R. Löscher (2012). Nitrous oxide dynamics in low oxygen regions of the Pacific: Insights from the MEMENTO database. Biogeosciences, 9(12), 5007–5022. https://doi.org/10.5194/bg-9-5007-2012.

Zamora, L. M., and A. Oschlies (2014). Surface nitrification: A major uncertainty in marine N2O emissions. Geophysical Research Letters, 41, 4247–4253. https://doi.org/10.1002/2014GL060556.

Zaehle, S., Friend, A. D., Friedlingstein, P., Dentener, F., Peylin, P., and Schulz, M. (2010). Carbon and nitrogen cycle dynamics in the OCN land surface model: 2. Role of the nitrogen cycle in the historical terrestrial carbon balance. Global Biogeochemical Cycles, 24. doi:10.1029/2009GB003522.

Zaehle, S., Medlyn, B. E., de Kauwe, M. G., Walker, A. P., Dietze, M. C., Hickler, T., et al. (2014). Evaluation of 11 terrestrial carbon-nitrogen cycle models against observations from two temperate Free-Air CO2 Enrichment studies. New Phytologist, 202(3), 803–822. https://doi.org/10.1111/nph.12697.

Zickfeld, K., Eby, M., Matthews, H. D., and Weaver, A. J. (2009). Setting cumulative emissions targets to reduce the risk of dangerous climate change. Proceedings of the National Academy of Sciences of the United States of America, 106(39), 16129–16134. https://doi.org/10.1073/pnas.0805800106.

Ziehn, T., Chamberlain, M., Law, R., Lenton, A., Bodman, R., Dix, M., Stevens, L., Wang, Y., and Srbinovsky, J. (2020). The Australian Earth System Model: ACCESS-ESM1.5. Journal of Southern Hemisphere Earth Systems Science, 70, 193-214.